

# Design, development and analysis of a full carbon fibre reinforced composite chassis of an electric vehicle

Khoo, Raymond Rui Xiang

2015

Khoo, R. R. X. (2015). Design, development and analysis of a full carbon fibre reinforced composite chassis of an electric vehicle. Master's thesis, Nanyang Technological University, Singapore.

<https://hdl.handle.net/10356/62236>

<https://doi.org/10.32657/10356/62236>



**NANYANG  
TECHNOLOGICAL  
UNIVERSITY**

**DESIGN, DEVELOPMENT AND  
ANALYSIS OF A FULL CARBON  
FIBRE REINFORCED COMPOSITE  
CHASSIS OF AN ELECTRIC  
VEHICLE**

**KHOO RUI XIANG RAYMOND**

**SCHOOL OF MECHANICAL AND AEROSPACE  
ENGINEERING**

**2015**

DESIGN, DEVELOPMENT AND ANALYSIS OF A FULL CARBON FIBRE  
REINFORCED COMPOSITE CHASSIS OF AN ELECTRIC VEHICLE

KHOO RUI XIANG RAYMOND

2015



KHOO RUI XIANG RAYMOND

# **DESIGN, DEVELOPMENT AND ANALYSIS OF A FULL CARBON FIBRE REINFORCED COMPOSITE CHASSIS OF AN ELECTRIC VEHICLE**

**KHOO RUI XIANG RAYMOND**

School of Mechanical and Aerospace  
Engineering

A thesis submitted to the Nanyang Technological University  
in partial fulfilment of the requirement for the degree of  
Master of Engineering

**2015**





---

# Acknowledgement

---

## **ERIAN and NTU**

I would like to thank ERI@N and NTU for the financial support that enabled me to embark on EVA development project.

## **TUM-CREATE**

I would like thank TUM-CREATE for providing this opportunity to work on project EVA, coordinating overseas training opportunity and entrusting me with the responsibility in the design and development of the EVA's vehicle structure.

## **Ng Heong Wah, Associate Professor, Supervisor, NTU**

I would like to thank Professor Ng, who has not only recommended this rare project opportunity but also the unwavering guidance, knowledge, assistance, time and encouragement to the author during the development of project EVA.

## **Project EVA Development Team, TUM-CREATE**

I would like to thank fellow project members for the patience in working out project details, the late nights spent together to develop and assemble EVA and providing me with enriching advices and experiences. It was one of the most enriching work experience for me thus far, being exposed to knowledge from multiple disciplines allowed me to have a broad perspective on prototype vehicle development. This superb team made EVA a reality.

## **Staff of Hope Technik and Admiralty International**

I would like to acknowledge staff of Hope Technik and Admiralty International for their patience, understanding and perseverance to achieve higher when high requirements and quality was demanded. Their openness to manufacturing knowhow in the field of composite manufacturing and vehicle design assisted me greatly in this project.

## **Family and Friends**

I am indebted to my parents and friends for their unwavering support, be it financially or emotionally. Their presences and encouragements allowed me to achieve what I struggle to think was possible before.



---

# Content

---

<b>Acknowledgement.....</b>	<b>i</b>
<b>List of Abbreviations.....</b>	<b>xix</b>
<b>Abstract .....</b>	<b>xxiii</b>
<b>Chapter 1: Introduction .....</b>	<b>1</b>
<b>1.1 TUM CREATE.....</b>	<b>1</b>
<b>1.2 Project EVA Background.....</b>	<b>1</b>
<b>1.3 Thesis Scope and Objectives of Project EVA .....</b>	<b>4</b>
1.3.1 Crash Worthiness and Safety .....	4
1.3.2 Structural Stability, Strength and Durability .....	4
1.3.3 Limitations .....	5
<b>1.4 Thesis Structure.....</b>	<b>5</b>
<b>Chapter 2: Literature Review.....</b>	<b>7</b>
<b>2.1 Introduction and Organization.....</b>	<b>7</b>
<b>2.2 Vehicle Crashworthiness .....</b>	<b>7</b>
2.2.1 Brief History of Crashworthiness .....	7
2.2.2 Crash Energy Absorption.....	8
2.2.3 Occupant Safety Cell and Crumple Zone .....	8
2.2.4 Crash Test Standards.....	9
<b>2.3 Vehicle Structure Requirements.....</b>	<b>11</b>
2.3.1 Torsional Stiffness .....	11
2.3.2 Bending Stiffness .....	12
2.3.3 Eigen Frequency/Natural Frequency/Noise Vibration Harshness .....	13
2.3.4 Dynamic Driving Loads.....	14
<b>2.4 Vehicle Structure Layout.....</b>	<b>15</b>
2.4.1 Ladder Frame / Body on Frame Design.....	15
2.4.2 Space Frame Design .....	15
2.4.3 Unibody/Monocoque Design .....	16

2.4.4	Carbon Monocoque Design .....	17
2.4.5	Multi-Material Hybrid Design .....	19
<b>2.5</b>	<b>Mass Reduction and Future Influences.....</b>	<b>21</b>
2.5.1	Advantages and Drawbacks of Weight Reduction .....	25
<b>2.6</b>	<b>Materials .....</b>	<b>26</b>
2.6.1	Metallic Materials .....	26
2.6.1.1	Crash Structures .....	28
2.6.2	Other Materials .....	30
2.6.3	Carbon Fibre Composites .....	31
2.6.3.1	Brief History of Carbon Fibre and Its Applications .....	31
2.6.4	Structural Joint of Carbon Fibre Composites.....	35
2.6.4.1	Mechanical Fasteners .....	35
2.6.4.2	Adhesive Joints .....	37
2.6.4.3	Metallic Inserts.....	39
2.6.5	Failure Criteria for Carbon Fibre Composite.....	40
2.6.5.1	Maximum stress/strain criteria (Non-Interactive) .....	40
2.6.5.2	Tsai-Hill and Tsai-Wu Criteria (Interactive).....	41
2.6.5.3	Composite Laminate Strength.....	42
<b>2.7</b>	<b>Concluding Remark .....</b>	<b>43</b>
<b>Chapter 3:</b>	<b>Development Setup, Considerations and Limitations...</b>	<b>45</b>
<b>3.1</b>	<b>Crashworthiness Development Challenges.....</b>	<b>45</b>
3.1.1	Crash Energy Approach for Frontal Impact.....	46
3.1.2	Photogrammetry Study of Frontal Crash Tests.....	47
3.1.3	Side Impact Collision Mechanics .....	49
3.1.4	Equivalent Quasi-static Crash Load.....	52
3.1.5	Structure Crash Load Path .....	53
3.1.6	Carbon Composite Crash Structure .....	53
3.1.7	Limitations of Carbon Composite Failure Models .....	55
3.1.8	EVA CFRP Structure Failure Criteria .....	57
3.1.9	EVA CFRP Structure Natural Frequency .....	58
3.1.10	EVA Crash Energy Management Approach.....	58
<b>3.2</b>	<b>EVA Preliminary Packaging and Design Decisions .....</b>	<b>58</b>

<b>3.3</b>	<b>Groundwork for Composite Structure Development .....</b>	<b>59</b>
3.3.1	Production Method and Material Selection .....	59
3.3.2	Material Property Testing .....	60
3.3.2.1	Property Test for CFRP and Structural Adhesive .....	60
3.3.3	Composite Joining Methods and Adhesive.....	65
3.3.4	Manufacturing Control.....	66
3.3.4.1	Layup and Manufacturing Constraints .....	66
3.3.4.2	Plies Overlap and Drop Off.....	67
<b>3.4</b>	<b>Concluding Remark .....</b>	<b>68</b>
<b>Chapter 4:</b>	<b>Development of EVA Vehicle Structure.....</b>	<b>71</b>
<b>4.1</b>	<b>FEA Simulation Definition of the Materials and Modelling Assumptions</b>	<b>72</b>
4.1.1	Fast Layup Changes with Shell Laminate Model .....	72
4.1.2	Static Simulation of Dynamic Loading using Inertia Relief.....	73
4.1.3	Clean-up of CAD Geometry, Meshing and Ply Layup Definitions.....	74
4.1.4	Constraints Conditions and Assumptions in FEA Model .....	77
4.1.5	Load Application in FEA Model .....	79
4.1.6	FEA Model Development Plan and Limitations.....	80
<b>4.2</b>	<b>FEA Model H0 (Preliminary).....</b>	<b>81</b>
4.2.1	Purpose and Objective of Model H0.....	81
4.2.2	Simulation Results of Model H0.....	82
4.2.3	Structural Design Challenges Identified in Model H0.....	84
<b>4.3</b>	<b>FEA Model H1 (Intermediate) .....</b>	<b>84</b>
4.3.1	Purpose and Objective of Model H1 .....	84
4.3.2	Envelope Contour Plots .....	85
4.3.2.1	Failure Due to Geometric Influence of Model H1 .....	85
4.3.2.2	Results of Multiple Failures of the Composite Vehicle Structure Under Crash Loads of Model H1 .....	86
4.3.3	Solutions to Front Crash Load Path Structure Failure in Model H1.....	86
<b>4.4</b>	<b>FEA Model H2 (Final) .....</b>	<b>88</b>
4.4.1	Purpose and Objective of Model H2.....	88
4.4.2	Vehicle Structure Performance of Model H2 under Crash Loads .....	89

4.4.3	Geometric Structure Design Comparison of Model H0, H1 and H2 .....	89
4.4.4	Side Impact Crash Simulation Result and Novel Side Crash Beam Structure	91
4.4.5	Result of Bending and Torsion Stiffness Simulation of Model H2 .....	96
4.4.6	Development of Auxiliary Components .....	97
<b>4.5</b>	<b>Front and Rear Aluminium Crash Structure/Crumple Zone.....</b>	<b>97</b>
4.5.1	Aluminium Failure Model Verification with Published Experimental Data	98
4.5.2	Crash Structure Detailed Geometry Development .....	99
4.5.3	Experimental Test Specimens and Simulation Verification .....	101
<b>4.6</b>	<b>Concluding remark .....</b>	<b>105</b>
<b>Chapter 5:</b>	<b>Manufacturing and Assembly of EVA .....</b>	<b>107</b>
<b>5.1</b>	<b>Manufacturing and Final Assembly .....</b>	<b>107</b>
<b>5.2</b>	<b>Tokyo Motorshow 2013 .....</b>	<b>111</b>
<b>5.3</b>	<b>Vehicle Structure Performance by Physical Evaluation .....</b>	<b>112</b>
<b>Chapter 6:</b>	<b>Conclusions .....</b>	<b>113</b>
<b>6.1</b>	<b>Conclusions .....</b>	<b>113</b>
<b>6.2</b>	<b>Recommendations for Future work.....</b>	<b>114</b>
<b>6.3</b>	<b>Conferences and Publications by the Author .....</b>	<b>115</b>
<b>References.....</b>		<b>I</b>
<b>Glossary .....</b>		<b>XII</b>
<b>Appendix A.....</b>		<b>A</b>
<b>Appendix B.....</b>		<b>C</b>

---

## List of Figures

---

Fig 1.1 TUM CREATE research structure [1]-----	1
Fig 1.2 Total annual mileage comparison between private cars and taxi in Singapore [2].-----	2
Fig 1.3 160KWh fast charging allow recharge of 200km range in 15 minute.-----	3
Fig 1.4 Proposed shift change and charging break. -----	3
Fig 2.1 Rigid passenger cell marked out in bold outlines on the side view of vehicle structure with crumple zones and seatbelts. (Daimler Global Media, Mercedes-Benz 111 series) (1959 to 1968).-----	9
Fig 2.2 Force interactions between vehicle structure and subsystems.-----	11
Fig 2.3 Illustration on how torsion stiffness of a vehicle structure is measured, constraints at suspension attachments points [8] -----	12
Fig 2.4 Illustration on how bending stiffness is measured, constraints at suspension attachments points. [8]-----	12
Fig 2.5 Noise and vibration mode map and primary body frequency design target by Malen [10]-----	14
Fig 2.6 Quasi-static design load factor for structural requirement under various dynamic driving scenarios extracted from Malen [10].-----	14
Fig 2.7 (Left) Open section ladder frame chassis of the 1920s [14] (Right) Modern ladder frame structure on a SUV which shows significant adaptation for packaging-----	15
Fig 2.8 (Left) Audi A8 Aluminium space frame body in white (Red : casting, Blue : extrusion, Green : sheet) [15] (Right) Example of a tubular space frame vehicle structure for a 2 seater. -----	16
Fig 2.9 Unibody of the 1934 Citroen 11 CV, produced till 1956. [14]-----	16
Fig 2.10 Exploded view of Mercedes S-Class hybrid steel and aluminium BIW structure with exterior panels. [16] -----	17



Fig 2.11 McLaren first carbon composite formula 1 monocoque shell 1981 [17]-----	18
Fig 2.12 (Left) Lamborghini Adventador Carbon Monocoque, (Right): McLaren MP4-12C carbon tub [17]-----	18
Fig 2.13 Aluminium structure with carbon transmission tunnel joined by a structural, hot curing adhesive (left) and aluminium front structure (right) [16] -----	19
Fig 2.14 McLaren MP4-12C - Powertrain and vehicle structure without exterior panel. [17] -----	20
Fig 2.15 BMW i3: Aluminium ladder frame structure and carbon monocoque life cell. [18] -----	20
Fig 2.16 BMW i3 cut away section illustration of the carbon monocoque life module with the base structure [19], Traditional ladder frame design similar to BMW i3 [14] -----	21
Fig 2.17 Breakdown of real world fuel consumption of a hybrid vehicle [20].-----	22
Fig 2.18 (Right) shows the total all greenhouse gas emissions in different sectors converted to CO <sub>2</sub> equivalent. (Left) shows the distribution of emissions of greenhouse gas between transport types in Singapore [29]. -----	23
Fig 2.19 Evolution of weight in compact-class cars [31] -----	23
Fig 2.20 Synergistic effect of Vicious Mass Cycle (left) and Virtuous Mass Cycle (right)-----	24
Fig 2.21 Efficiency benefit sequence: Mass reduction of passenger cabin and synergistic effect will lead to greater fuel efficiency and secondary mass reduction [20]. -----	24
Fig 2.22 Bulk mass inelastic collision illustration representing collision of vehicle with different mass m1 is lighter than m2.-----	25
Fig 2.23 Stress - Strain diagram of various materials and their failure characteristics under tensile failure [33] Area under the plot shows energy absorption limit of materials. -----	26
Fig 2.24 Total Elongation (%EL) vs. Ultimate tensile strength (UTS) "banana curve of automotive steels" [37] -----	27
Fig 2.25 Exploded view of the aluminium body structure of the Audi A8 [16] -----	28
Fig 2.26 Folding of thin wall stainless steel structure under axial crushing [40] -----	29

Fig 2.27 Fold formation and Load-Displacement of different phase and cycle of thin-wall square stainless steel profile. -----	29
Fig 2.28 Different types of crush initiators for box extrusion profiles. -----	30
Fig 2.29 (Top) ABD Matrix and illustrated coupling effects, (Bottom) ABD coupling mathematic relationship between stress and strains [48] -----	32
Fig 2.30 Unidirectional prepreg tape [49] -----	33
Fig 2.31 Multi-axial non-crimped fabrics held together with glass fibre stitching [50] -----	33
Fig 2.32 Different types of weave pattern on woven fabric and their influence in handling and mechanical properties. [51]-----	34
Fig 2.33 Different types of braided fabrics and their influence in handling and mechanical properties [50]-----	34
Fig 2.34 Macro level FEA of twill weave fabric [52] -----	34
Fig 2.35 Composite strength in unidirection loading depending on angle and fibre volume fraction [52] -----	35
Fig 2.36 Comparison of stress concentration factors of holes in composites and metal. [55] -----	36
Fig 2.37 Mode of failure of bolted joints in advanced composites [56]-----	37
Fig 2.38 Type of adhesive joints in composites [54] -----	38
Fig 2.39 Adhesive stresses in tapered and no tapered bonded joints [54] -----	38
Fig 2.40 Big head threaded inserts and spiked inserts [62] [63] -----	39
Fig 2.41 Cast Aluminium front shock tower support structure of the BMW i3 bonded to the carbon monocoque life cell. (Picture taken by author at the 2013 Tokyo Motorshow) -----	39
Fig 2.42 (Left) Maximum stress envelope (Right) Maximum strain envelope. [47]--	40
Fig 2.43 (Left) Different failure modes envelope for varying angle unidirectional composite plates. (Right) Type of failure modes of unidirectional lamina [65] -----	41

Fig 2.44 (Left) Failure envelope of biaxial loading (Right) Failure envelope for transverse and shear loading for Tsai-Wu, Tsai-Hill, Max-strain, Max-stress and Hashin-Rotem failure criteria. (Daniel and O.hais) -----	42
Fig 3.1 Illustration of frontal collision set up, A and B are identical vehicle impacting the barriers, red reference line shows the point of impact. -----	46
Fig 3.2 Illustration of crumple zone deformation and total crash energy absorbed and the end of collision position of the vehicle. -----	47
Fig 3.3 FMVSS 301 full width vehicle crash test showing the amount of deformation and time duration of the impact -----	47
Fig 3.4 Photogrammetry of frontal offset crash test, yellow indicated distance is approximately 1m. -----	49
Fig 3.5 (Left) Illustration of conservation of momentum in a side impact collision. (Right) shows the velocity profile of colliding vehicle. -----	50
Fig 3.6 Illustration showing the door crumple zone $\Delta$ and the space between the interior door panel and the occupant $\Delta 0$ . -----	50
Fig 3.7 Side impact collision events alongside with velocity time diagram of $M_1$ , $M_2$ and the occupant. The slope of the purple arrows is the acceleration rate of the occupant.-----	51
Fig 3.8 Side impact velocity profile (left) without improvement in vehicle side impact strength and door gap reduction and (right) with improvement in both vehicle side impact strength and door gap reduction. -----	52
Fig 3.9 Illustration on crash load path through structural members in (top) frontal offset collision and (bottom) side impact collision. -----	53
Fig 3.10 Formula 1 nose cone under crash test fractures and delaminates as the crash progresses, breaking apart and absorbing energy cushioning the impact. [78] -----	54
Fig 3.11 Comparison of dissipated energy of steel and CFRP crash absorption cone [82] -----	55
Fig 3.12 Structural components in complexity hierarchy levels [64] -----	60
Fig 3.13 (Top) Chemical and mechanical test coupons, (left and bottom right) resin vacuum infusion resin flow test for sandwich structure (bottom left) adhesive test coupon showing failure at the bond surface. -----	64

Fig 3.14 Explosion view of the major composite panels that makes up EVA's monocoque structure. -----	65
Fig 3.15 Examples of good and bad adhesive joining methods [55] -----	66
Fig 3.16 Illustration the largest [0,90] ply that could be obtained from a [-45/+45] roll. -----	67
Fig 3.17 Distributed ply overlap to reduce excessive thickness and enhance strength	68
Fig 3.18 Amount of recommended overlap -----	68
Fig 3.19 Staggering ply drop off. -----	68
Fig 4.1 Main development topics for EVA electric taxi project.-----	71
Fig 4.2 Ply stack plot of composite shell -----	73
Fig 4.3 (Left) Quasi-static full width frontal crash simulation without inertia relief with fixed support at the rear crash structure (Right) Quasi-static full width frontal crash simulation with inertia relief showing realistic static equivalent of dynamic frontal crash showing low loading in rear crash structure. -----	73
Fig 4.4 Procedure of geometric surface clean up to element generation. In step 2 division or partition line can be drawn to define area of different ply layup or control the characteristic of meshing. -----	74
Fig 4.5 An Example of the definition of different ply layup zone in ABAQUS of the windscreen roof structure -----	75
Fig 4.6 Example of the ply book which defines layup in each assigned zone.-----	75
Fig 4.7 The use of discrete coordinates to define layup direction in various region --	76
Fig 4.8 (Top) Cross-section illustration of a laminated joint (Middle) Tie constraints on laminate nodes to adhesive nodes (Bottom) The exaggerated shearing deformation shown under joint loading. -----	77
Fig 4.9 The inertia load exerted by the battery cells during frontal offset crash scenario defined using pressure loading condition. -----	79
Fig 4.10 (Left) Frontal offset crash structure load on the peripheral of the crash structure mounting using line load condition (Right) Roof crush loading test using pressure loading condition-----	79

Fig 4.11 Composite Vehicle Structure Development Map-----	80
Fig 4.12 H0 Model of EVA taxi concept (with propose layup and structure components-----	81
Fig 4.13 Example of early initial package definition that is used to design H0 model	81
Fig 4.14 Deformation contour plot of the vehicle floor when an area the size of average footwear is subjected to 80kg load.-----	82
Fig 4.15 (Top) shows the max-strain failure concentration points for the ply 1 at 0.4% strain (bottom left and right) shows symmetric ply 1 failure points at high stress concentration points. (Blue shows compression loading and red shows tensile loading)-	83
Fig 4.16 H1 Model of EVA Taxi vehicle structure with H1 vehicle package model.	84
Fig 4.17 Envelope failure plots of (left) Model H0 and (right) Model H1. The envelope plots shows that failure is more widespread on the crash rail of model H1.-	86
Fig 4.18 (left) Part 581 (NHTSA) crash compatibility, (right) proposed change to crash structure height and allow better load path and brake booster clearance.----	87
Fig 4.19 Model H2 of EVA Taxi vehicle structure along with H2 vehicle package model-----	88
Fig 4.20 Model H2 front and back view in element mesh -----	88
Fig 4.21 Deformation contours of (Left) Model H1 (Right) Model H2with clipping at 30mm with full width frontal crash.-----	89
Fig 4.22 Use of aluminium adapters to extend mounting points allowing structure to have a cleaner and smoother load path.-----	89
Fig 4.23 Tsai hill envelope plot with clipping set at 1.0 (Top left and Right) Model H0 under full width frontal crash (middle left and right) Model H1 under full width frontal crash and (bottom left and right) Model H2 under full width frontal impact. Model H2 shows significant improvement in strength even when same laminate thickness is used.-----	90
Fig 4.24 Quasi-static side crash load simulation Tsai-Hill envelope plot. (left) with exterior door panel surface (right) with crash beam and door interior panel.	92
Fig 4.25 Quasi-static side crash load simulation Tsai-Hill envelope plot (Left) crash beam only (right) interior door panel envelope plot.-----	92

Fig 4.26 Carbon fibre kevlar composite crash beam of EVA electric taxi prototype.	93
Fig 4.27 (left) Torsional loading deformation plot (right) bending loading deformation plot. (Deformation exaggerated by 15 times) -----	96
Fig 4.28 (left) bending stiffness benchmark comparison (right) BMW torsional stiffness comparison (Vertical axis in Nm/degree°, horizontal axis in Years). -----	96
Fig 4.29 Auxiliary FEA simulation conducted to ensure strength of functional critical components in respective load scenarios.-----	97
Fig 4.30 (Top right) Force-time plots of FEA simulation (Top left) Force-displacement plot of experimental results. (Middle and bottom) AL6063-T5 FEA material model simulation with comparison with experimental data [92]-----	98
Fig 4.31 Alternative machined groove to trigger asymmetric folding (blue) -----	99
Fig 4.32 Subassembly of front crash structure with easily replaceable bumper assembly. -----	100
Fig 4.33 Quasi-static crushing of TUM-CREATE electric taxi aluminium crash structure for crash initiator design verification (above) experiment, (below) Explicit FEA simulation in ABAQUS.-----	101
Fig 4.34 (left) crushing of low speed crash structure (middle) progressive folding of main crash beam (right) Progressive folding not affected by centre comp bracing -----	102
Fig 4.35 (Left) 15 degree angled impact (Right) stability of crash structure maintained -----	102
Fig 4.36 Force vs time plot for frontal impact at 0 degrees. -----	103
Fig 4.37 Force vs time plot for frontal impact at 15 degrees.-----	103
Fig 4.38 Project EVA electric taxi aluminium crash structure. -----	104
Fig 5.1 Manufacturing and assembly sequence of EVA BIW structure (Caption below) -----	108
Fig 5.2 Component assembly of EVA Electric Taxi (Caption below) -----	109
Fig 5.3 Snippets of author working with EVA.-----	110

Fig 5.4 Compilation of pictures from the launch of EVA electric taxi at Tokyo Motor Show 2013.-----	111
Fig 5.5 Illustration of the carbon composite vehicle structure of EVA electric taxi prototype. -----	112

---

## List of Tables

---

Table 2.1 Human tolerance limits in crash survival in different directions [5].	8
Table 2.2 List of common crash standards and their test setup (Crash test dummies, Speed, direction, impact) [7]	10
Table 2.3 Material performance index comparison between typical materials in tension with average specification values [42]	30
Table 3.1 Calculated quasi-static crash loads for vehicle weighing 1500kg	53
Table 3.2 Predicting the biaxial strength of a unidirectional composite [85].	56
Table 3.3 Predicting the maximum strength of multidirectional composite [85].	56
Table 3.4 An example of a composite mechanical and chemical property test programme [89]	61
Table 3.5 (Top) Equivalent Tape (Lamina) property for FEA simulation and (Bottom) 3M DP490 adhesive performance [89].	62
Table 3.6 Fibre Volume and Porosity Content [89].	63
Table 4.1 Elements, nodes and element type for H0, H1 and H2 simulation development model.	78
Table 4.2 Plybook and layup of EVA's Carbon Kevlar sandwich front door panel, where FD_CRASH_B_1, FD_CRASH_B_2, FD_CRASH_B_3 the composite crash beams.	95





---

## List of Notations

---

$1-, 2- \text{ and } 3- \text{ axes}$	Principal material coordinate system
$a$	Acceleration
$A_{ij}, B_{ij}, D_{ij}$	Various stiffness coefficients
$Area^{lwf}$	Vehicle structure contact area from suspension attachment point
$B$	Bending stiffness
$C_{ij}$	Stiffness coefficient
$d$	Deci (1000)
$E$	Young modulus (Pa)
$F^b$	Applied force for vehicle structure bending deflection
$F_t$	Applied force for vehicle structure torsional deflection
$G$	Gravity
$i, j, k$	Subscript of coordinate system
$K$	Body-in-white torsional stiffness
$L$	Light weight index
$m_1, m_2$	Lumped mass
$m$	Meter
$m_{bw}$	Mass of body in white (closures) [kg]

$S_s$	Static Torsional Stiffness [ $Nm/^\circ$ ]
$t$	Time
$t_o$	Initial time [s]
$u$	Displacement
$v$	Velocity [ $m/s^2$ ]
$V_f$	Final Velocity [ $m/s^2$ ]
$w^t$	Distance between shock towers
$\theta$	Angle [ $^\circ$ ]
$\rho$	Density [ $kg/m^3$ ]
$\sigma$	Stress [Pa]
$\delta^b$	Bending deflection
$\Delta$	Door thickness
$\Delta_0$	Distance between door and occupant

---

## List of Abbreviations

---

ABD Matrix	Anisotropic coupling coefficient
ABS	Anti-lock Braking System
AFRP	Aramid Fibre Reinforced Plastics (Kevlar)
AHSS	Advanced High Strength Steel
BEV	Battery Electric Vehicle
BIW	Body-In-White
BVID	Barely Visible Impact Damage
CAE	Computer Aided Engineering
CCR	Crush Compression Ratio
CDM	Continuum Damage Mechanics
CFRP	Carbon Fibre Reinforced Plastics
CG	Center of Gravity
CLT	Classic Laminate Theory
CMH17	Composite Military Handbook
CO <sub>2</sub>	Carbon dioxide
CZone	Crush Zone (Engenuity)
DCB	Double Cantilever Beam
DOE	Design of Experiment
DP	Dual Phase

ESC/ESP	Electronic Stability Control
ESP	Electronic Stability Program
EuroNCAP	European New Car Assessment Programme
FEA	Finite Element Analysis
FMVSS	Federal Mobile Vehicle Safety Standard
FRP	Fibre Reinforced Plastic
FSV	Future Steel Vehicle
GFEI	Global Fuel Economy Initiative
GFRP	Glass Fibre Reinforced Plastics
GHG	Green House Gases
HIC	Head Injury Criterion
HRCT	High resolution CT scan
ICCT	International Council on Clean Transportation
ICE	Internal Combustion Engine
IEA	International Energy Agency
IIHS	Insurance Institute for Highway Safety
ITF	International Transport Forum
LCC	TUM Composite institute
LTA	Land Transport Authority
MDB	Mobile Deformable Barriers
MPG	Miles Per Gallon
MQB platform	Volkswagen Modular Transverse Matrix (Modularer QuerBaukasten)

NHTSA	National Highway Traffic Safety Administration
NTU	Nanyang Technological University
NVH	Noise Vibration Harshness
ODB	Offset Deformable Barrier
OEM	Original Equipment Manufacturer
PHEV	Plug in Hybrid Electric Vehicle
RP	Research Programme
RSM	Response Surface Methodology
SEA	Specific Energy Absorption
SOB	Small Overlap Barrier
TRIP	Transformation Induced Plasticity
TUM	Technische Universität München
UD	Uni-directional
UNECE	United Nations Economic Commission for Europe
UNEP	United Nations Environment Programme
USAF	United States Air Force
USNCAP	United States New Car Assessment Programme
WWFE I	World Wide Failure Exercise Phase I
WWFE II	World Wide Failure Exercise Phase II
WWFE III	World Wide Failure Exercise Phase III



---

## Abstract

---

Design for steel vehicle structures is a well-researched topic and has many research publications covering important aspects and factors that affects the design of a vehicle structure including manufacturing techniques and limitations. However published literature for developing carbon fibre composite vehicle structure are very limited, many focus only in sub-components carbon composite implementation without considering overall structural requirements and application. Many considerations used in steel vehicle structures are not valid with the use of carbon fibre composite due to the differences in material mechanical property especially in the area of crashworthiness. New design considerations have to be devised for developing carbon composite vehicle structures. The EVA electric taxi project provided the foundation to achieve that. The EVA project aims to develop an efficient, fully functional, prototype electric vehicle for tropical megacities and will feature a full carbon fibre composite structure to reduce overall weight and prototyping cost. Listed below was the responsibility of the author in EVA project.

- In-charge of vehicle crashworthiness development
- Providing crash load requirements to all sub-system design
- Carbon composite material property testing
- Conduct FEA analysis of the vehicle structure
- Define layup for the whole vehicle structure consisting of 68 composites panels
- Develop design solutions for weakness in vehicle structure
- Design of aluminium crash structure
- Experimental verification of aluminium crash structure
- Oversees the body in white structure overall assembly and tolerance.
- Assembly of EVA

A comprehensive literature review of vehicle crash standards and crashworthiness design along with vehicle structure performance requirements was carried out to understand the design criteria of vehicle structures. These are further complimented by review of material mechanical properties, property degradation under failure and how to simulate these failures in Finite Element Analysis (FEA). The advantages, limitations and complexity to perform such simulations will be evaluated to formulate a realistic achievable vehicle structure development targets and steps in this report. Methods to simplify complex dynamic load problems into equivalent quasi-static load will also be explored to speed up development process. The multi-disciplinary nature of the vehicle project would requires multiple systems integration resulting in strict design space restrictions within the vehicle package in which key factors that affect efficient vehicle structure performance for crashworthiness will be identified. Furthermore a brief design methodology to work around these restrictions will be explored. Results of the development along side with findings and observations will be documented in the later section of the thesis showing how goals and objectives of a lightweight crashworthy prototype vehicle



structure were achieved. The final weight of composite vehicle structure came in at 220kg at the end of the development which is 100-150kg lighter than comparable steel vehicle structure in this vehicle size and class. Subsequently EVA electric taxi concept was officially presented at Tokyo Motor Show in late November 2013.

# Chapter 1: Introduction

## 1.1 TUM CREATE

TUM CREATE (Campus of Research Excellence and Technological Enterprise) is a research collaboration between two leading universities NTU (Nanyang Technological University) and TUM (Technische Universität München) funded by NRF (National Research Foundation of Singapore) focusing on electromobility.

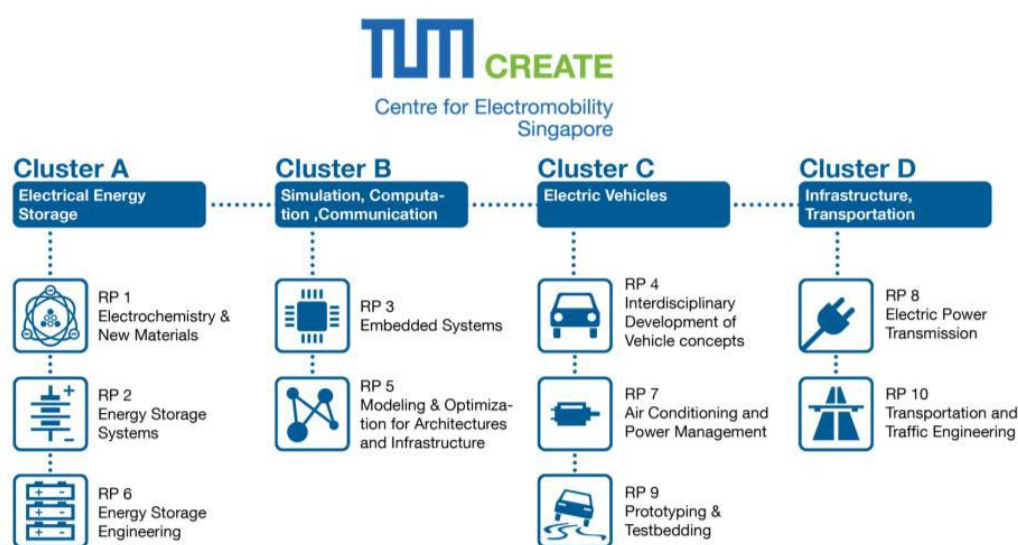


Fig 1.1 TUM CREATE research structure [1]

The research programme structure is divided into 10 research project groups in 4 main topic clusters employing approximately 120 scientists shown in Fig 1.1. The research programme covers multi-disciplinary mobility topics ranging from developing battery chemistry for next generation future electric vehicles to unique urban vehicles concepts. Infrastructure research on traffic engineering and optimized integration of electric charging infrastructure in urban environment and its effect on the existing power grid were also explored. This multidisciplinary research approach covers almost all major areas concerning future urban mobility.

## 1.2 Project EVA Background

In the first phase of TUM CREATE, one of the milestones was to develop a fully functional electric vehicle prototype which would feature new ideas and technologies conceived and developed from research project groups from 1 to 10. The project focuses on solutions for tropical megacities such as Singapore, where hot tropical climate challenges the cooling and climate control systems energy requirements to maintain comfort can severely affect electric vehicle driving range. This project will be the first fully functional electric prototype vehicle

that was conceptualized, designed, developed and built in Singapore. Upon completion, the vehicle will serve as a research platform for electric vehicle trials, test and data collection for further research. A team of approximately 30 PhD students from TUM and NTU was tasked to develop this electric vehicle with additional support from engineers and students pursuing masters' or bachelors. The team consists of automotive interior and exterior designers, engineers specialized in low voltage, high voltage, cooling systems, controls, software, battery pack, chassis and structure. This project set to explore possibilities for electro mobility in the near future in order to spur industrial interest and research in new electric vehicle concepts. With EVA project as a precursor, we aims to develop state of the art research, design and prototyping development knowhow in Singapore. RP 9 plays a crucial role in engineering, coordinating, managing integration of concepts/ideas and into the vehicle package from various RP.

The vehicle development started with a series of studies and surveys conducted to narrow down the type of vehicle concept that will have greatest influence in technology in local context, the results of the evaluation narrows down to electrification of the taxis in Singapore. The most influencing factor was the high utilization of taxis in Singapore. Taxis forms 3% of the vehicle population but account for 15% of all vehicles mileage. Replacing 3% of taxi on the road with zero emission vehicles can drastically reduce emissions compared to replacing 3% private cars. Taxis in Singapore are often two shift taxi, which meant two or more drivers will take shifts to drive the taxi. Such shift work meant the taxi will be literally driving 24/7 nonstop. This poses a big challenge for current electric vehicles where significant amount of time is required for recharging, thereby reducing taxi uptime and flexibility. If this challenge were to be accomplished, its public visibility could increase people's awareness towards electric vehicles as taxi is classified as a form of public transportation in Singapore and is very visible. Such exposure can spur the market to move towards electric vehicles.



Fig 1.2 Total annual mileage comparison between private cars and taxi in Singapore [2].

Further definition and benchmarking were conducted to obtain average trip distance, driving cycle, occupancy rate including qualitative surveys to identify passenger/driver behaviour and habits. These coupled with business model (cost), discussion with taxi companies and relevant government ministries on future development plans allow us to align our concept vehicle

direction. Subsequently these information was used to evaluation various energy storage option. The most economic and infrastructural feasible solution was the fast charging approach as it makes the most sense in both cost and operation. Furthermore with the low energy density of current battery technology, a large battery (1000kg) is required to have sufficient range for a complete shift. Fast charging allow taxi drivers to quickly recharge during their breaks and allowing a smaller battery (500kg - ½ shift) to be fitted in the vehicle, increasing efficiency (less mass) and reduce initial battery cost. The benefit of fast charging allow lesser behavioural habit changes by taxi drivers. The expected behavioural plan for a two shift taxi is shown in Fig 1.4.

Using battery and technology prices in 2011, the results of cost calculations is promising from the total cost of ownership perspective. Electric taxi will be cost less than current diesel taxis over its lifespan even after factoring the cost of 2 battery pack replacement (due to battery degradation) over its 8 years lifespan. Maintenance and running cost is also reduced due to the simplicity and efficiency of electric powertrain. Furthermore a 60% reduction of well to wheel CO<sub>2</sub> emission is expected from taxi electrification when considering the natural gas dominant power generation in Singapore.

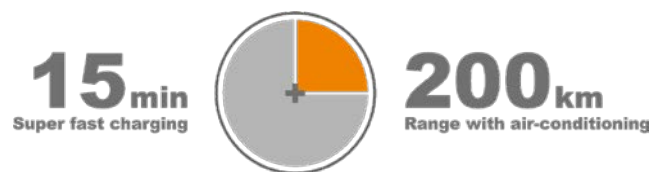


Fig 1.3 160KWh fast charging allow recharge of 200km range in 15 minute.

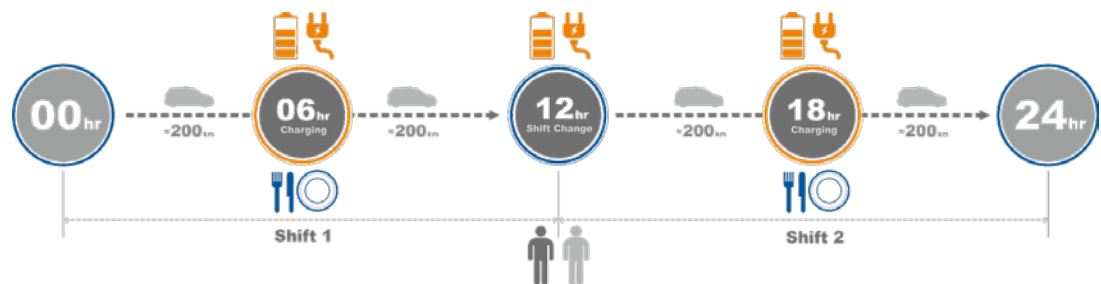


Fig 1.4 Proposed shift change and charging break.

EVA taxi, will be developed from a ground up so as to open up design possibilities that is not possible with conversion of existing sedans models. Roadworthiness of concept research vehicle is one of the main priorities thus, occupant safety, structure durability and design is paramount. The required charging rate and driving range meant that a 50 KWh battery pack 2000mm (L) x 1250mm (width) x 200mm (height) (500kg) was required. The battery can only be mounted in the centre of the car due to safety and weight distribution reasons. The integration of the large battery onto existing vehicle (especially ICE vehicles) require extensive modification to vehicle structures such as removing the central tunnel and floor of the passenger cabin as there is no existing space allocated that is sufficient for the battery. This

integration will also encroach into passenger cabin requiring windscreen, dashboard and roof height changes to ensure occupants have sufficient headroom and space. This necessitate a complete redesign of the passenger cabin and adjacent support structure. Furthermore the remaining existing vehicle structure (such as crumple zones) may require additional reinforcement due to the large added mass of the battery. The amount of retrofitting work would be required at nearly every corner of the vehicle and such retrofitting work will have many structural compromises, reducing structural efficiency. By developing a new vehicle structure, engineers and designers will be allowed to explore radical new design and styling ideas that can improve user experience and technical solutions can be implemented easily without design restriction imposed by conversion from existing vehicle. Without the conversion restriction, the vehicle structure can be more efficiently designed to integrate the large battery pack structurally.

### **1.3 Thesis Scope and Objectives of Project EVA**

The author was tasked as part of his master's thesis to develop carbon monocoque structure for EVA with key focus on crashworthiness and structural integrity. To achieve these goals, the design has to consider structural aspects of all components and systems. The thesis will focus on carbon composite vehicle design, construction methodology with definition of fibre orientation layup and engineering assumptions and considerations to meet structural and crashworthiness development requirements.

There are vast amount of current literature on engineering methodology and design optimization for metallic body vehicles development but information on designing and optimizing fibre composite usage in vehicle monocoque structure is scarce or limited in scope. Existing metallic vehicle structure development and optimization methodology have severe shortcomings especially when applied to composite materials particularly on crashworthiness development due to large difference in material behaviour. In the aerospace industry there are still ongoing studies and research done on improving crashworthiness of aircraft structures to increase survivability in accidents. This thesis will focus on prototype composite vehicle structure development with consideration to crashworthiness design in an attempt to fill the literature gap on composite passenger vehicle structure.

#### **1.3.1 Crash Worthiness and Safety**

EVA Taxi will be developed as a fully functional road worthy prototype, significant attention and resources had to be allocated to ensure the design meets safety requirements particularly in terms of occupant protection in an event of a severe collision when driven on public roads.

#### **1.3.2 Structural Stability, Strength and Durability**

During the developing process, crashworthiness, safety, structure stability, strength, resilience for vibrations and dynamic loading during operation was considered. This is to ensure that the vehicle structure reliability and premature failure does not occur. Furthermore, rectification after production would be costly and difficult.

### 1.3.3 Limitations

Realistic targets have to be imposed for project EVA due to limited manpower and development time. Experimental crash test of the vehicle structure will not be possible as only a single prototype will be constructed. Thus, the design of the vehicle structure will be verified by means of computer simulation and sub-component level test coupon test. A crash worthy vehicle structure requires huge amount of man hours to develop, as the only responsible person working on vehicle structure design, non-design critical requirement are given lower priority. Solutions to satisfy those requirements are typically integrated without excessive detailed engineering work. The project will follow concurrent engineering method. As such it is often required to carry out late design changes in response to revision changes.

- 1) Air bag safety systems were left out as the manpower and cost to design a custom airbag system was not feasible and too resource intensive. Furthermore reliability of air bag triggering sensors cannot be verified with untested structures.
- 2) Noise Vibration and Harshness was left out as this factor was not the main objective of the structure design, doing so will require significant investment in development time and resources. However the vehicle structure was designed to ensure that main natural frequency of the structure does not coincide with the cyclic loading frequency.

## 1.4 Thesis Structure

The thesis will be structured in the following 5 main chapters

2. Literature Review
3. Development Setup, Considerations and Limitations
4. Development of EVA vehicle structure
5. Manufacturing and Assembly of EVA
6. Conclusion



---

## Chapter 2: Literature Review

---

### 2.1 Introduction and Organization

The literature review is divided into 5 sections. The first section will cover a brief history of crashworthiness, human tolerance limit in crash and the concept of crashworthiness in vehicle structure. In addition review of current crash test standards and how these standards bring about safer crashworthy vehicles. The next section will cover vehicle structure performance requirements such as torsion stiffness, bending stiffness and natural vibration frequency. The review of vehicle structure performance will be further complimented by the review of the current state of the art vehicle structure design, trends and weight reduction that is driving the next evolution in vehicle structure design. The last section will focus on review of material properties of both metal and composite, the onset of failure and damage evolution to computer simulation complexity in composite materials.

### 2.2 Vehicle Crashworthiness

#### 2.2.1 Brief History of Crashworthiness

In a modern vehicle structure, crashworthiness is one of the most important design criteria. Millions of lives were saved by advances in vehicle crashworthiness spurred on by crash safety regulations and vehicle technology innovations from early 1920s. From the mid-1970s Institutions and various research centres such as NHTSA (1970) (National Highway Traffic Safety Association), EuroNCAP (1979) (European New Car Assessment Program) and IIHS (1959) (Insurance Institute of Highway Safety) were formed and have been continuously improving testing methodologies and implementing new standards for vehicles design and safety. Since then, there have been big strides in developments of occupant safety. Occupants in modern day passenger vehicle are likely to walk away with minor scratches/injury in an accident that would have them seriously injured if they were in a vehicle built years before. This example was clearly shown by IIHS 50th anniversary crash demonstration of 2009 Chevrolet Malibu and 1959 Chevrolet Bel Air [3].

The need to quantify probability of crash related injuries spurs the development of the modern crash test dummy that accurately replicate human biomechanical behaviour with high bio-fidelity. The Hybrid 3 is the current state of the art front crash test dummy family which comprises of the 50<sup>th</sup>, 95<sup>th</sup> percentile male dummy and 5<sup>th</sup> percentile female dummy to cover population anatomical distribution. They were also complimented by a group of hybrid 3 child crash dummies representing 10, 6, and 3 year old child. The dummies are fitted with a multitude of sensors to record data during a crash. The data were analysed post-crash to rate the probability of injury. A front crash dummy is not equipped to measure side impact accurately, thus a family of side impact dummy was developed with specifically designed ribs to accurately measure the injury probability on side impact.



### 2.2.2 Crash Energy Absorption

A typical vehicle collision lasts approximately 100 milliseconds [4] and within this short period of time, the vehicle will undergo a sudden change in velocity (deceleration), the occupant in the vehicle will also undergo a similar change of velocity. Such sudden deceleration/acceleration will impose large forces on the occupants. The human tolerance limits under such forces were first studied by the US air force research, using cadaver or living human as test subject under severe acceleration to obtain the human tolerance limits for the design parameters for military jets/weapons. The limits of human tolerance limit for survival in a fully restraint position is listed in Table 2.1 which are obtained from extensive study of aircraft accidents and injury in US Air Force [5].

Table 2.1 Human tolerance limits in crash survival in different directions [5].

Direction of Accelerative Force	Occupant's Inertial Response	Tolerance Level
Headward (+ Gz)	Eyeballs Down	20-25 G
Tailward (- Gz)	Eyeballs Up	15 G
Lateral Right (+ Gy)	Eyeballs Left	20 G
Lateral Left (- Gy)	Eyeballs Right	20 G
Back to Chest (+Gx)	Eyeballs Out	45 G
Chest to Back (- Gx)	Eyeballs In	45 G

Note: Reference: Crash Survival Design Guide, TR 79-22.  
(0.10 Second time duration of crash pulse; full restraint)

The general public have little understanding about crash safety and survivability. When seatbelt was first introduced, there was huge scepticisms about its effectiveness. The public's initial misconception was that the seat belt will limit their chances in escaping from fire or when the vehicle crash into water bodies by trapping them to the seats. They would prefer to be thrown clear by not wearing seatbelt than being trapped in a crash. However studies shows that properly restrained occupants are more likely to survive in fire/water situation than unbelted occupants because belted occupant are more likely to stay conscious after a crash to save themselves. Furthermore, fire and drowning cases in vehicle crash are statistically rare compared to other type of accidents. By not belting up occupants are also less likely to be ejected out of the car in a roll over crash.

### 2.2.3 Occupant Safety Cell and Crumple Zone

Modern vehicles are designed to absorb the crash energy to protect the occupants. Crumple zones is used to cushion or absorb the collision energy by collapsing in a crash. The crumple zones controls the occupant acceleration by controlling the rate of crash energy absorption in order to stay within the tolerance acceleration limit shown in the Table 2.1. Crumple zones are located around the perimeter structure surrounding the occupants with larger crumple zone area in the front and rear and smaller crumple zone on the sides shown in Fig 2.1.

Austin [6] concluded that the amount of intrusion into the occupant compartment affects the severity of the injuries. Furthermore he states the importance of survival space in a crash where surrounding structures are sufficiently rigid to prevent excessive intrusions, this is well documented in many other literatures on crashworthiness. The principle of a safe structure consists of a strong and rigid frame that surrounds the occupant. Crash energy absorbing structure (crumple zone) is mounted around this rigid frame and is designed to plastically deform at a lower load, allowing it to absorb crash energy while maintaining survival space is shown in Fig 2.1.

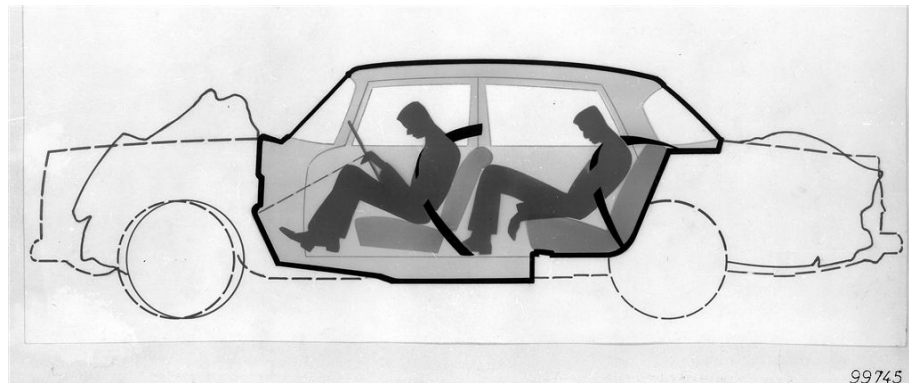


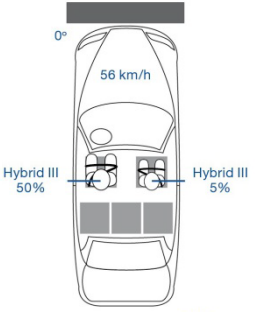
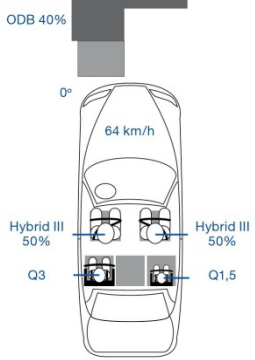
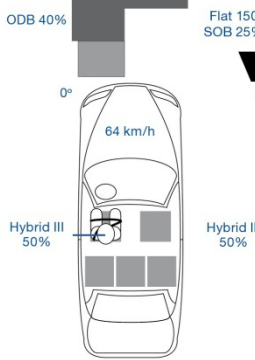
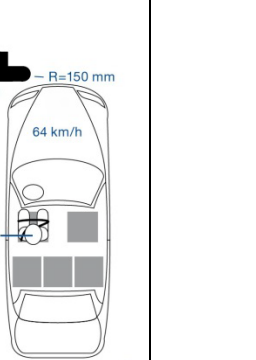
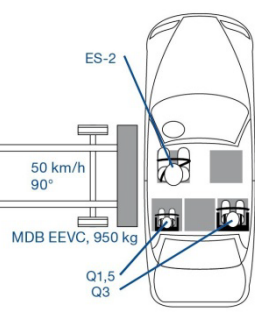
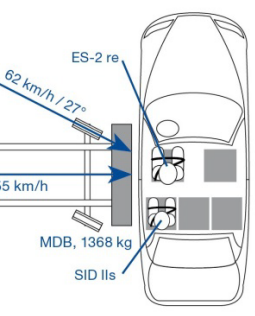
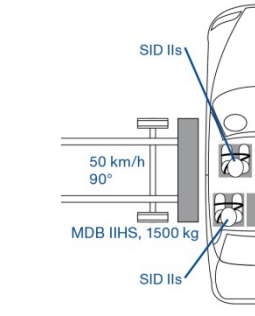
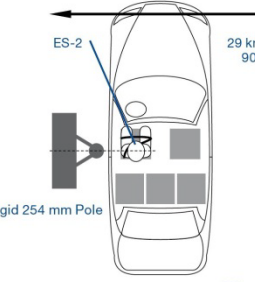
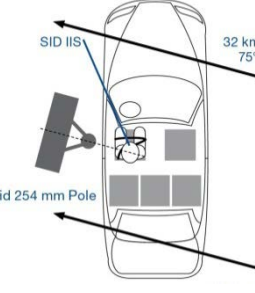
Fig 2.1 Rigid passenger cell marked out in bold outlines on the side view of vehicle structure with crumple zones and seatbelts. (Daimler Global Media, Mercedes-Benz 111 series) (1959 to 1968).

## 2.2.4 Crash Test Standards

Institutions and organisation such as IIHS, NHTSA, EuroNCAP had developed a series of standardized crash test to benchmark crash safety between differing models and class. These crash test standards were developed from years of data from real accidents statistics. In recent years, there have been an increased weightage placed on pedestrian safety, active safety for collision mitigation and avoidance system and performance of electronic stability program (ESP). These active systems aim to prevent collision before it happens. However for the development of EVA, focus will still be on basic passive crash safety as current active systems cannot completely prevent collisions and engineering a matching active systems will be too expensive and not the main aim for this project. Table 2.2 showing, the list of common passive crash test standard and their test parameters.

These existing crash test standards are constantly re-evaluated, revisions or new tests are often implemented on a basis to improve overall safety. In a historic example, accidents statistics indicate that head on collisions mostly occurs in offset engagement. When the offset crash test was introduced, majority of vehicles perform poorly in the misaligned collision. As a result, the frontal offset crash standard was introduced in the 1995 to encourage the OEMs to design vehicles that can better withstand offset impact. Today, most modern vehicles ace this crash test standard. The constant revising standards meant that vehicles scoring 5 stars rating a decade ago could possibly manage only 3 stars in the latest rating standards.

Table 2.2 List of common crash standards and their test setup (Crash test dummies, Speed, direction, impact) [7]

	Euro NCAP	U.S. NCAP	IIHS
Full Width			
ODB/SOB			 
MDB			
POLE			

These are the reasons why crash standards are highly regarded by the consumers when purchasing a new car. The consumers' demand for safer vehicles promotes OEM to develop vehicles with higher crash safety. Majority of new cars have excellent crash safety ratings as a result. The progress of advancement in crash safety is evident by the 50<sup>th</sup> anniversary crash demonstration by IIHS [3]. The crash test standards are explained in greater detail in Appendix A.

## 2.3 Vehicle Structure Requirements

The vehicle structure essentially forms the backbone of the vehicle, major components are mounted directly or indirectly to it. To support these components rigidly, the structural design have to be well thought out. The vehicle structure is also subjected to many different structural requirements, such as stiffness, strength and fatigue resistance. Vehicle structure are broken down into different zones for development such as the passenger cell and crumple zone. The safety passenger cell requires higher stiffness and strength than crumple zone to ensure that the cell hold up during the collapse of crumple zone during absorption crash energy.

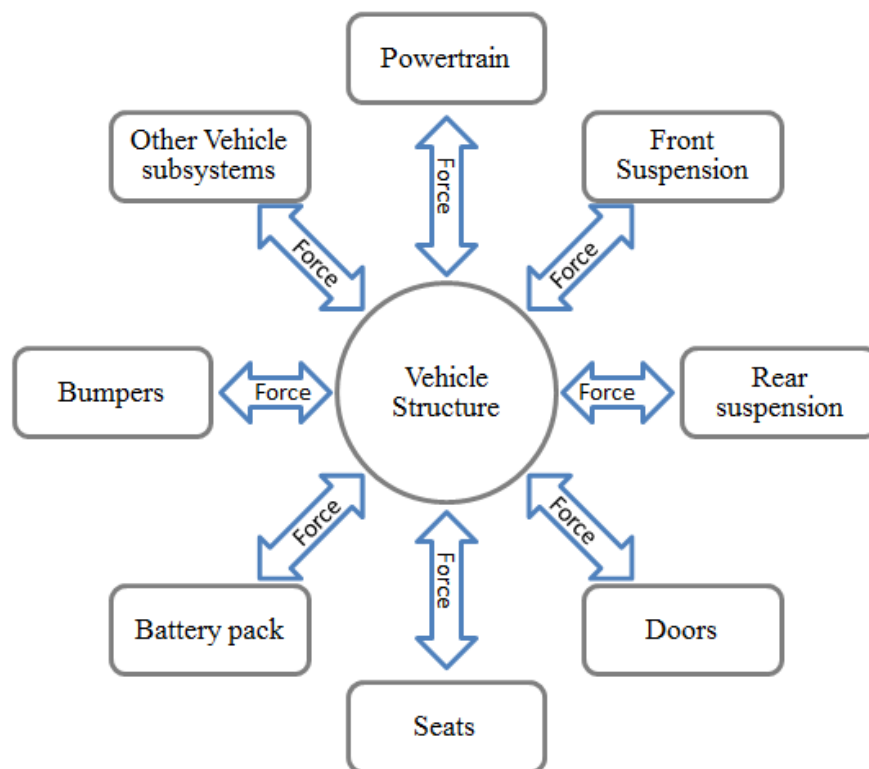


Fig 2.2 Force interactions between vehicle structure and subsystems.

### 2.3.1 Torsional Stiffness

Torsional stiffness measures the structure's ability to resist structural twisting flexure under unbalanced loading of the wheels on uneven road surfaces between the front and rear axle as shown in Fig 2.3. Low torsional stiffness may result in the inability to open or close the doors when parked on uneven ground due deformed door frame. The unit for torsional stiffness is

measured in Nm/degree. This requirement ensures the front and rear suspension is aligned under demanding loading conditions. Handling can be erratic if the vehicle structure does not have sufficient torsional stiffness to maintain alignment between the front and rear suspension. The development of better stability and driving dynamics made high torsional stiffness essential design criteria in modern vehicles.

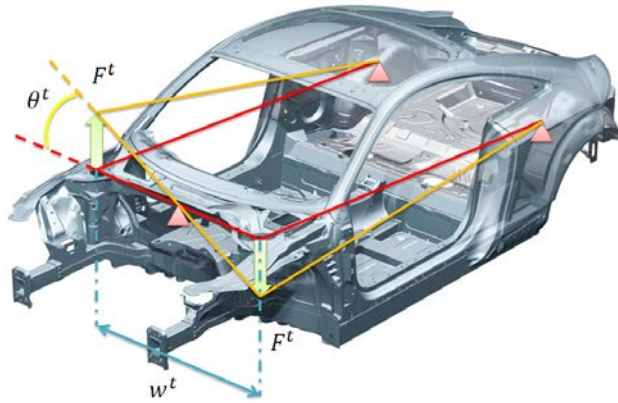


Fig 2.3 Illustration on how torsion stiffness of a vehicle structure is measured, constraints at suspension attachments points [8]

The torsion stiffness  $K$  of the vehicle structure in  $Nm/degree$  °

$$K = \frac{F^t w^t}{\theta^t}$$

Where  $F^t$  = applied force,  $w^t$  = distance between shock tower,  $\theta^t$  = angular deflection.

### 2.3.2 Bending Stiffness

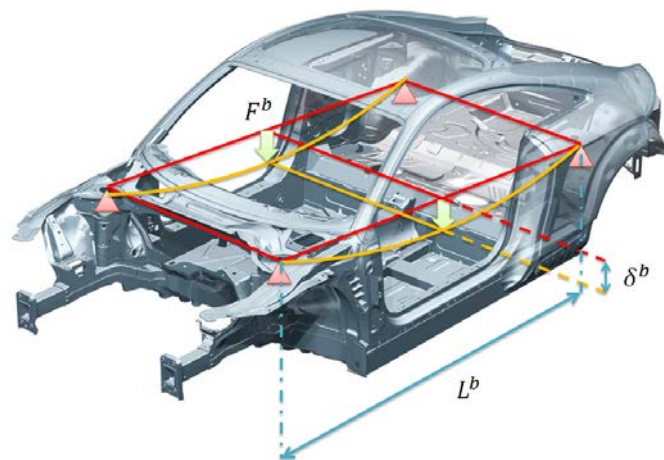


Fig 2.4 Illustration on how bending stiffness is measured, constraints at suspension attachments points. [8]

Bending stiffness measures the structure's ability to carry load at the centre of the vehicle between the front and rear wheels as shown in Fig 2.4. Bending stiffness is measured in N/mm and determines the vehicle flexure under load. Bending stiffness is measured by simply supporting all suspension attachment points with an applied a load to the structure. Sufficient stiffness ensures the vehicle structure does not deform excessively while carrying heavy loads. Similar to the requirement of torsional stiffness, a vehicle structure that flex excessively will counteract the suspension intended response resulting in poor controllability under driving condition or result in a jammed door as distorted doorframe clinching the door under heavy load. The bending stiffness of the vehicle structure  $B$  in  $N/mm$ :

$$B = \frac{\sum F^b}{\delta^b}$$

### 2.3.3 Eigen Frequency/Natural Frequency/Noise Vibration Harshness

The natural vibration frequency of an object with elastic properties depends on the mass and elastic stiffness. The natural frequency of the vehicle structure is important for identifying points of fatigue weaknesses and also comfort. Resonance vibration will occur if the load frequency matches the natural frequency of the structure and this can result in excessive oscillation and noise. In the worst case, premature failure can occur due to excessive deflection similar to the oscillation that caused Tacoma narrows bridge collapse [9].

It is important that the first vibration mode does not coincide with the excitation vibration frequency of reciprocating forces in the vehicle. Excitation can come from road vibrations, unbalanced rotating parts and aerodynamic forces. Different modes of structural excitation response must be examined, particularly the primary torsion frequency and bending frequency mode requires more attention. Higher order vibration responses are usually smaller in magnitude and are generally ignored as the primary and secondary vibration frequencies are the ones with the largest amplitude.

Natural frequency of 22 to 30 hertz range is often the design target for vehicle structure as shown in studies of Malen [10] and Pfestorf [11]. This frequency range is at the threshold of human hearing range where hearing sensitivity drops. Humans' sensitivity for touch also decreases in this range, a vehicle structure with natural frequency in this range will appear quiet and vibration free. However during design Body-in-White (BIW) structures are much lighter compared to fully assembled vehicle, therefore the vibration frequency of the BIW should be in the region from 45 – 60 hertz. Fig 2.5 shows the noise and vibration mode map for vehicular vibration.

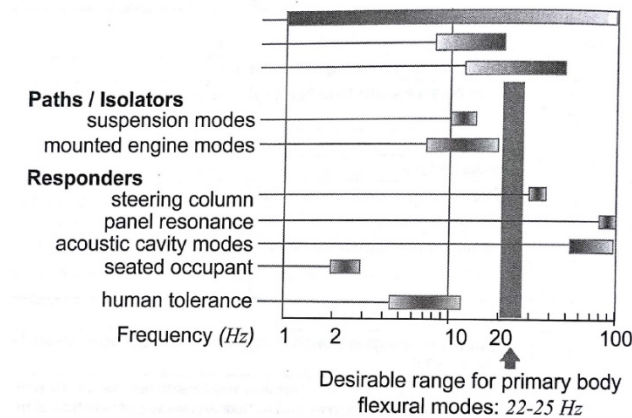


Fig 2.5 Noise and vibration mode map and primary body frequency design target by Malen [10]

### 2.3.4 Dynamic Driving Loads

A vehicle structure also has to ensure that it can handle the rigour of daily driving including occasional curb strikes and potholes. Malen [10] and Seiffert [12] have calculated and simplified dynamic load as a factor of static load shown in Fig 2.6. According to Jäger [13], dynamic driving loads are significantly lower than crash loads in the order of 10 times the magnitude, however attention should be given to dynamic load points to ensure that they were designed with the required stiffness, strength and fatigue resistance for daily operation.

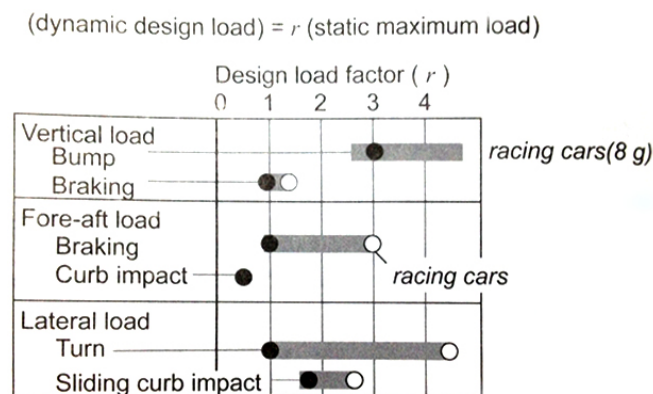


Fig 2.6 Quasi-static design load factor for structural requirement under various dynamic driving scenarios extracted from Malen [10].



## 2.4 Vehicle Structure Layout

### 2.4.1 Ladder Frame / Body on Frame Design



Fig 2.7 (Left) Open section ladder frame chassis of the 1920s [14] (Right) Modern ladder frame structure on a SUV which shows significant adaptation for packaging

In the 1920s, a majority of vehicle structure were designed around a ladder frame design shown in the left figure of Fig 2.7, where the passenger cabin is mounted on top of the ladder frame which replicates the design used on horse carriages. This design layout is known as body on frame vehicle structure. This design was initially preferred because it allows manufacturers to base the same support structure and powertrain on multiple exterior cabin design variants, minimizing the engineering effort and cost to develop a new drive train for a new model. Ladder on frame is still the preferred structural type for heavy-duty commercial vehicles such as trucks and buses of which variant on cabin and outfit is still important (i.e tipper truck, cargo truck to cement mixer). One key advantage of the ladder frame is that the cabin can be easily isolated from the powertrain vibration via a series of vibration isolators, increasing comfort in the cabin. However the main challenge of traditional ladder frame design is the lack of sufficient torsion rigidity [10]. Driving dynamics development on suspension systems increases structural torsion stiffness requirement. This coupled with lightweight design, antiquate traditional ladder frame design in passenger vehicles as space frame and unibody design are far superior.

### 2.4.2 Space Frame Design

Space frame is defined as a frame structure in space. The space frame forms a strong truss structure near the extremity of the vehicle shown in Fig 2.8. Exterior panels which contribute little to structural strength are then mounted on the space frame to complete the exterior look and design of the vehicle. This construction method varies slightly from the unibody design where exterior panels are used to create sections of the structure frame as shown in Fig 2.10. This construction method allows lightweight design especially in aluminium where extrusion and casting parts can be readily used.

The tubular space frame design, relies on the similar concept as space frame construction. The only difference is the structure consists of only beam and truss sections, these sections interconnect to form a strong and stiff space frame structure. Fig 2.8 shows an example of a tubular space frame vehicle structure.





Fig 2.8 (Left) Audi A8 Aluminium space frame body in white (Red : casting, Blue : extrusion, Green : sheet) [15] (Right) Example of a tubular space frame vehicle structure for a 2 seater.

### 2.4.3 Unibody/Monocoque Design

The advances in materials and capabilities to manufacture complex geometry and shapes lead proliferation of the unibody design. Citroen was one of the first OEM to utilize this construction technique with Citroen Traction Avant (1930) shown in Fig 2.9 similarly iconic cars such as the Citroen 2CV, Volkswagen Beetle and the Mini are based on unibody design. Fig 2.10 shows a modern Mercedes unibody design, it consists of multiple stamped/formed sheet metal put together to form a network of boxed sections, bulkhead and tubes as structure of the vehicle. This design is particularly well suited for high volume production due to short cycle time between stamped/formed panels production. Unibody design allow structural load bearing members and sections to be placed at structure extremities. These structure sections with exterior panels effectively increases torsional and bending stiffness further.



Fig 2.9 Unibody of the 1934 Citroen 11 CV, produced till 1956. [14]



Fig 2.10 Exploded view of Mercedes S-Class hybrid steel and aluminium BIW structure with exterior panels. [16]

#### 2.4.4 Carbon Monocoque Design

Monocoque means singular body, by engineering definition it is identical to unibody where the outer skin is both the exterior and loads bearing structure. The term monocoque is generally used when describing unibody made of carbon fibre composite material. The unique anisotropic property of carbon fibre composite allows engineers to have a higher degree of structural design freedom and capability. More information about carbon fibre will be covered in Section 0. The designer can optimize the strength/stiffness of the structure by aligning carbon fibre along the direction of the load path. Coupled with fibre orientation variation, engineers can easily increase the strength/stiffness on critical areas by increasing the number carbon fibres plies, unlike formed metals. Carbon fibre was initially developed for aerospace application and McLaren was the first to introduce the carbon fibre monocoque in Formula 1 in 1980s as shown in Fig 2.11. The brittle nature of failure raise initial concerns on its crashworthiness. Inevitably McLaren was involved in a crash and all critics were baffled how well the carbon fibre monocoque structure managed to maintain its structure integrity while absorbing large amount of crash energy. Carbon composite forever changed motor racing and the benchmark for crash safety in Formula 1 and motorsport since.



Fig 2.11 McLaren first carbon composite formula 1 monocoque shell 1981 [17]



Fig 2.12 (Left) Lamborghini Aventador Carbon Monocoque, (Right): McLaren MP4-12C carbon tub [17]

Carbon composite monocoque structures are still relative rare in mass market vehicles and are more commonly found on premium supercars (McLaren F1, McLaren MP4-12C, Pagani Huayra, Aston Martin one 77) as shown in Fig 2.12. However, recent improvement in manufacturing techniques, resin systems and cost of producing carbon fibre, the cost have plummeted making it feasible to be implemented on mid end model vehicle with up to 10,000 unit/year series production.

### 2.4.5 Multi-Material Hybrid Design

In modern vehicle structure construction, the distinctions between vehicle structure types are blurred. There are minute differences between unibody, monocoque and space frame vehicle structure. Modern vehicle structures are often combinations of various vehicle types in order to achieve the most efficient body structure. Majority of series production vehicles employs the combination of space frame and unibody construction and a variety mix of materials for better structural and package integration efficiency. This fusion of multi-material design allows engineers to select the best material for the each structural application. The selection of different materials allows more efficient uses of material, reducing weight and improves performance. Fig 2.10 shows the exploded view of the hybrid steel and aluminium body in white structure with exterior panels of a Mercedes S-Class. The BIW lightweight index has been improved by 50% compared to the predecessor model [16]. Fig 2.13 shows the body structure of Aston Martin Sport car utilizing a carbon composite transmission tunnel. These are just some examples of such multi-material hybrid vehicle structure design.

In the higher performance segment, hybrid structure type can be easily identified. McLaren MP4-12C as shown in Fig 2.14 features a carbon fibre composite monocoque tub without roll cage or roof structure, the engine and rear drivetrain is mounted on an aluminium space frame which is then bolted structurally to the carbon fibre monocoque, the front end is configured in a similarly manner with a bolted on crash structure. The McLaren MP4-12C structure features a hybrid design combination of composite monocoque for the occupant tub and space frame construction similar to multi-material construction.



Fig 2.13 Aluminium structure with carbon transmission tunnel joined by a structural, hot curing adhesive (left) and aluminium front structure (right) [16]





Fig 2.14 McLaren MP4-12C - Powertrain and vehicle structure without exterior panel. [17]

Another hybrid structure example is the BMW i3, it is the first mid-range volume production electric vehicle to feature state of the art carbon monocoque safety cell. The hybrid vehicle structure is based on a combination of an aluminium ladder frame and a modern rigid CFRP monocoque glued and bolted together as shown in Fig 2.15. This hybrid design is an evolution from traditional ladder on frame construction. The ladder frame is efficient to house the large and thick battery pack at the center of the car. The design uses unique attachment points at front strut towers to the A-pillar in order to increase torsional rigidity through direct structural connection to the stiff carbon safety cell to mitigate the low torsional performance of typical ladder frame design. BMW also employ plastic exterior body panels allowing significant weight savings and dent protection compared to vehicles of similar weight class. The BMW i3 weigh in at just 1200kg with battery pack, it is one of the lightest electric vehicle in its vehicle class today.

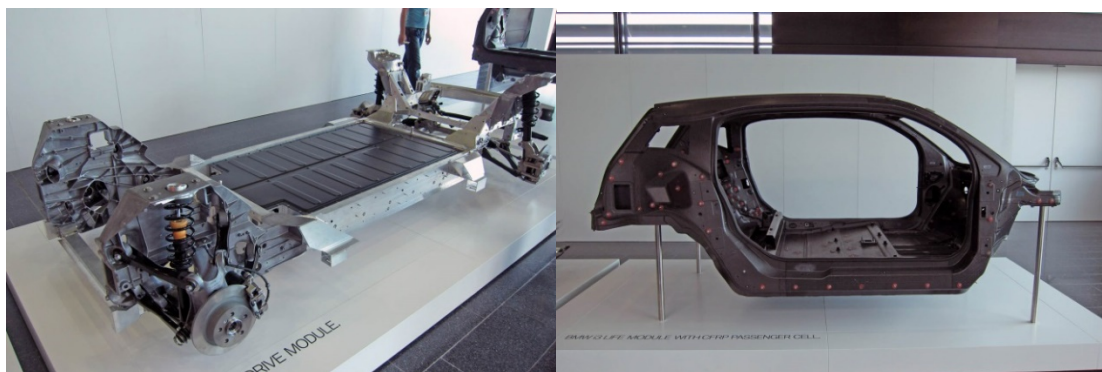


Fig 2.15 BMW i3: Aluminium ladder frame structure and carbon monocoque life cell. [18]

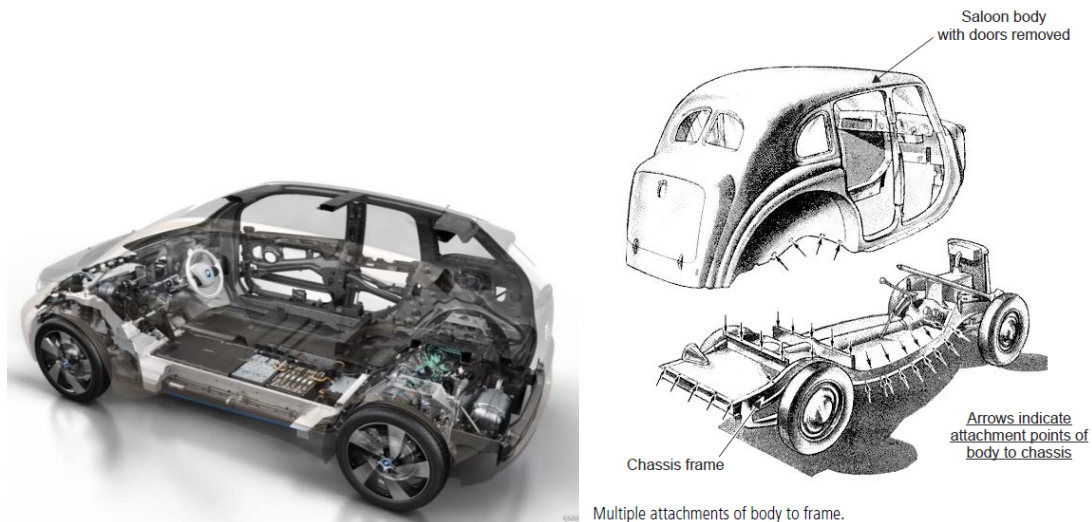


Fig 2.16 BMW i3 cut away section illustration of the carbon monocoque life module with the base structure [19], Traditional ladder frame design similar to BMW i3 [14]

## 2.5 Mass Reduction and Future Influences

Efficiency is the buzzword to sustainability, systems have to be lean and fat free. Having unnecessary mass is similar to climbing a mountain weighed down with items you would not need, which requires you to expend more energy, effort and slows you down. The same could be said for current fleet of passenger vehicles, reduction in weight and increase in efficiency can dramatically improve performance and reduce power requirements. Heavier vehicles require more energy in city traffic stop-go driving cycle, they also require a more powerful engine to provide the same acceleration performance compared to a lighter car [20]. With current transportation forming a large part of a city's GHG emissions, improvement in efficiency can dramatically reduce emissions shown in Fig 2.18.

On the global front, the "Global Fuel Economy Initiative" (GFEI), a partnership of FIA foundation, the IEA, the International Transport Forum (ITF), and the United Nations Environment Programme (UNEP), estimated that a 50% improvement in fuel economy is achievable using existing technologies or emerging technologies within the next decade and concludes that such emissions targets are realistic to achieve [21]. This is further verified with studies done by Makino [20], Zuldema [22], Knittel [23] and Lutsey [24]. Policy makers saw the need to bring about new and more stringent emission standards to prompt OEM to develop more efficient vehicles. These standards are designed to be technology neutral to promote uptake of emerging automotive technologies. Makino [20] studied and breakdown possible areas of improvement that can be achieved and approximated reduction each area have for fuel consumption and GHG emissions shown in Fig 2.17.

To achieve the goals of sustainability, automotive manufacturers are aiming at weight reduction to improve efficiency in an effort to meet the upcoming stringent emissions and fuel efficiency legislative requirements. Automotive manufacturers are also trying to reverse this mass gain trend shown by [25] [26] [27] [28] alongside with the development of efficient state

of the art hybrid drivetrains, improved aerodynamics, energy recovery systems to further boost efficient use of available power.

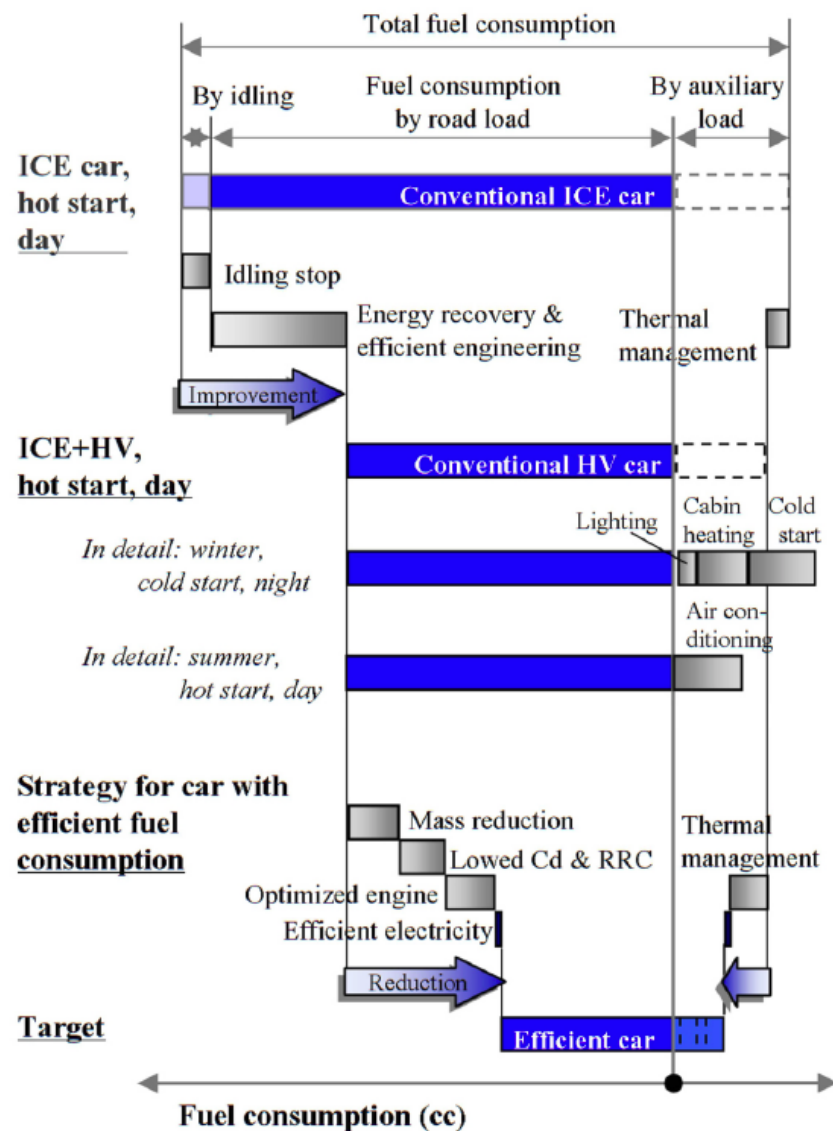


Fig 2.17 Breakdown of real world fuel consumption of a hybrid vehicle [20].

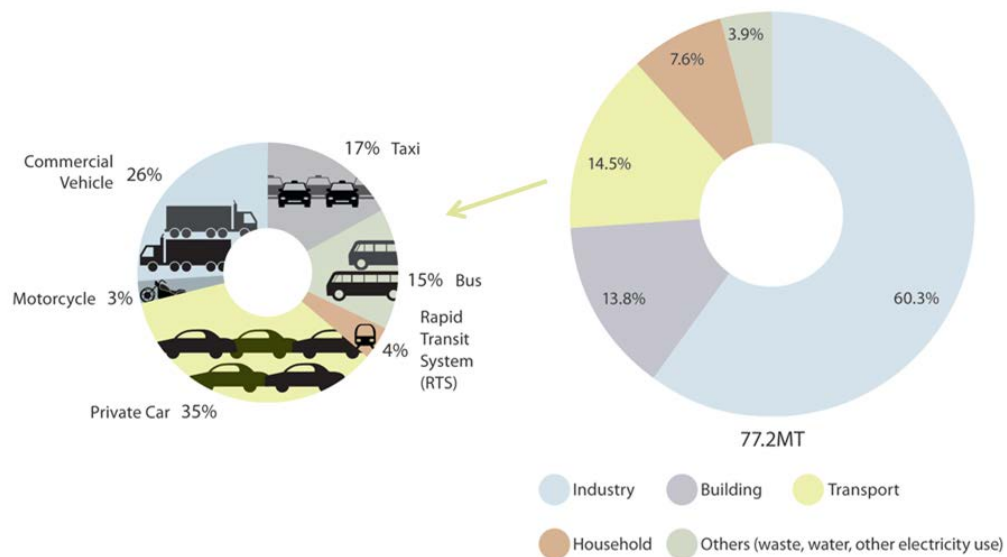


Fig 2.18 (Right) shows the total all greenhouse gas emissions in different sectors converted to CO<sub>2</sub> equivalent. (Left) shows the distribution of emissions of greenhouse gas between transport types in Singapore [29].

Since the 1970s vehicles are gaining weight, Fig 2.19 shows the evolutionary weight growth of main series model from Toyota, Ford, Volkswagen and Citroen from 1970 to 2002. Crash loads are the determining factor for the size structural members as show in Future Steel Vehicle [30]. A significant portion of this weight gain was due to increasing crash safety requirements however the exact effect cannot be easily quantified. The other portion of mass growth was attributed to demand for features and electronics (hi-fi systems, multiple speakers system, electrically actuated seats, etc). These additional features quickly inflate the total vehicle weight with synergistic mass cycles.

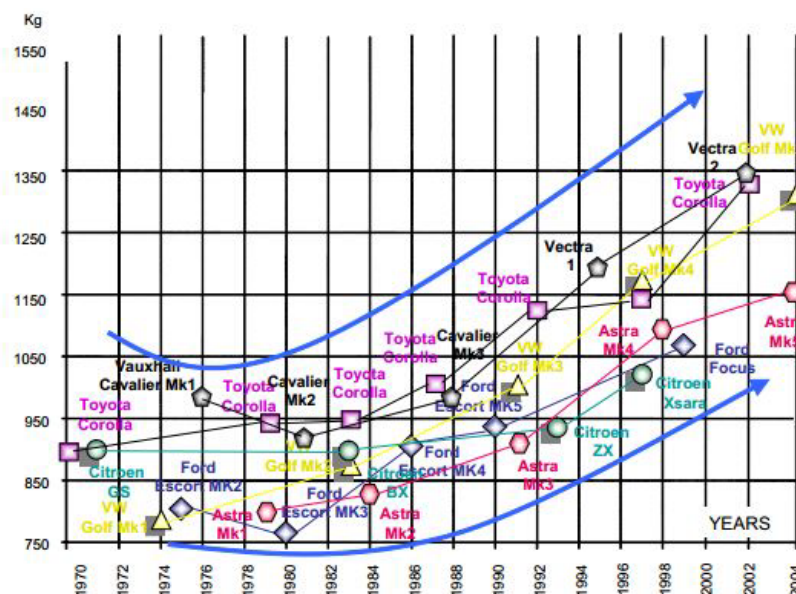


Fig 2.19 Evolution of weight in compact-class cars [31]



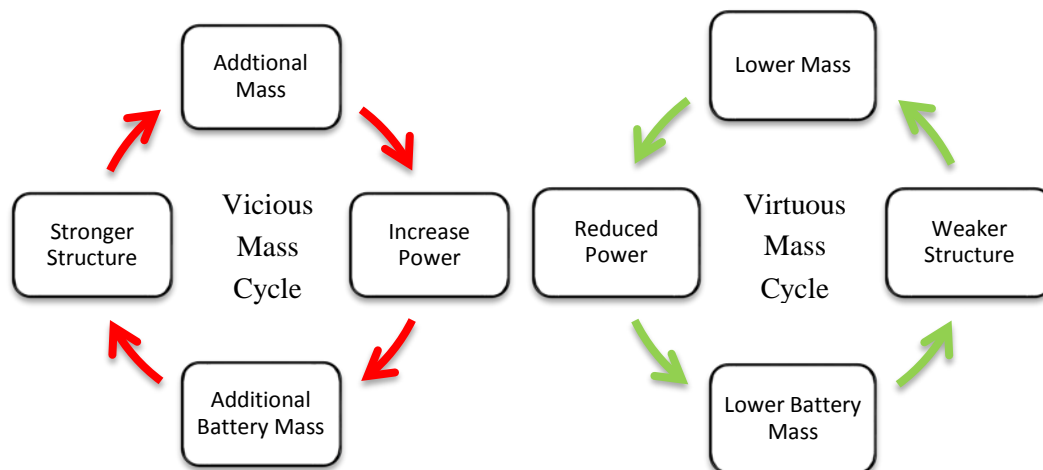


Fig 2.20 Synergistic effect of Vicious Mass Cycle (left) and Virtuous Mass Cycle (right)

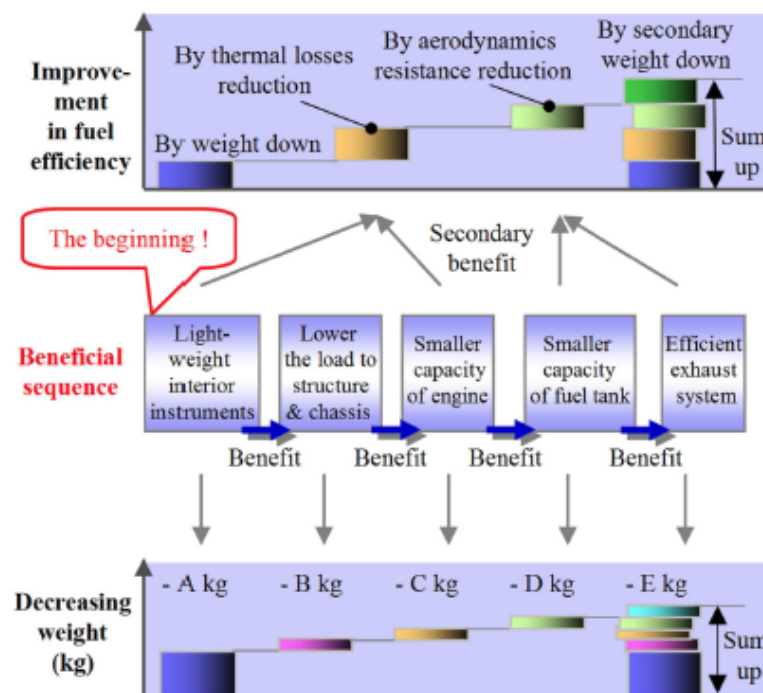


Fig 2.21 Efficiency benefit sequence: Mass reduction of passenger cabin and synergistic effect will lead to greater fuel efficiency and secondary mass reduction [20].

The synergistic mass cycle effect is often also known as mass compounding effect or secondary mass effect. The cycle is illustrated in Fig 2.20. The vicious synergistic mass cycle initiate with mass increase. Thus to maintain the performance level, this additional mass would require more power and with higher power you need heavier systems and larger battery. At the same time vehicle structure needs to be strengthened to support the additional mass. This further weight gain for structure, systems and battery will go into the feedback loop in an

iterative cycle until the convergence of a new mass equilibrium. The synergistic mass effect can also be reversed for weight lost, compounding mass reduction can be achieved. Fig 2.21 [20] shows that small reduction of mass can bring a synergistic virtuous mass cycle effect down throughout various subsystems level within the vehicle, particularly if initial weight reduction comes from non-structural components (i.e. interior components). These parts that are further down the structural hierarchy contribute significantly more to the mass compounding effect.

### 2.5.1 Advantages and Drawbacks of Weight Reduction

There are many advantages from weight reduction, from lower emissions, better acceleration performance and reduced material use to better fuel consumption. However this weight reduction brings about some negative effects. Nolan [32] examined the mass incompatibility between vehicle footprint and its effect on occupant injury risk in a crash. He found that in a fleet of heavier vehicles, a lighter vehicle fare worse in an accident. This difference is explained by the inherent physics of colliding objects with different mass. This mass incompatibility can be simply explained by inelastic collision as shown in Fig 2.22, where  $m_1$  (lower mass) experiences a greater velocity change than heavier  $m_2$  when they collide (inelastically). The larger velocity change in  $m_1$  means that during the collision,  $m_1$  experiences higher acceleration levels than  $m_2$ . The greater acceleration faced by  $m_1$  would result in higher occupant injury. This simplified explanation corresponds to the statistics from NHTSA which finding suggests that a vehicle weighting twice as much as the other (heavier 1818kg vs lighter 909kg), the occupants of the lighter vehicle are 8 times more likely to be killed than the occupants of the heavier vehicle even when both the vehicles are rated to have the same crash safety standard rating in a full frontal crash test. This also shows that, vehicle weight offers no safety advantage or disadvantage in single-vehicle crashes. Nolan's research also shows that automotive manufacturers' compliance to voluntary standard crash structure height (NHTSA part 581) increases compatibility resulting in a significant reduction in injury risk of occupants in mass incompatible crashes.

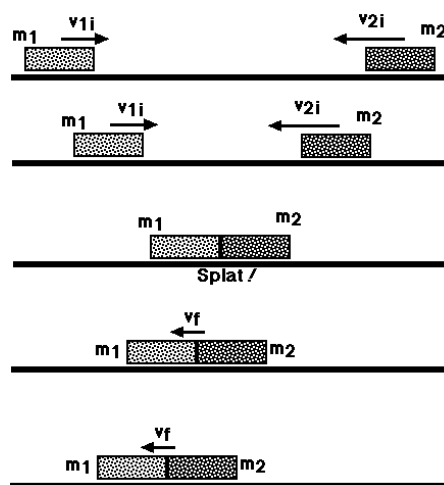


Fig 2.22 Bulk mass inelastic collision illustration representing collision of vehicle with different mass  $m_1$  is lighter than  $m_2$ .

This weight reduction trends towards efficiency and sustainability can have an initial negative effect. However initial mass incompatibility will be unavoidable, but once a critical number of overweight vehicles are replaced with lightweight vehicles, the balance should tip over easily to favour lightweight vehicles.

## 2.6 Materials

Materials have many different properties such as ductile, brittle, high strength, elastic modulus, low density, high density, yield strength and strain rate hardening effect. Various portions of vehicle structure such as crumple zone and passenger safety cell favour different material properties that either provide strength or energy absorption characteristics. Materials with higher performance particularly in specific strength, specific stiffness and specific energy absorption (SEA) are of interest to vehicle structure design engineers. These dominating material properties determines its engineering applications. Fig 2.23 shows the differences in stress, strain and failure points for CFRP, steel, GFRP and plastics under tensile failure. The area under the stress strain plot shows the total energy absorption under deformation. This ability to deform plastically to absorb energy is particularly useful in design of crash worthy structures.

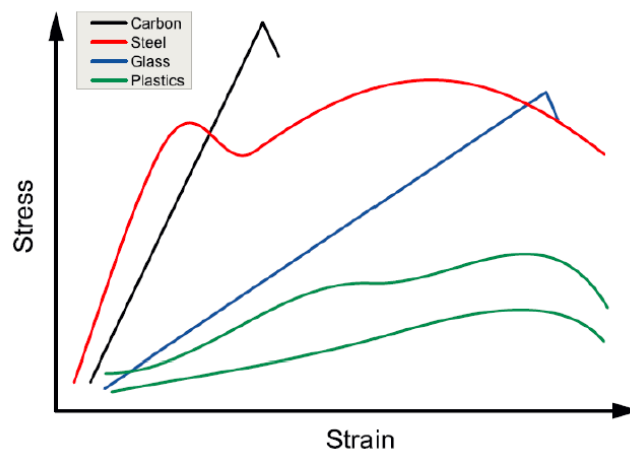


Fig 2.23 Stress - Strain diagram of various materials and their failure characteristics under tensile failure [33] Area under the plot shows energy absorption limit of materials.

### 2.6.1 Metallic Materials

Steel consists of alloying element of iron and carbon. It is one of the most widely used material in the automotive industry for body structure. It is extremely suitable for high volume production due to the short stamping cycle time. There are varying strength grades from 300MPa to over 1000MPa depending on heat treatment, microstructure grain refinement, precipitation hardening, transformation hardening and alloying elements [34] [35]. Fig 2.24 shows the property summary of these different automotive steel grades. The modern steel has extremely high tensile strength. These are known as AHSS (Advanced High Strength Steel). Automotive manufacturers are increasing its use in modern vehicles to reduce weight. The

application of such high strength steel depends on its formability (forming limit diagrams) and manufacturing limitations. Higher tensile strength grade are generally more expensive and cannot be used for complex geometries due to the limitation in flexibility/forming limit for manufacturing [36]. The development of highly formable steel also made manufacturing of complex structure from a single sheet possible.

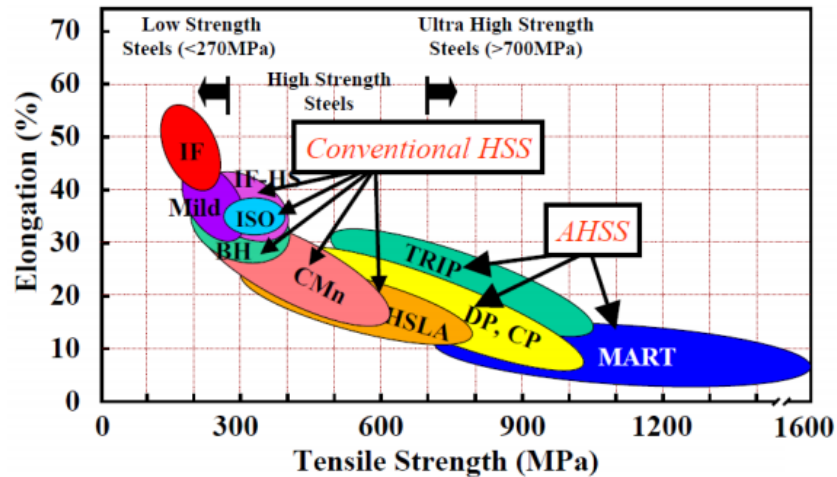


Fig 2.24 Total Elongation (%EL) vs. Ultimate tensile strength (UTS) "banana curve of automotive steels" [37]

In general vehicle's crash energy absorption structure requires to be constructed of a material that can undergo high plasticity at high stress prior to failure so as to extend the Specific Energy Absorption (SEA) capabilities. The increase use of AHSS allows structure sections to have thinner skins while achieving the same strength and reduced weight. The decrease in thickness can affect the structural stiffness due to buckling instability and much more attention have to be given to optimize the geometric cross-section and second moment of area to avoid buckling failure. For automotive exterior panels, the selection of material is also important. Higher yield strength material will be less likely to be dented when impacted by stones or foreign objects compared to a lower yield strength material as higher yield strength allows more energy to be absorbed without plastic deformation. This meant that the vehicle can be made more resistance to dent from stone, hail and door impact from adjacent vehicle.

Low density material such as aluminium can be chosen for better buckling performance for long beam application because material thickness have to increase to achieve same strength as steel, the increased thickness adds additional off axis stability due to increase in out of plane stiffness. Aluminium more resistant to corrosion compared to steel and does not have a fatigue limit, however well-designed aluminium structures will not have any fatigue related issues over its lifetime. Strain rate hardening is another material property to consider. For steel in general, strength increases with strain rate and aluminium are generally considered to be non-strain rate sensitive, thus it is superior for application in vehicle crash structure, allowing engineers to easily control the crash energy management at any collision speed. Aluminium also boasts an average SEA rate of 20kJ/kg [38]. Current modern aluminium structure weighs

20-30% lighter than that of a conventional steel vehicle structure. Aluminium vehicle structure absorbs crash energy in the same way similar to steel, primary through deformation, folding and fracturing. A lightweight aluminium vehicle structure Audi A8 is shown in Fig 2.25.

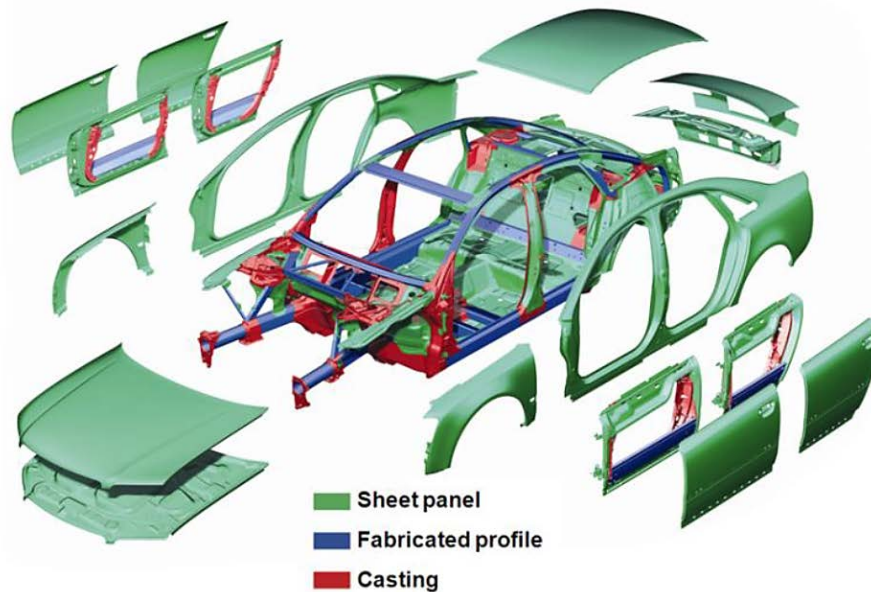


Fig 2.25 Exploded view of the aluminium body structure of the Audi A8 [16]

### 2.6.1.1 Crash Structures

One of the criteria for crash worthiness, is the controlled absorption of crash energy. The progressive deformation of the crash structure creates an opposing reaction force to decelerate the vehicle. The most effective means to absorb this energy is by means of progressive axial crushing. Wierzbicki [39] pioneered the mechanics of progressive axial collapse of thin wall structures. The plastic hinging and folding of material during the crushing of the structure is where the main bulk of energy is absorbed shown in Fig 2.26. Thus the selection of suitable energy absorbing material rely mainly on the material's plastic deformation performance.

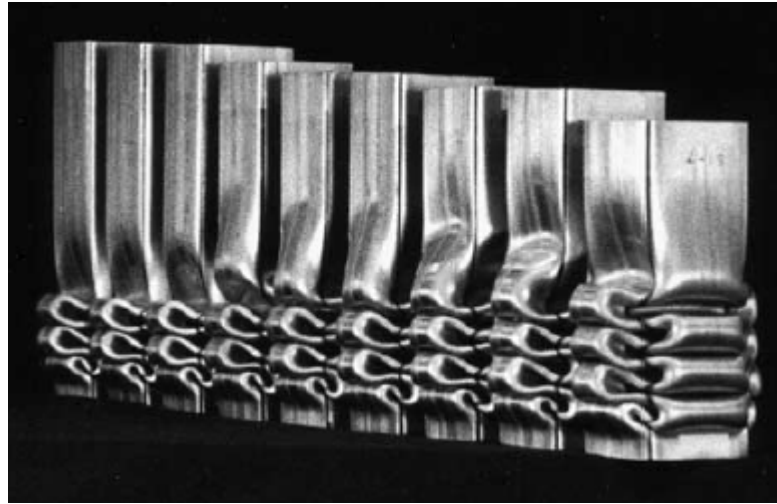


Fig 2.26 Folding of thin wall stainless steel structure under axial crushing [40]

In axial crushing, a preceding high peak force (100kN) is required to trigger the folding process as shown by experiments conducted by DiPaolo in Fig 2.27. After the folding process was initiated, an oscillating force-displacement cycle will dominate, creating a rise and fall cyclic axial reaction load. In an ideal load absorbing profile, the load displacement curve should be flat to create an even and consistent energy absorbing profile. The high initial peak is unfavourable as it may trigger/initiate folding at the base of the crash structure rather than at the crash front. If the folding process occurs at the base it can cause stability problems in crash structure. Thus, it is imperative that during the energy absorption process the structure does not bent or breakaway due to fractures developed by the folding process. Such breakaways create gaps in the energy absorption curve and can severely compromise crash worthiness as energy absorption is terminated prematurely. Effective crush triggers/initiator have to be developed to ensure the folding initiates at the crash front and reduce the peak initial force. Fig 2.28 shows the various type of crush trigger/initiator.

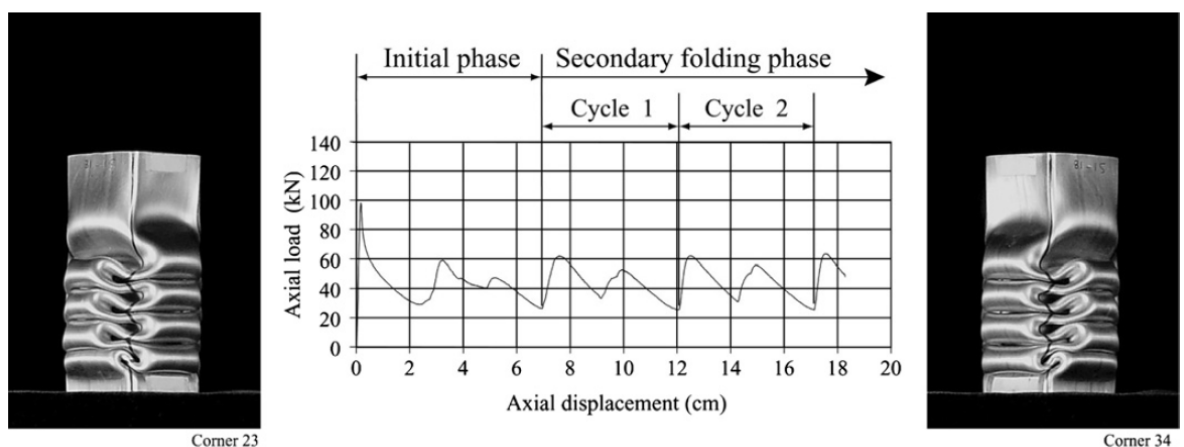


Fig 2.27 Fold formation and Load-Displacement of different phase and cycle of thin-wall square stainless steel profile.

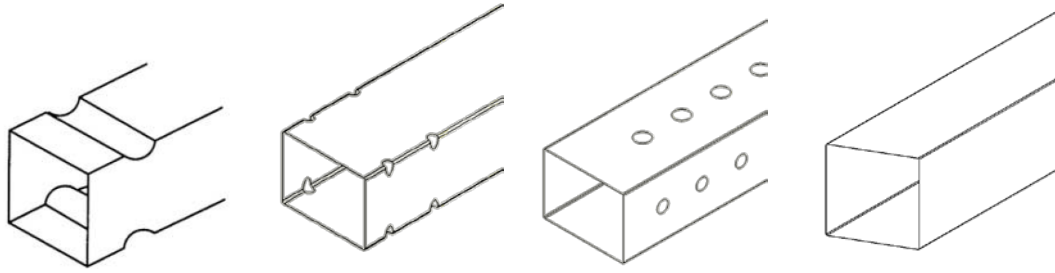


Fig 2.28 Different types of crush initiators for box extrusion profiles.

## 2.6.2 Other Materials

Current vehicle structures mostly consist of steel and aluminium, however new designs are moving towards multi material composite construction. Other materials such as magnesium, titanium, stainless steel, glass fibre composites, plastics and rubber are also used for their respective dominant material performance and application. Ashby [41] first developed materials selection method using material performance index for engineering applications.

Table 2.3 below shows the material performance index [41] of an assortment of materials commonly used for structural applications. Glass fibre reinforced plastics (GFRP), Aramid fibre reinforced plastics (AFRP) where UD (50%) meant uni-directional and fibre volume fraction respectively.

Table 2.3 Material performance index comparison between typical materials in tension with average specification values [42]

Material	$\rho \left[ \frac{kg}{dm^3} \right]$	$E [MPa]$	$R_m [MPa]$	$\frac{1}{\rho} \left[ \frac{dm^3}{kg} \right]$	$\frac{E}{(g\rho)} [km]$	$\frac{R_m}{(g\rho)} [km]$
Steel	7.85	210,000	700	0.1274	2675.16	8.92
Aluminium	2.7	70,000	400	0.3700	2592.60	14.80
Magnesium	1.74	45,000	300	0.5750	2586.07	17.24
Titanium	4.5	110,000	1,000	0.222	2444.44	22.22
GFRP – UD (50%)	2.25	39,000	1,150	0.4444	1766.90	52.10
CFRP – UD (50%)	1.5	120,000	1,700	0.6667	8155.88	115.53
AFRP – UD (50%)	1.32	31,000	1,250	0.7576	2393.97	96.53
Wood	0.5	12,000	100	2.0000	2400.00	20.00

## 2.6.3 Carbon Fibre Composites

Carbon fibre are made from very thin fibres of carbon atoms chemically bonded along the axis of the fibre, resulting in a material that is exceptionally strong, weight for weight stronger than steel. When aligned in matrix material (either thermoset or thermoplastics), thousands of these carbon fibre reinforces each other to form extremely strong and rigid carbon fibre composite. Due to the alignment of reinforcing fibres the strength of carbon fibre composite is anisotropic, extremely stiff and strong along fibre direction and weak in transverse tensile direction. Carbon fibres is bundled together to form a tow. Next, the tow is used to create woven, weave or stitched fabric which allow easier placement and alignment of carbon fibre. Carbon fibre directionality can be mixed in a stack of different layers and plies to form a laminate as shown in Fig 2.31.

### 2.6.3.1 Brief History of Carbon Fibre and Its Applications

Carbon fibre first commercial use was the incandescent lamp filament by Thomas Edison [43]. The carbonization process allows carbon fibre to withstand high temperature and have good electric conductivity. It was not until the 1950s where it was discovered that by applying tension during the carbonization process, high mechanical properties can be obtained. Carbon fibre was primary used for military application due to its superior mechanical properties particularly in area of naval and aviation. Its inherent corrosion resistance and high specific strength opened new performance possibility for rocket motor casing and aircraft structure. The mass commercialization and technology transfer didn't start until after the 1970s. Since then, its application and global growth expanded rapidly, gaining significant market share in aviation, automotive, sporting goods and wind turbines blades [44].

Lightweight high strength materials have always been the pinnacle for aerospace applications, every kilogram saved on an airliner contributes to thousands of dollars savings in fuel cost over its life time. CFRP's high fatigue resistance and anisotropic properties allow engineers to better utilize and optimize for load application [45] in primary and secondary structures. Boeing 787 Dreamliner is the first commercial airliner to feature 50% weight percentage which amounts for 80% by material volume resulting in a 20% efficiency improvement compared to previous generation of aircraft [46]. With a fifth the density of steel, CFRP lightweight high strength performance, resistance to corrosion and low thermal expansion property has benefited the aviation/space industry and in high performance engineering applications. Particularly in motorsports, it made significant impact with increased structural stiffness in both torsional and bending modes in a lightweight high strength package. Carbon fibre composite structure provided a huge performance advantage over other motorsport racing teams without it. With the recent advances in composite production, manufacturing cycle time and matrix technology, carbon fibre are starting to make economic sense in mid-range passenger vehicles to as tooling cost for carbon fibre are much lower than their metallic counterpart. The BMW i3 and Alfa Romeo 4C are example of such mid-range vehicles with safety cell structure constructed out of CFRP.



Unlike isotropic materials, carbon composites is anisotropic. Its mechanical properties differs in different directions. This property is perfectly suited for components that are loaded uniaxially, as material can be optimally orientated. Carbon fibre forms the reinforcing components of CFRP, which are held together by matrix of either thermoset or thermoplastics material. The strengthening concept of the construction is similar to steel rebars in concrete structures. Composites are not just limited to long fibre reinforcement but also can have particulate or short fibre (aligned, partially aligned or random) reinforcement. Carbon fibre composites are usually constructed by laying up plies of carbon fibre fabric sheets to form a laminate structure. Fig 2.32, Fig 2.33 and Fig 2.31 show the different types of fabrics, woven, non-crimp and tape. Laminates with different orientation alignment will results in anisotropic performance which can be calculated with classical laminate theory (CLT) [47] and ABD matrix shown in Fig 2.29. Its couplings between bending extension and shear can be calculated, the ABD matrix and illustration of the load couplings are shown in Fig 2.29.

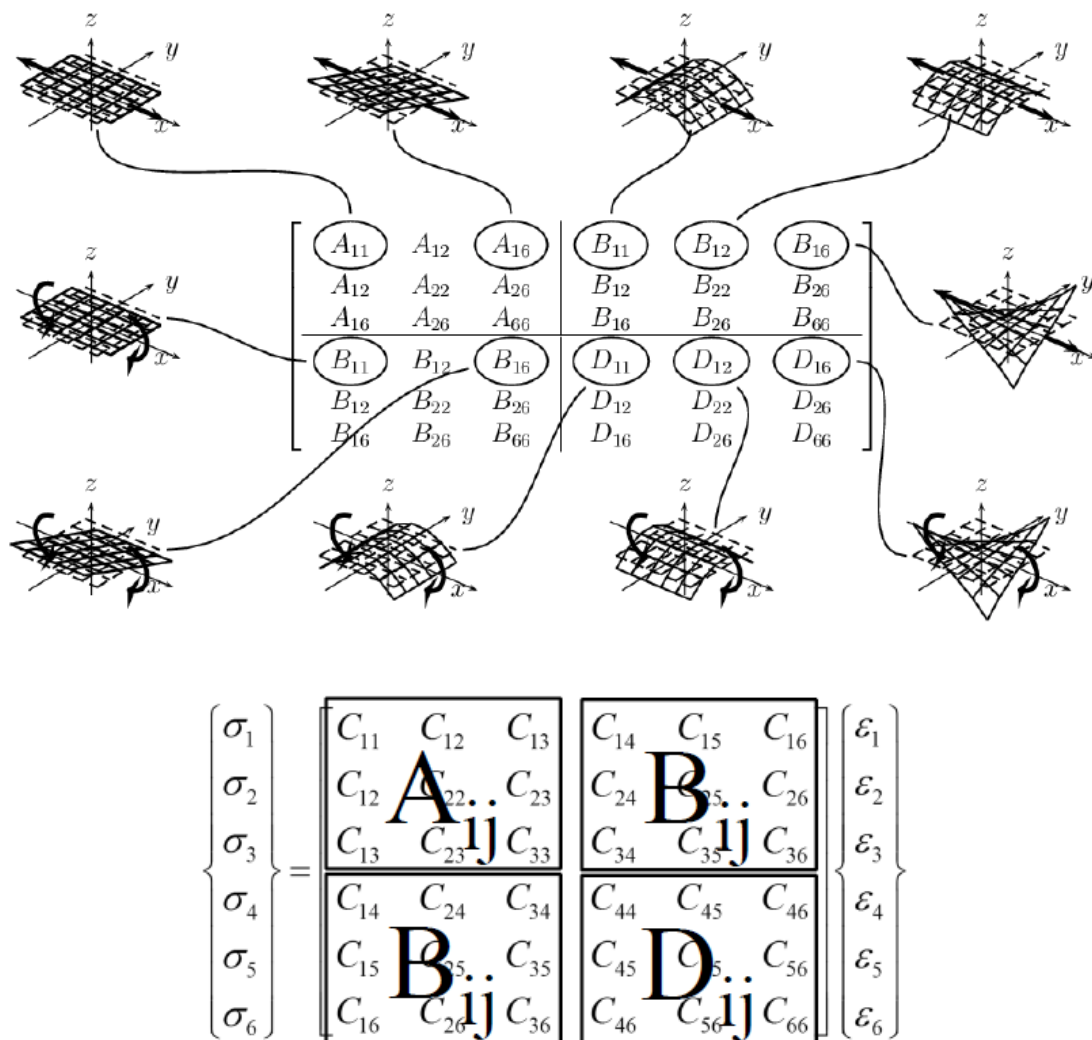


Fig 2.29 (Top) ABD Matrix and illustrated coupling effects, (Bottom) ABD coupling mathematic relationship between stress and strains [48]

Besides CLT, there are also analytic plate approaches if load cases are simple. These analytic methods can be easily found in most composite textbooks such as [47] by Daniel and Ishai. The coupling between bending, extension and shear allow engineers to design a material that deforms a predefined way under load. Carbon fibres are commercially available in different forms: woven Fig 2.32, braided cylindrical fabric in Fig 2.33, multi-axial non-crimped fabrics Fig 2.31, unidirectional pre-preg (pre-impregnated carbon fibre) or randomly aligned short fibre matt. There is a another classification of tow size which indicates the number fibre filaments in each bundle, the spools normally comes in 1k, 3k, 5k, 12k or 30k bundles. These spools bundles can then be used to create weaved fabrics or uni-directional tape.



Fig 2.30 Unidirectional prepreg tape [49]

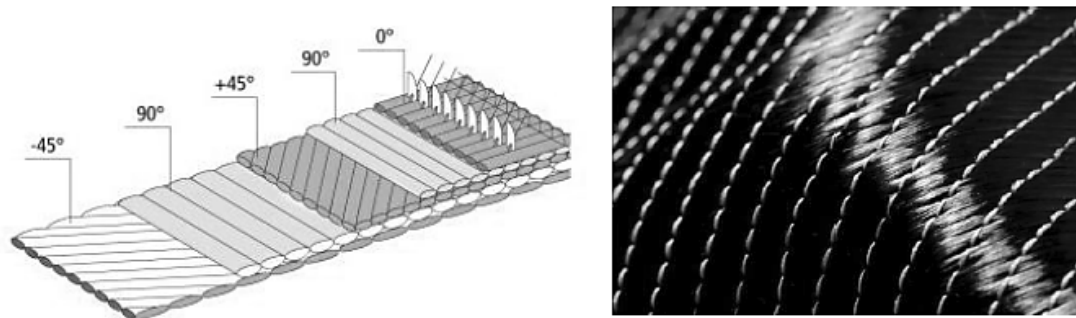


Fig 2.31 Multi-axial non-crimped fabrics held together with glass fibre stitching [50]

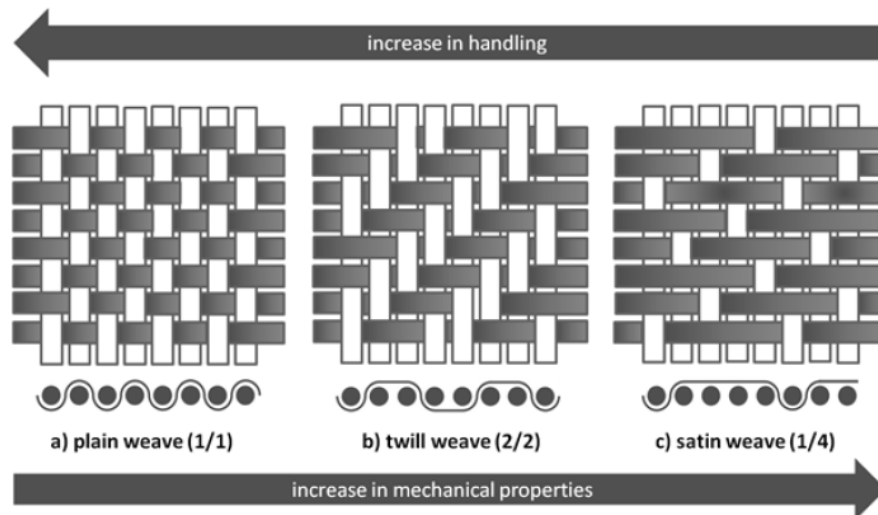


Fig 2.32 Different types of weave pattern on woven fabric and their influence in handling and mechanical properties. [51]

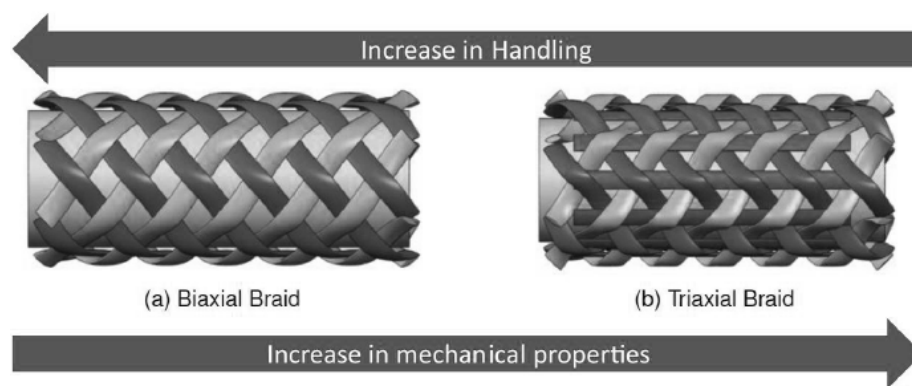


figure 58: different types of braids and their influence [LCC12b]

Fig 2.33 Different types of braided fabrics and their influence in handling and mechanical properties [50]

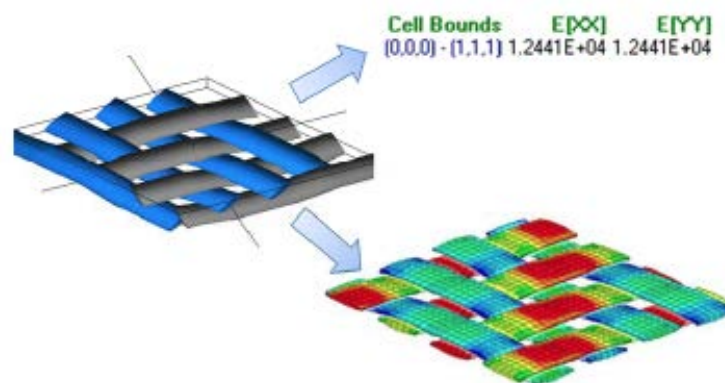


Fig 2.34 Macro level FEA of twill weave fabric [52]

In general, woven fabric are easier to handle and have better smeared properties, however they are mechanically weaker due to kink in the tow from each weave as shown in Fig 2.34 compared to non-crimp fabric or unidirectional, however weaves are more resilient to delamination within a ply. A general rule construct a stronger laminate, there must be a reinforcing cross ply to reinforce the unidirectional layers after a significant number of unidirectional plies was laid down. Hart Smith [53] deduced the 10 percent rule which states that each 45° or 90° ply on average contribute one tenth of the strength of a 0° ply to the overall performance of the laminate. These reinforcing layers have inter-laminar influence on each other, changing the dominant failure modes when used in crash energy absorption application. The strength of the laminate can be calculated accurately with this 10 percent rule.

The flexibility and variability of carbon fibre placement allows precise engineering for strength and stiffness. Engineers can increase number of plies to increase strength or align fibre direction to increase stiffness and strength. For metallic structure using stamping technology there will be a variation of thickness due to the forming process, in areas subjected to stretching, obtaining precise thickness after forming will be much more difficult.

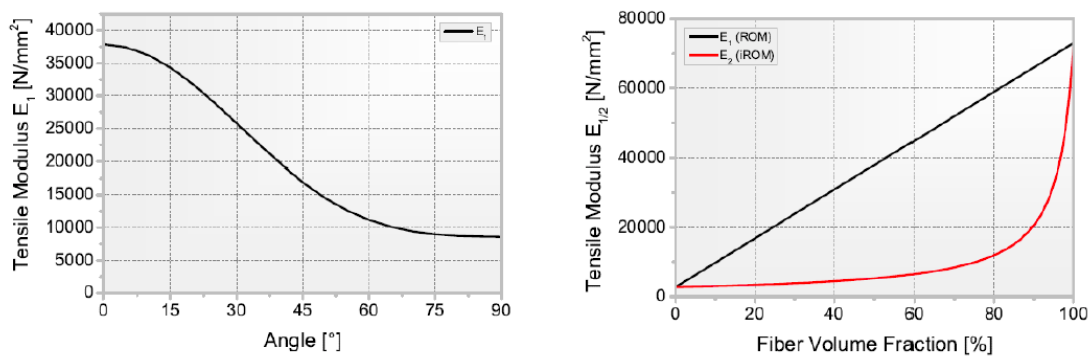


Fig 2.35 Composite strength in unidirection loading depending on angle and fibre volume fraction [52]

## 2.6.4 Structural Joint of Carbon Fibre Composites

The difference in material mechanical performance between CFRP and metal means that different considerations is required to obtain a good structure connection/joint. For composites in general, due to the lack of plasticity behaviour to redistribute high stress concentration, failure to consider stress concentration of joints can easily result in premature failure of joint. One of the most effective methods to reduce stress concentration is to employ adhesive joint. Hart Smith [54] had researched on the multiple types of adhesive joints and the techniques employed to increase the joint strength.

### 2.6.4.1 Mechanical Fasteners

Mechanical fasteners is one of most common form of structural joints for composite structures. Composite are more sensitive to stress concentrations due to the anisotropic nature of fibre reinforced composites as shown in Fig 2.36 compared to ductile metallic isotropic material.

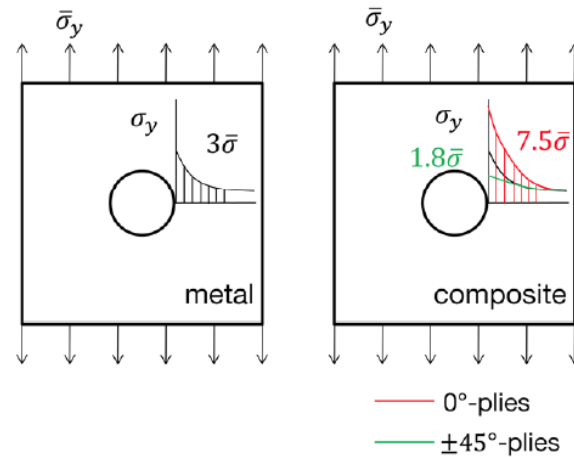


Fig 2.36 Comparison of stress concentration factors of holes in composites and metal. [55]

A composite plate with quasi-isotropic or orthotropic layup will have the best load capacity if loading direction cannot be determined. Hart Smith's analytical study on mechanical fastened joints of composites suggested that with the best designed bolted composite joints can only be 50% as strong as the equivalent perfect composite plate [56]. The primary mechanism in composite mechanical fastened joint strength is in the bearing loading capacity of the bolted joints and the interval between the fasteners. In addition, over-tighten fasteners results in localized matrix cracks and delamination, resulting in lower bearing load capacity. In a study done by Liu [57] the drilling process caused delamination around mechanically drilled hole which have to be considered when designing bolt fasteners for composites. In another study done by Gibson [58] to study the effect of cycling loading on fastened joints, suggested that joints could significantly reduce fatigue life limit due to high stress concentration and the most common mechanical fastened failure is shown in Fig 2.37.

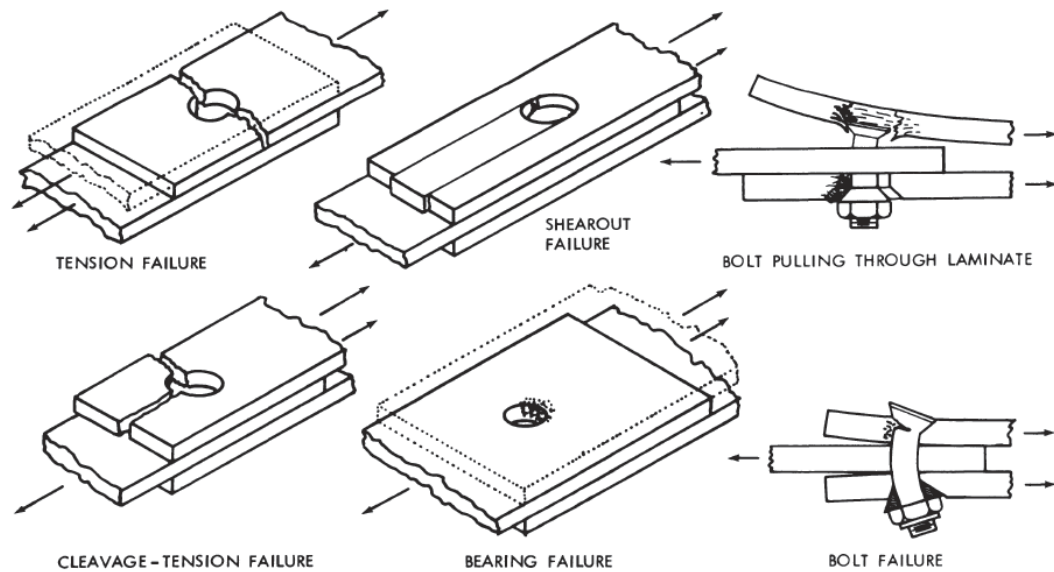


Fig 2.37 Mode of failure of bolted joints in advanced composites [56]

#### 2.6.4.2 Adhesive Joints

Adhesive bonding is one of the most common forms of structural attachment method for the design of lightweight composite structures. Fig 2.38 shows the different types of adhesive joints. Adhesive joints in principle are structurally more efficient than mechanical fastened joints. Adhesive joints allow stresses to be distributed reducing stress concentrations. Adhesive generally have a lower strength than the carbon fibre composite, thus Hart-Smith [56] suggested that composite plates should have bond length of 30-50 times the thickness to ensure that stresses can be transmitted across without exceeding adhesive strength limit, isolating failure out of adhesive joint area. Design of adhesive joint requires understanding principal loading direction. Adhesive is the weakest when it faces loads that result in peel stress while it is the most resilience when loaded in shear. This characteristic is similar welded/spot welded joint and membrane design methodology mentioned by Malen [10]. Hart-Smith suggested using stepped lap joint or scarf joint joining method to adhere two thick composites laminate. He also pointed out the peel stress can be reduced in joints design through scarfing and plies drop off to reduce peel stresses as shown in Fig 2.39. These designs reduces peel stress by reducing the bending stiffness at the edge of the adhesive joint.

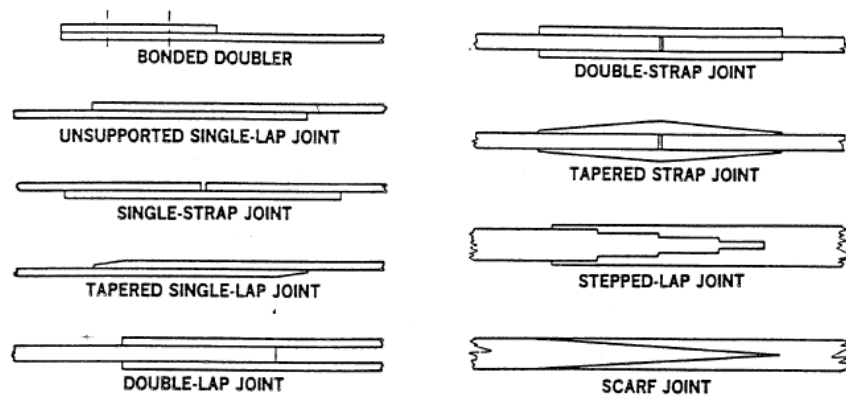


Fig 2.38 Type of adhesive joints in composites [54]

Adhesive joints are also highly sensitive to manufacturing defects such as ill-prepared bonding surfaces, contamination of bond surfaces, poor bonding technique, steep angled joint assembly between adhesive parts of more than  $30^\circ$ , presence of moisture on bond surfaces and temperature [59]. The poor fit of mating surface can result in stress concentration within the adhesive particularly in areas where adhesive is thinner. Adhesive which are brittle in nature and can develop cracks overtime, which can lead to stress concentration and subsequent failure of the adhesive joints. Effect of factors affecting performance of adhesive are described in more detail by Hart-Smith in [59] [60] [61].

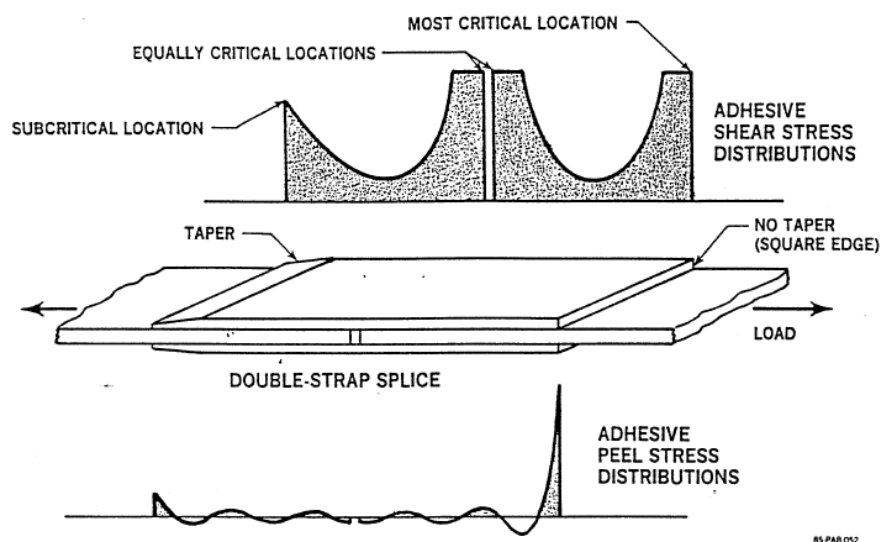


Fig 2.39 Adhesive stresses in tapered and no tapered bonded joints [54]



### 2.6.4.3 Metallic Inserts

For structural attachment to composite surfaces, another excellent method is the use of inserts and big heads shown in Fig 2.40 which distribute the stress. The unique spike feature and large bond area on the inserts allows load spreading over a large area positively engaging the strong carbon fibres, reducing stress concentration and bearing loads on the composite plate allowing larger force transfer than a whole through bearing loading. Sandwich insert typically require inserts to be bonded via adhesive to the core material of the sandwich, particularly in hollow sandwich like nomex honeycomb, resin or adhesive have to fill the immediate space vacated by the placement of the insert to ensure good force transmission. In general, the design of the inserts is to distribute the load via adhesive bonds to the sandwich structure reducing stress concentration.

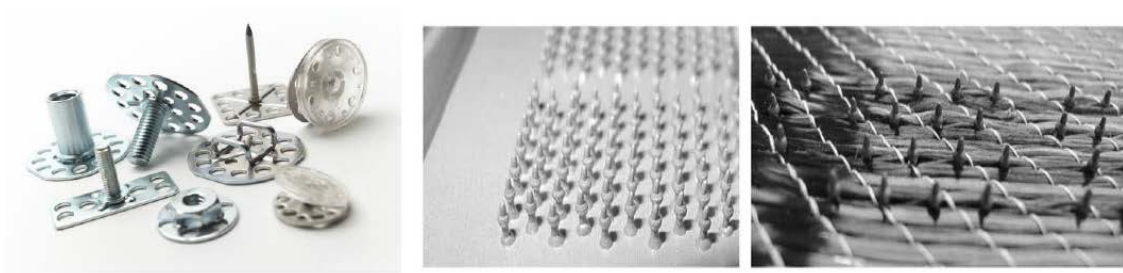


Fig 2.40 Big head threaded inserts and spiked inserts [62] [63]

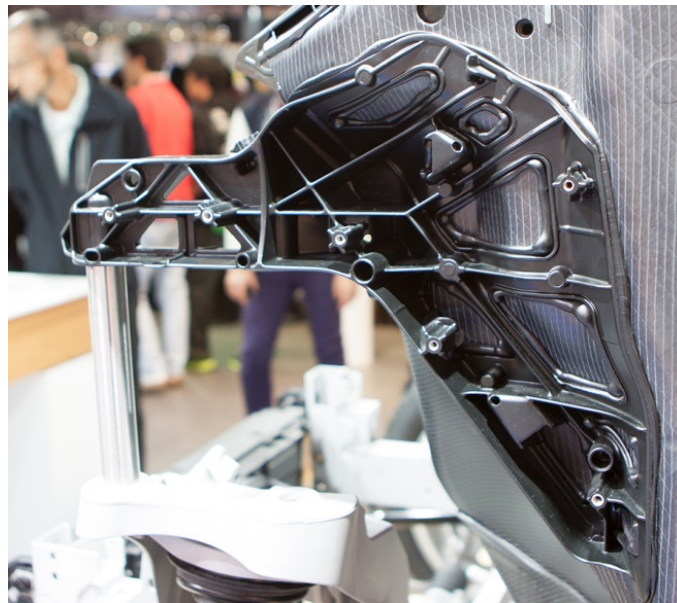


Fig 2.41 Cast Aluminium front shock tower support structure of the BMW i3 bonded to the carbon monocoque life cell. (Picture taken by author at the 2013 Tokyo Motorshow)

These inserts or studs can also be used for attachment of component and mounting of sub-systems. Directly fastening of components to composite surface is generally not recommended shown in Fig 2.41.



Combination of two structural joint methods can be beneficial. The use of fasteners in conjunction with adhesive bonding when properly designed function as crack arrester by resisting peel stresses mentioned by Barnes [64] .

## 2.6.5 Failure Criteria for Carbon Fibre Composite

Failure criteria for anisotropic material is different compared to isotropic material due to the differing failure mechanism. Failure of composite can occurs in many modes as shown in Fig 2.43. In long fibre carbon fibre composite failure occurs with either fibre or matrix failure either by tension, compression or shear. Failure characteristic is dependent on fibre volume ratio, void ratio, strength of fibre and matrix material. In lamina failure, there are a variety of approaches focusing on different mechanics of failure theory, some provides a slightly more conservative criteria, while some to a lesser extent. Predicting and calculating exact failure modes of failure is very challenging when developing a large multi component composite vehicle structure due to the complex geometry and forces interaction and distribution between parts. Diving into complex failure mechanisms can be futile as manufacturing accuracy and variations in hand layup components and adhesive joining of components can easily invalidate any accurate failure assumptions and calculations. Therefore in this development process, relatively simple and conservative failure models will be used to calculate laminate failure to mitigate the reduction in strength brought forth by less than ideal manufacturing quality.

### 2.6.5.1 Maximum stress/strain criteria (Non-Interactive)

Maximum stress and strain criterion is one of the most well used non interactive failure criteria for determining composite failure. This group of failure criteria associates with different failure modes particularly in fibre fracture, transverse matrix cracking and shear matrix cracking. The non-interactive nature of the criteria can lead to errors in strength predictions under multi-axial stress state in a structure.

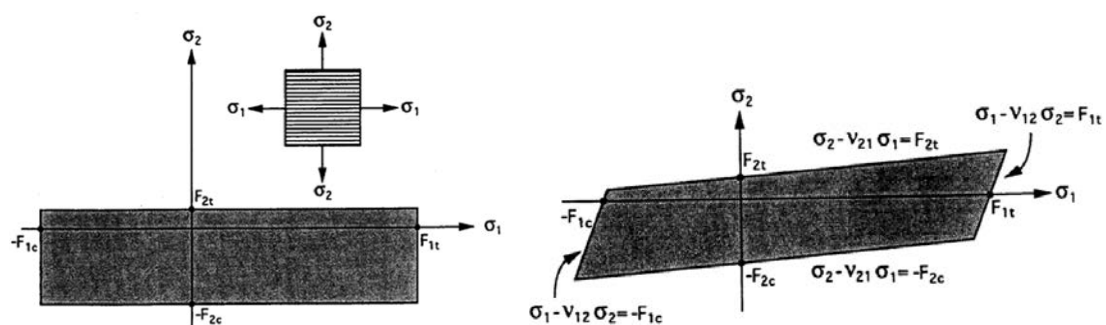


Fig 2.42 (Left) Maximum stress envelope (Right) Maximum strain envelope. [47]

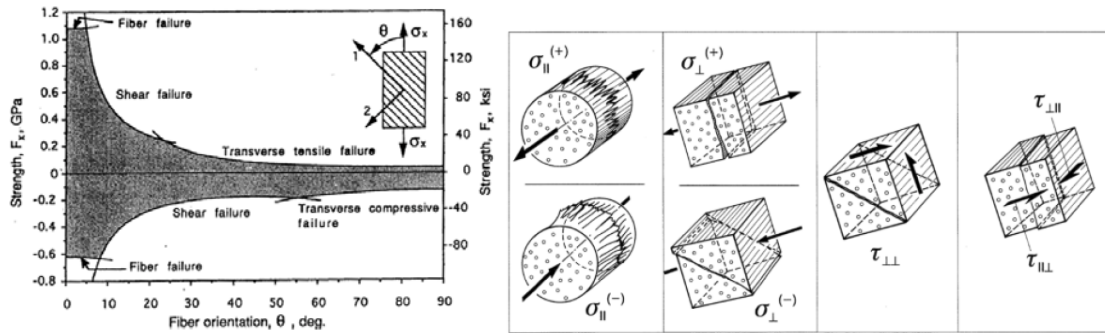


Fig 2.43 (Left) Different failure modes envelope for varying angle unidirectional composite plates. (Right) Type of failure modes of unidirectional lamina [65]

### 2.6.5.2 Tsai-Hill and Tsai-Wu Criteria (Interactive)

Tsai-Hill failure criteria is an adapted extension of Von-Mises criteria for isotropic materials which accounts for interactions between tensile stresses and shear stresses. While Tsai-Wu uses polynomial tensors interactively to determine failure envelope. Both of these criteria focus mainly of bulk laminate failure concept using isotropy assumption and cannot take into account of different damage mechanism in laminate that are naturally anisotropy. However Tsai-Hill and Tsai-Wu are the most used failure criteria to determine failure in composites. Its accuracy can be further improved by varying experimentally obtained coefficient parameters. Its simplistic mathematical approach allows it be easily programmed for used with FEA. The main drawback of this approach is that it does not distinguish the modes of failure. The basic form of Tsai-Wu criteria is shown below.

$$F_i \sigma_i + F_{ij} \sigma_i \sigma_j \leq 1$$

Where  $i, j = 1 \dots 6$  where  $F_i, F_{ij}$  are obtained experimentally and  $F_{ii}F_{jj} + F_{ij}^2 \geq 0$  condition is satisfied to ensure the envelope is closed and convex.

The basic form of Tsai-Hill criteria is show below. The drawback of the Tsai-Hill criteria is that it does not differentiate tensile from compressive stresses. Thus when using Tsai-Hill criteria, one have to consider the loading direction.

$$\left(\frac{\sigma_1}{\sigma_{1u}}\right)^2 + \left(\frac{\sigma_2}{\sigma_{2u}}\right)^2 - \frac{\sigma_1 \sigma_2}{\sigma_{1u}^2} + \left(\frac{\tau_{12}}{\tau_{12u}}\right)^2 = 1$$

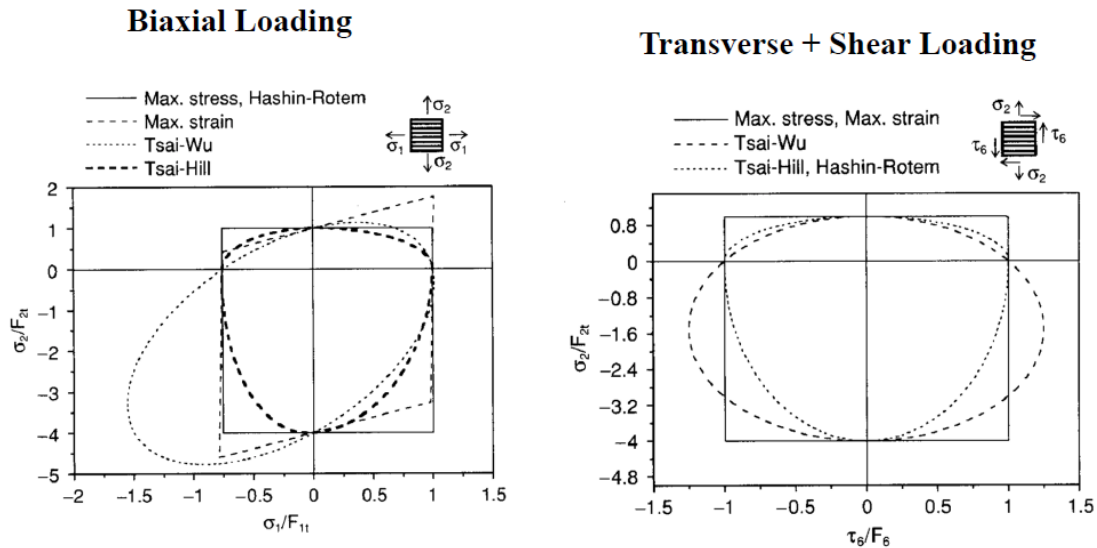


Fig 2.44 (Left) Failure envelope of biaxial loading (Right) Failure envelope for transverse and shear loading for Tsai-Wu, Tsai-Hill, Max-strain, Max-stress and Hashin-Rotem failure criteria. (Daniel and O.hais)

There are many alternative interactive or non-interactive failure criteria such as Puck [65], Hashin-Rotem [66], Azzi-Tsai [67], Hoffman [68], Chamis [69] and many more. Each failure criteria offer characteristics such as simplicity of use or ability to determine the mode of failure under prescribe loading stress. However identifying exact failure can have limited contribution to the development process when there is significant shortcomings in manufacturing accuracy. To make up for the lack of accuracy a more conservative approach is typically desired. Fig 2.44 shows the difference in failure envelope of various failure criteria, the outline shows that some criteria are more conservative in compression loading while some are more conservative in tensile loading. Therefore a combination of composite failure criteria can be used according to which failure region is more conservative.

### 2.6.5.3 Composite Laminate Strength

The failure criteria describe previously is more centred towards lamina failure. Predicting the strength of laminate before failure requires more considerations, particularly the progressive accumulation of damage or reduction in laminate stiffness which eventually leads to ultimate failure. This is a difficult task, as there are many more mechanism affecting the failure such as delamination, intra and inter-laminar characteristics. Depends on the layup of the laminate, the progressive onset of failure can occur progressively [70] or abruptly [71]. The typical procedure to predict the strength is via lamina strain and stress analysis lamina failure criteria, stiffness degradation model and finally laminate failure criterion. Failure of lamina can be predicted by failure criteria mentioned previously. However when it comes to stiffness degradation model, the rate of degradation depends on the onset of matrix cracking or fibre failure. A number of models have been proposed to determine the ultimate laminate failure but in large scale complicated structure with large variation in layup, the progression for stiffness degradation from one part of the structure can result in failure at another section of the

structure due to stress redistribution. In most cases the stress redistribution process can be complicated and inaccurate due to failure of geometrically complex laminate coupled with combination failure mechanism of structural joints, adhesive and inserts. For loading of simple composite structure the modelling of such failure are much simpler and straight forward. Even with accurate FEA modelling coupled with calibrated material failure model, it will be too computationally intensive to simulate the progressive failure of a large structure. Therefore one of the most reliable ways to verify its performance is by conducting physical experimental testing, however such destructive development methods does not make sense for prototype development.

## 2.7 Concluding Remark

This review chapter covered several vehicle structure design concepts, general crashworthiness design, the most influential crash test standards and safety. Additionally, touched on briefly, the basic vehicle structure requirements for passenger vehicles and the dynamic performance requirements. Furthermore, a short overview on how mass reduction increases the vehicle performance and efficiency along with the environmental and safety impacts inherited by the mass reduction. The environmental challenges is one of the primary motivation to explore the possibility of lightweight vehicle structure. Aligning with the EVA project's aim of a realizing a fully functional prototype featuring a highly efficient structure. This presents a development challenge particularly in development methodology due to the limited literature on composite vehicle structure design with consideration for crash safety. This set the foundations for further investigations. Material characteristic and basic failure criteria of CFRP along with general composite designs, such as adhesive, joints and inserts were explored. In additional, a close design analysis of the state of the art composite vehicle structure particularly the electric variant, the BMW i3, revealed insights on some of the design constraints revolving about composites vehicle structure. The author also studied several metallic vehicle structures, their load paths and crash energy management characteristics concurrently with the mechanics of metallic progressive axial crushing in crash energy absorption. In the next chapter, a deeper analysis in the forces involved in crash test standards and subsequently the conversion to equivalent quasi-static crash loads will be carried out. Additionally, topics such as limitations of accurate composite failure simulation, superiority of carbon composite in crash energy absorption, material selection process, adhesive joint design and design for manufacturing along with material characterisation by laboratory coupon test will discussed.



---

## Chapter 3: Development Setup, Considerations and Limitations

---

After the brief review of crash worthy vehicle structure design, metallic and composite material and current trends of the automotive industry towards lightweight sustainable vehicles. This chapter will cover the design setup, considerations and limitations for development of the vehicle structure. In order to create a safe prototype platform for future research, the vehicle structure has to efficiently regulate the deceleration by energy absorbing crumple zones, reducing forces subjected to the occupant and maintain survivable space by minimizing intrusion. To achieve this goal, the author will review the physics and mechanics of collision, derive equivalent quasi-static crash loads, state of the art simulation for composites, material selection, selection of production process and obtaining mechanical property from test coupons. In the closing sections of the chapter, a brief overview on the constraints of adhesive joints design, definition of manufacturing guidelines for ply overlap along with infusion test on sandwich panel using vacuum assisted resin infusion (VARI) process will be discussed to define the limiting boundaries and development approach.

### 3.1 Crashworthiness Development Challenges

In literature and books, it is relatively easily find information on concept of crash worthiness and desired qualities of an ideal vehicle structure. Future Steel Vehicle (FSV) Phase 1 [72] and Phase 2 [30] covered this aspect of literature comprehensively (approximately 1800 pages) on the concept, engineering design, crashworthiness, cost and manufacturing optimization for modern steel vehicle structure. However detailed literature on how to develop carbon fibre composite vehicle structure is limited and inconclusive. Many of the methods used by FSV are only applicable to metallic materials that deform plastically, such methods are not suitable for development of crashworthy composite vehicle structures. A brief review of composite aircraft structure development methods revealed the limited applicability in passenger vehicles due to the differing design aims. In aircraft structure design, the loads are dominated by aerodynamic and structure load under routine operations coupled with a safety factor of up to 2.5 and the main design concern is resistance to fatigue failure and residual strength after damage. The aircraft structure focuses on crack arresting design and ample structure reserve strength if part of the structure was compromised due to damage. On the other hand, vehicle structures focuses on the rate of energy absorption through the crushing of crumple zones. The design requirements is vastly different as crash loads dominates the design criteria/requirements. Crash loads are in the region of 20 to 30 times of normal operation loads, meeting crash load requirements often easily exceed the fatigue and normal operating load requirements of the vehicle structure. As a result of that, the strength and rigidity of the occupant safety cell and the energy absorption rate of the crumple zones are the main design objective in a vehicle structure. The large ratio between maximum design load and operation load and different structure aims meant that methodology between aircraft design cannot be exchanged without additional consideration. Thus a new simplified approach to develop composite prototype

vehicle has to be considered. In the following sub-sections, an approach is proposed for the simplification of dynamic crash load to equivalent quasi-static crash load, through crash mechanics and photogrammetry analysis for front and side impact.

### 3.1.1 Crash Energy Approach for Frontal Impact

In front impact crash test, USNCAP uses full width frontal impact and EuroNCAP uses the frontal offset impact test. In Fig 3.1 shows the illustration of a frontal collision setup for deformable barrier and rigid barrier, vehicle A and B are identical and the deformable barrier have the same characteristic in absorbing impact similar to the crumple zone of the car. To have a fair comparison, we will also assume that both crash tests occur at the same speed. The dotted red reference line indicates the point of impact and the crash absorption characteristic is taken as ideal constant crash force with crumple deformation.

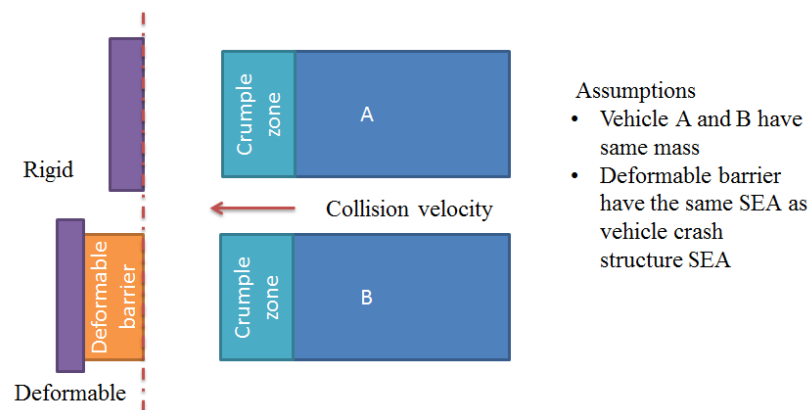


Fig 3.1 Illustration of frontal collision set up, A and B are identical vehicle impacting the barriers, red reference line shows the point of impact.

In Fig 3.2 shows the end of the collision event and the total crash energy being absorbed. For the rigid collision (A) and deformable barrier collision (B) the displacement from the reference line is identical and the total crash absorbed energy is also identical, in the scenario for the deformable barrier collision there is more crumple zone left compared to collision with the rigid structure, the deformable absorbs part of the crash impact energy. The frontal offset impact (C) have a larger displacement from the reference line due to the partial engagement of the vehicle crash structure, the resulting crash energy absorb is the identical as (A) and (B). The illustrations in Fig 3.1 and Fig 3.2 shows the simplified crash mechanism for frontal impact. However in actual vehicle crash, the crash energy absorption characteristic is slightly different, the crash absorption will not be a flat force displacement plot but at a slightly increasing rate primarily due to the stability of the crash similar to crush compression ratio (CCR) for composite structure and secondarily due to interaction between vehicle components such as motor, gearboxes, suspension sub-frame shown in Fig 3.11. The optimization of crash performance contribution from these sub-systems is a secondary priority.

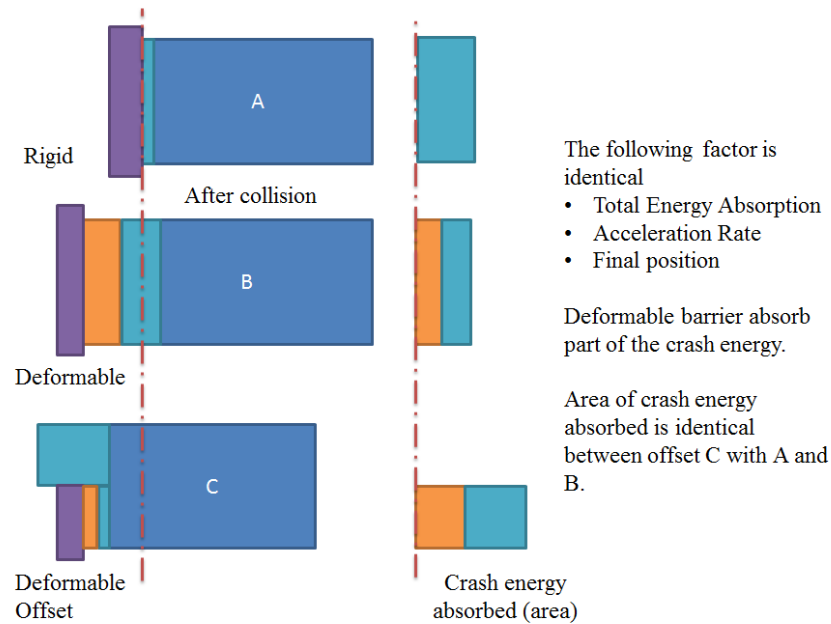


Fig 3.2 Illustration of crumple zone deformation and total crash energy absorbed and the end of collision position of the vehicle.

### 3.1.2 Photogrammetry Study of Frontal Crash Tests

For the mechanics of a vehicle crash, analysis is conducted on well-documented vehicle crash tests [73] [74] using photogrammetry to study the amount of deformation of crumple zone, crash duration and resulting acceleration. A number of recent FMVSS 301 (full width frontal collision) and EuroNCAP offset frontal crash videos were also studied to understand the mechanics of crashworthy vehicle.

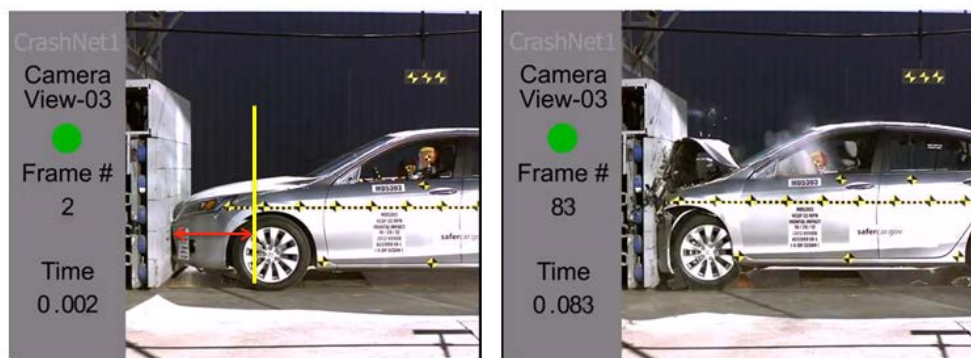


Fig 3.3 FMVSS 301 full width vehicle crash test showing the amount of deformation and time duration of the impact

Fig 3.3 shows a time-stamped FMVSS301 crash test video. Left shows the start of the collision event and on the right shows the end of the collision event, the yellow line marked the amount of deformation at the end of the collision. By referring to vehicle dimension specification the deformation at end of collision, the calculated photogrammetry of the deformation length is approximately 600mm in length. Given the duration of collision and



initial speed, we can calculate the amount of crash deformation. To simplify analysis, we will assume the collision event has constant acceleration with ideal constant force crumple zone.

$$Distance = \frac{1}{2}(V_1 + V_2)t$$

Where  $V_1$  is the initial velocity and  $V_2$  is the final velocity, where  $V_1 = 15.56\text{m/s}$  or  $56\text{kmh}$ ,  $V_2 = 0\text{m/s}$  and  $t = 0.083\text{ sec}$

$$Distance = \frac{1}{2}(15.56\text{m/s} - 0)0.083\text{s} = 0.645\text{m}$$

The calculated deformation is almost identical to photogrammetry analysis. Average crash force or quasi-static crash load can be calculated by

$$Acceleration = \frac{(V_1 - V_2)}{t} = \frac{(15.56\text{m/s} - 0)}{0.083\text{s}} = 187.47\text{m/s}^2$$

And with acceleration and vehicle weight we can calculate the average quasi-static crash force

$$Average\ Force = Mass \times Acceleration = 1500\text{kg} \times 187.47\text{m/s}^2 = 281.2\text{kN}$$

Considering if there are only main two crash energy absorption beam, each energy absorption beam will have to absorb an average of  $140.6\text{kN}$  of force over  $0.645\text{m}$  to achieve same acceleration as the vehicle in Fig 3.3.

For the 40% frontal offset collision into deformable barrier which simulate an offset collision with another vehicle. Assuming the deformable barrier has the same average crush force as the vehicle we can calculate the deceleration rate of the offset collision. Frontal offset collision test occurs at higher speed of  $64\text{km/h}$  and only engages one crash energy absorption beam. We can use:

$$Acceleration = \frac{140.6\text{kN}}{1500\text{kg}} = 93.7\text{m/s}^2$$

$$t = \frac{V_1}{a} = \frac{17.78\text{m/s}}{93.7\text{m/s}^2} = 0.189\text{s}$$

$$Distance = V_2t + \frac{1}{2}(acceleration)t^2 = 0 + \frac{1}{2}(93.7\text{m/s}^2)0.189\text{s}^2 = 1.67\text{m}$$

Considering offset deformable barrier is 500mm in depth, the aluminium honeycomb will stop crushing at  $2/3^{\text{rd}}$  of original length. The vehicle deformation can be calculated after subtracting barrier deformation.

$$\text{Distance} = 1.67\text{m} - 0.5 \times \frac{2}{3} = 1.34\text{m}$$

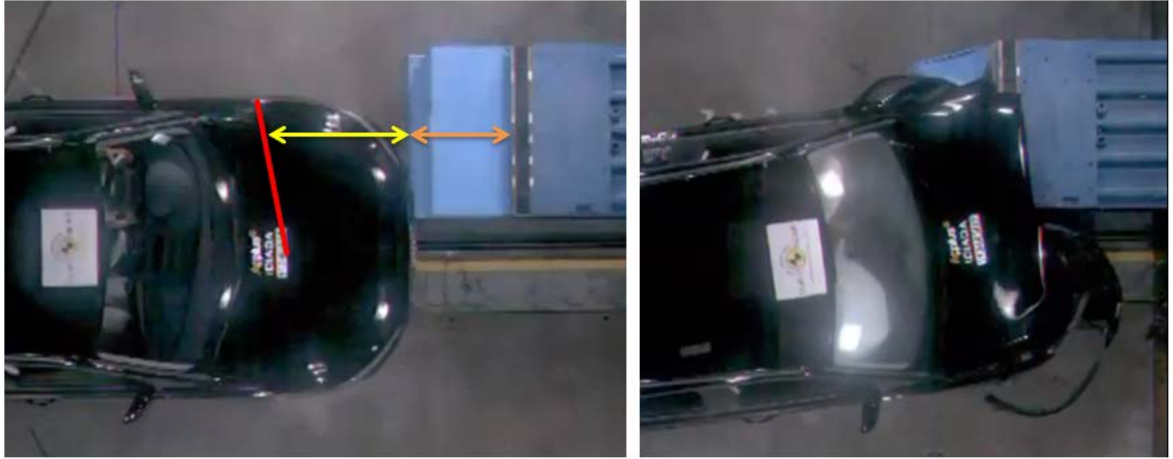


Fig 3.4 Photogrammetry of frontal offset crash test, yellow indicated distance is approximately 1m.

This calculation shows that deformation is up to 1.34m. However this is not the case as shown in Fig 3.4. This strongly suggests that the crash reaction is not constant but increasing as the crash deformation increase. This increase in crash force with deformation is clearly identified in simulation and experimental crash test from [72] [75]. This increase can be attributed by the crushing of the wheels, rims and suspension strut towers.

### 3.1.3 Side Impact Collision Mechanics

The mechanism of side impact collision protection is more challenging as there is a limited available crumple zone, it must utilize a different approach for management of crash energy. The protection method revolve around the concept of reducing the relative occupant acceleration to mitigate injury risk.

The side impact collision (MDB) in Table 2.2 shows the list of different side impact tests however the slight differences in the test does not change the impact mechanics for side impact significantly. One of the key challenges is the lack of side crumple zone and the three-point seat belt does little to restrain the occupant movement in a side impact. The side impact collision follows the same inelastic collision with conservation of momentum as shown in Fig 2.22. The final velocity of both vehicles are given as

$$M_1V_1 + M_2V_2 = (M_1 + M_2)V_F$$

Where  $M_1$  and  $M_2$  are the mass of the striking vehicle and impacted vehicle respectively and  $V_1$  and  $V_2$  is the velocity of striking vehicle and impacted vehicle respectively.

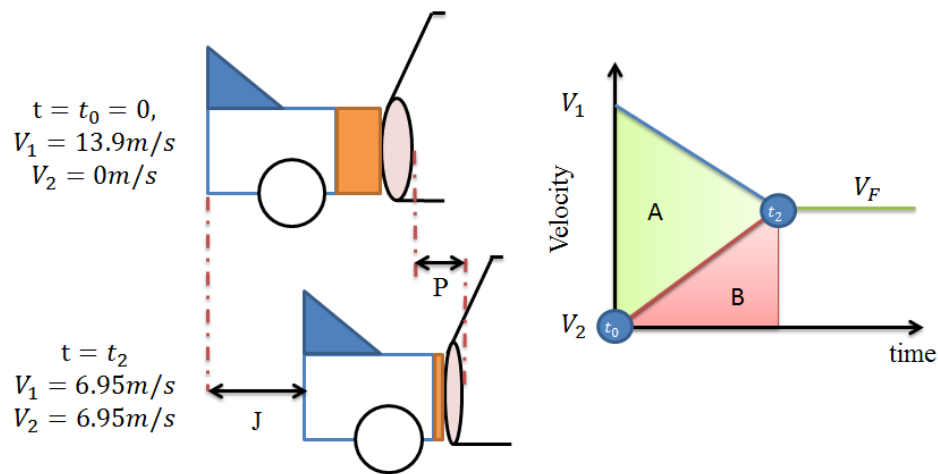


Fig 3.5 (Left) Illustration of conservation of momentum in a side impact collision. (Right) shows the velocity profile of colliding vehicle.

The chronological development of collision between two vehicles of identical mass at 50km/h is shown in Fig 3.5. The transfer of momentum results in the crash energy absorption of the doors and front crumple zone of the impacted vehicle and striking vehicle respectively. At time  $t_2$ , the end of the collision, the internal surface of the door moved by  $P$  and the striking vehicle covered a distance of  $J$  as the collision momentum moves the impacted vehicle into sideward motion. As a result, the occupant will come in contact with the internal door trim panel during the collision.

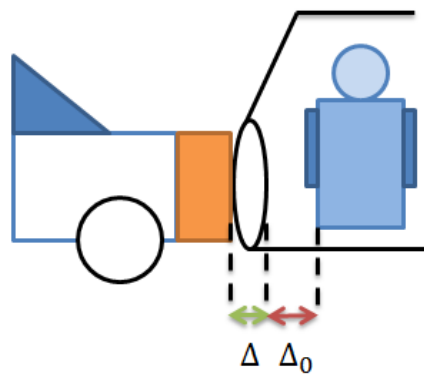


Fig 3.6 Illustration showing the door crumple zone  $\Delta$  and the space between the interior door panel and the occupant  $\Delta_0$ .

Due to the unconstraint nature of seat belt for side impact, we can assume negligible seat belt effort. However this does not mean the seat belt is useless, the seat belt contributes by keeping the occupant in his seat. In Fig 3.6 shows the position of occupant in a vehicle, where  $\Delta_0$  is the space between the occupant and the interior of the door and  $\Delta$  is the thickness of the door to

the door trim which helps in absorption of crash energy. At the start of a side impact/contact when  $t = t_0 = 0$  is  $\Delta$  and  $\Delta_0$  show in Fig 3.7 indicates thickness of door and space in between door and occupant. As the crash progresses, the impacted vehicle  $M_1$  will displace  $M_2$  due to transfer of momentum of the striking vehicle  $M_1$ . The occupant remained in the same reference point because the negligible restraint effect of seat belt.

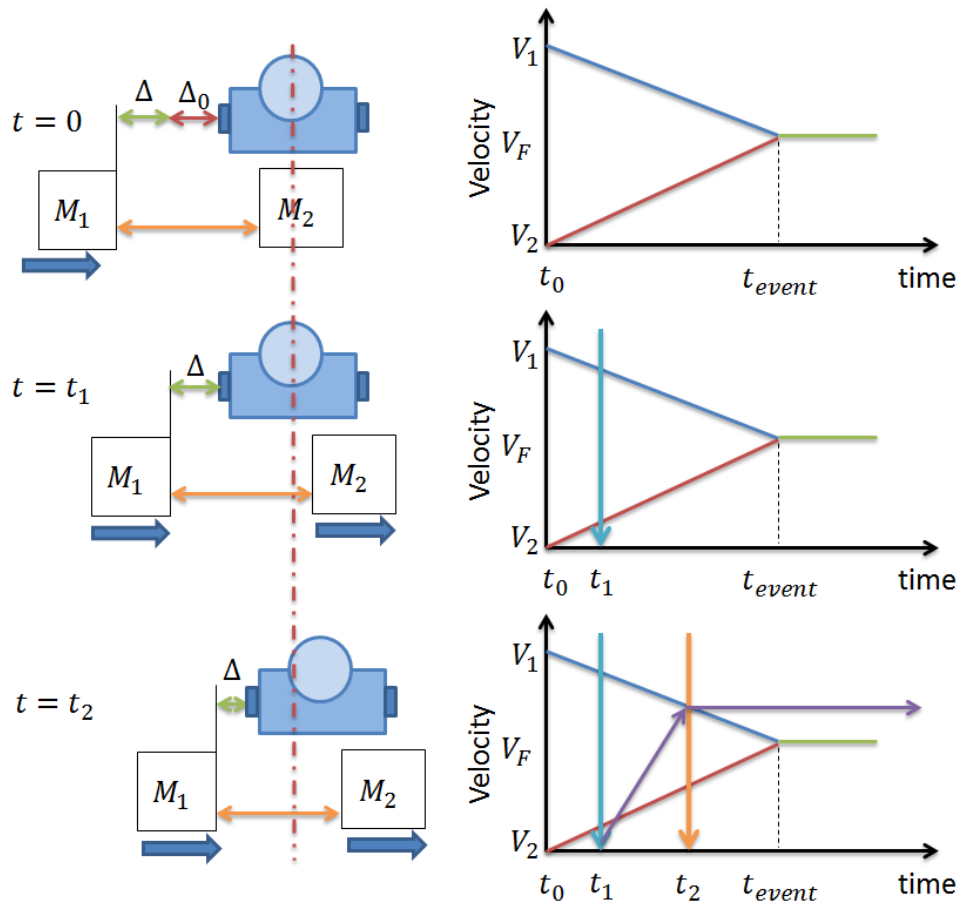


Fig 3.7 Side impact collision events alongside with velocity time diagram of  $M_1$ ,  $M_2$  and the occupant. The slope of the purple arrows is the acceleration rate of the occupant.

When  $t = t_1$ , the occupant will make contact with the internal door panel as  $\Delta_0$  reduces to zero. At this point the occupant will accelerate as crash forces are being physically applied on the occupant. In the final phase of the crash process at  $t = t_2$  where active momentum transfer is still occurring, the door crash structure  $\Delta$  will reach its limit of energy absorption and will accelerate occupant to the velocity of  $V_1$  at  $t = t_2$ . The velocity of the occupant after this point does not change even though  $V_f$  will be much lower because seat belts do not restrict sideward motion in the other direction.

The slope of the occupant velocity plot between  $t_1$  and  $t_2$  in Fig 3.7 indicates the acceleration of the occupant during the collision, to reduce injury risk to the occupant this slope has kept to a minimum. Considering the variables that can be changed,  $t_1$  can be made to start earlier and

$t_2$  made to occur later to reduce occupant acceleration. Reduction in  $t_1$  requires an increase in  $\Delta$  but this cannot be increased excessively as you need space to move your arm around, the gap originally used by  $\Delta_0$  can be filled up by an airbag cushioning impact against hard interior door trims thus increasing  $\Delta$  when the airbag is deployed. This is the reason side air bag systems is so effective in reducing injuries in a side impact. To increase the  $t_2$  timing, we have to delay the point where  $M_1$  comes in contact with the occupant. The stiffening and strengthening of the side structure will result in more efficient transfer of momentum, delaying  $t_2$ . This assist in reducing the apparent impact velocity on occupant as the crash energy will directly accelerate the bulk inertia of the whole vehicle. This is similar to the rigid wall frontal collision in Fig 3.2 except that the rigid wall is able to move due to momentum transfer. If the vehicle side structure is weak, the effective mass accelerated from the momentum transfer will be significantly lower. Thereby resulting in an occupant acceleration profile similar to a collision with high vehicle mass discrepancy as shown in Fig 2.22. The delay in  $t_2$  timing also reduces the final velocity of the occupants which help in reducing acceleration and injuries. In Fig 3.8 shows what can the two improvements mentioned earlier can do to reduce the acceleration imposed on the occupant during a side impact collision.

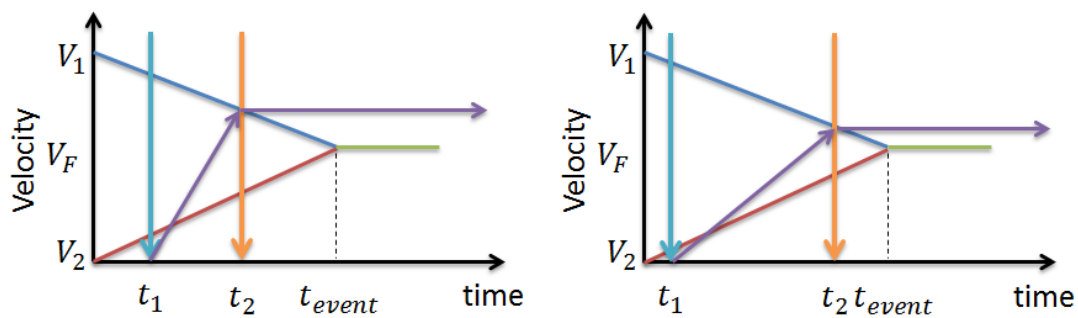


Fig 3.8 Side impact velocity profile (left) without improvement in vehicle side impact strength and door gap reduction and (right) with improvement in both vehicle side impact strength and door gap reduction.

### 3.1.4 Equivalent Quasi-static Crash Load

Quasi-static finite element simulation (implicit) is one of the simplest approaches to determine the strength of structures and is much easier to setup compared to dynamic simulation (explicit). The nature of crash is dynamic but we can develop ways to obtain the quasi-static crash loads using the simplified analysis of frontal and side impact made in the previous section. The use of quasi-static simulation in the initial phase of development avoids the complexity of penalty contact in dynamic simulation and also offers a large reduction in computation cost. From the earlier simplified mechanics of frontal and side crash we subsequent derive the following quasi-static load for a 1500kg vehicle listed in Table 3.1. The side impact, rear impact assumes a striking vehicle of the same mass with identical frontal crumple zone reaction loads. From roof crush benchmark, highest rating is given to vehicles roof that is able to withstand more than 4 times the vehicle weight. These quasi-static crash loads tallies with figures given by Malen [10] and Witteman [76]. These equivalent quasi-

static loads will be used in finite element analysis to develop the EVA composite vehicle structure.

Table 3.1 Calculated quasi-static crash loads for vehicle weighing 1500kg

Crash Test	Quasi-static crash load	Load application
Full Width Frontal Impact	320kN	Both front crash structure
Frontal Offset	160kN	Single front crash structure
Side Impact	320kN	Doors and B-pillar
Rear Impact	320kN	Both rear crash structure
Roof Crush	63kN (4x 1500kg)	Roof

### 3.1.5 Structure Crash Load Path

In a crash, the crash reaction forces will have to be transmitted to the rest of the vehicle, decelerating all components mounted to the vehicle structure. The distribution of these forces through structural members is known as load path. The stiff and strongest load path carries the highest load. Fig 3.9 shows the typical crash load paths for frontal offset impact and side impact collision. The strength of these load paths is critical in maintaining survival space for the occupant and transmitting load to the rest of the vehicle structure. If the load path structure deforms excessively, intrusion and deformation into the occupant safety cell structure will occur. Thus the stability of the structure depends on the design and efficient distribution of crash load paths. Inefficient crash load path requires excessive reinforcement which will increase the weight significantly.

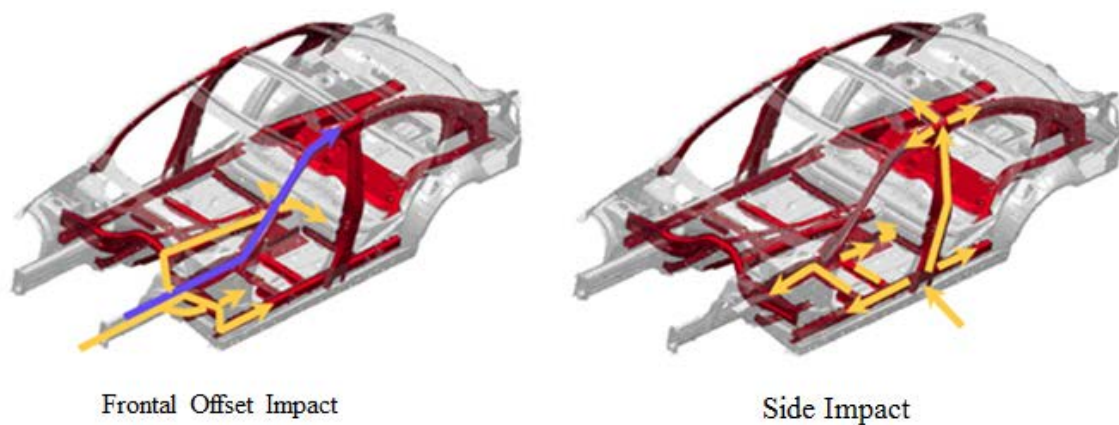


Fig 3.9 Illustration on crash load path through structural members in (top) frontal offset collision and (bottom) side impact collision.

### 3.1.6 Carbon Composite Crash Structure

In the previous section, we touch on the brief history of carbon fibre composite vehicle structure, it was found that carbon fibre composite race car in a crash outperforms a vehicle made from traditional metallic material. How does carbon fibre composite ace crashworthiness? A well-designed composite crash structure will pulverize on impact breaking into thousands of tiny debris absorbing crash energy by various composite failure modes such as fibre breakage

and matrix cracking. This pulverization process have very high SEA, which in an experiment conducted by Hermann et al [77] suggests that for carbon thermoset composites the SEA is approximately at 100kJ/kg, whereas SEA of aluminium and steel are approximately at 30kJ/kg and 20kJ/kg respectively varying mainly due to geometrical design. Therefore carbon composite structure can be up to 3 times lighter than a metallic crash structure.

The excellent SEA of carbon fibre composites is further enhanced by the material property which isolates damage in the crash front and maintains structure integrity in the safety cell, protecting the occupant. This phenomenon was documented by Barnes et al. [64]. Barnes also studied the crushing mechanics of carbon fibre composite. It is paramount that the energy absorbing fracturing mechanism is maintained at the crush front. A composite crash structure will lose its effectiveness if it failure occurs at the base of the crash rail, resulting in the separation from the vehicle structure and creating a gap in the crash energy absorption. This is similar to how crush front have to be maintained for metallic crash energy absorbing structure, except metallic crash structures are less sensitive due to ductility. Barnes identified the design criteria to ensure stability, known as crush compression ratio (CCR), which is the ratio of the compressive strength to the crush stress. He suggested, a range from 4 to 10, higher CCR would be more tolerance to varying angled crash situations and lower CCR meant otherwise. Geometric features such as curvature increase the crush stress due to hoop tension/compression forces creating a supporting force in direction transverse to the crash loads. The compressive strength of the base increases with the cross-section, Fig 3.10 shows the formula 1 nose cone crash structure in a crash test.



Fig 3.10 Formula 1 nose cone under crash test fractures and delaminates as the crash progresses, breaking apart and absorbing energy cushioning the impact. [78]

Carbon composite crash structure fails dramatically, breaking apart into small pieces shown in Fig 3.10. A typical ductile metallic crash structure under axial crush plastically folds to form a pleated structure. Once the crash structure is fully pleated at approximately 1/3 of the original length, reaching the maximum folding capacity, the structure will become uncrushable. This meant that metallic crash structures only have a useful crash energy absorption length of 2/3 of the original crash length. Carbon composite crash structure can utilize nearly the full crash length for controlled energy absorption, the pulverization of material prevents material the build-up of incompressible debris which occurs in metallic crash structure. The lack of folding mechanism in composite crash structure pulverization process causes less fluctuation in the absorption process as shown in Fig 3.11. Extensive research in axial crushing of composite tubes were carried out by McGregor [79], Tomton [80] and Hull [81].



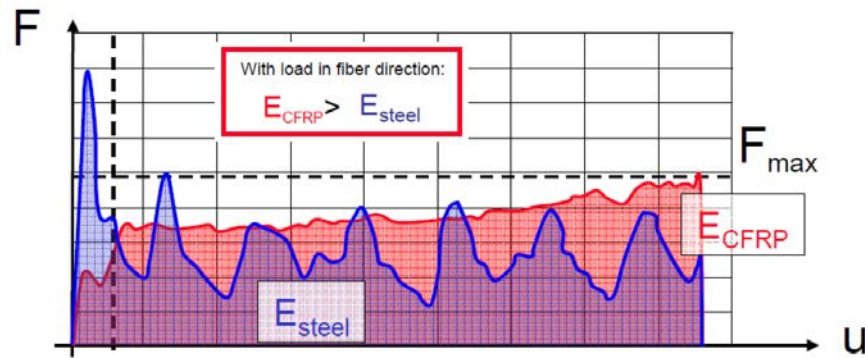


Fig 3.11 Comparison of dissipated energy of steel and CFRP crash absorption cone [82]

However, there is little available literature about angled crushing (non-axially aligned) of composite tubes. The availability of such literature will be useful in real world application for design of vehicle crash structure where the angle of crash is unpredictable. A method to mitigate varying angle of crash is by implementing high CCR. However high CCR requires a large base cross-section for composite crash structure which is challenging to integrate to the package due to the design space required. Furthermore the complexity of composite failure mechanism, modelling failure in order to verify crashworthiness of structure can be computationally costly and economically difficult to justify.

### 3.1.7 Limitations of Carbon Composite Failure Models

As design of EVA vehicle structure can only be verified through computer simulation as only one prototype will be made, an important prerequisite is the ability to accurately verify the performance in a dynamic crash scenario. It is important to understand the current state of the art failure models for composites. One of the most comprehensive literature is the Worldwide Failure Exercise (WWFE) [83] [84]. Under WWFE, leading theories on composite failure were tested in various scenarios in a blind test and later verified with experiment results. Hinton [85] summarized the general performance of these theories in Table 3.2 and Table 3.3. The conclusion suggest that multiple theories were able to predict the failure with reasonable accuracy for uni-directional lamina composite but no single failure theory can accurately predict failure of multi-directional laminate structures. Table 3.2 and Table 3.3 shows the performance of each failure theory with reference to each test parameter, few theories performed well in this aspect. These test numbers indicate the normalized result compared to actual experimental results on different biaxial loading given by stress ratio column. It demonstrates the limits of accuracy and weakness of the current state of the art theories.



Table 3.2 Predicting the biaxial strength of a unidirectional composite [85].

Test case	Stress-ratio	ZNOVIEV	WOLFE	TSAI	Sun(NL)	SUN(L)	ROTEM	PUCK	MCCARTENY	HART-SMITH2	HART-SMITH1	EDGE	ECKOLD	CHAMIS-2
0 LAMINA UNDER SHEAR+TRANSVERSE	SR = 1/0	1	1	1	1	1	1	1	1	1	1	1	1	1
0 LAMINA UNDER SHEAR+TRANSVERSE	SR = 0/1	1	1	1	1	1	1	1	1	1	1	1	1	1
0 LAMINA UNDER SHEAR+TRANSVERSE	SR = -1/0	1	1	1	1	1	1	1	1	1	1	1	0.29	1
0 LAMINA UNDER SHEAR+TRANSVERSE	SR = 0.35/1	1.21	0.96	1.21	1.05	1.05	1.05	1.05	1.05	1.05	1.05	1.05	1.21	1.05
0 LAMINA UNDER SHEAR+TRANSVERSE	SR = -0.73/1	0.63	0.76	0.63	0.6	0.6	0.6	0.6	0.6	0.63	0.63	0.63	0.55	0.6
0 LAMINA UNDER SHEAR+LONGITUDINAL	SR = 1/0	1	1	1	1	1	1	1	1	1	1	1	1	1
0 LAMINA UNDER SHEAR+LONGITUDINAL	SR = -1/0	1	1	1	1	1	1	1	1	1	1	1	1	1
0 LAMINA UNDER SHEAR+LONGITUDINAL	SR = 0/1	1	1	1	1	1	1	1	1	1	1	1	1	1
0 LAMINA UNDER SHEAR+LONGITUDINAL	SR = 20.7/1	1.05	0.831	1.05	0.92	1.05	1.05	0.92	1.05	1.05	1.05	1.05	0.778	1
0 LAMINA UNDER SHEAR+LONGITUDINAL	SR = 7.2/1	0.71	0.71	0.71	0.71	0.76	0.71	0.71	0.71	0.71	0.71	0.71	0.65	1
0 LAMINA UNDER SHEAR+LONGITUDINAL	SR = -13.6/1	1.3	0.98	1.18	1.3	1.3	1.16	1.3	1.3	1.3	1.3	1.3	1.02	1
0 LAMINA UNDER LONG. +TRANS.	SR = 18.8/-1	1.125	0.955	0.77	1.125	1.125	1.1	1.125	1.125	1.05	1.13	0.84	0.87	0.67
0 LAMINA UNDER LONG. +TRANS.	SR = 9.3/-1	1.54	0.99	0.88	1.54	1.54	1.34	1.2	1.54	1.36	1.54	1.54	0.9	0.45
0 LAMINA UNDER LONG. +TRANS.	SR = 4.23/-1	1.195	0.96	0.95	1.195	1.195	1.17	1.08	1.195	1.2	1.2	0.84	0.91	0.33
0 LAMINA UNDER LONG. +TRANS.	SR = -1/0	1	1	1	1	1	1	1	1	0.505	1	1	1	1.6
0 LAMINA UNDER LONG. +TRANS.	SR = 1/0	1	1	1	1	1	1	1	1	1	1	1	1	1
0 LAMINA UNDER LONG. +TRANS.	SR = 0/-1	1	1	1	1	1	1	1	1	1	1	1	1	0.28

Accuracy within  $\pm 10\%$   
 Accuracy within  $\pm (>10<50)\%$   
 Accuracy greater than  $\pm 50\%$

Table 3.3 Predicting the maximum strength of multidirectional composite [85].

Test case	Stress Ratio	ZNOVIEV	WOLFE	TSAI	Sun(NL)	SUN(L)	ROTEM	PUCK	MCCartney	HART-SMITH2	HART-SMITH1	EDGE	ECKOLD	CHAMIS-2
30/90 UNDER SHEAR+DIRECT STRESSES	SR = -2.3/1	0.656	0.32	0.531	0.85	0.675	0.809	0.85	0.675	0.737	0.62	0.74	0.225	1
30/90 UNDER SHEAR+DIRECT STRESSES	SR = 1/1	0.818	0.21	0.535	0.91	0.436	0.927	0.91	0.436	1.08	1.08	1.08	0.393	1
30/90 UNDER SHEAR+DIRECT STRESSES	SR = 0/1	0.914	0.38	0.613	1.11	0.449	0.967	1.11	0.449	0.974	0.83	1	0.336	1
30/90 UNDER SHEAR+DIRECT STRESSES	SR = -1/0	0.608	0.53	0.534	0.84	0.734	1.222	0.84	0.734	1.18	1.15	1.18	0.814	1.94
30/90 UNDER SHEAR+DIRECT STRESSES	SR = 1/0	0.87	0.444	0.445	0.9	0.528	0.733	0.9	0.528	0.89	0.89	0.89	0.371	1.16
30/90 UNDER DIRECT STRESSES	SR = 1/2.86	1.272	0.909	1.02	1.23	0.238	1.318	1.23	0.238	1.43	1.43	1.43	0.41	1.09
30/90 UNDER DIRECT STRESSES	SR = 1/-1.44	0.916	0.55	0.43	1.06	0.55	1.06	1.06	0.55	1.53	1.53	1.53	0.183	1.03
30/90 UNDER DIRECT STRESSES	SR = -1/2.3	1.2	1.71	1.88	1.84	1.81	2.11	1.84	1.81	2.25	2.25	2.25	1.4	2.83
30/90 UNDER DIRECT STRESSES	SR = 1/1	0.937	0.883	0.19	0.91	0.194	0.963	0.91	0.194	1.342	1.31	1.342	0.808	0.59
30/90 UNDER DIRECT STRESSES	SR = -1/0	1.824	1.49	1.07	2.06	1.69	1.771	2.06	1.69	1.35	1.35	1.35	0.842	1.75
30/90 UNDER DIRECT STRESSES	SR = 1/0	0.814	0.765	0.45	0.78	0.672	0.938	0.78	0.672	1.09	1.04	1.04	0.67	0.69
0/90/45 UNDER DIRECT STRESSES	SR = -1/0	1.614	1.401	1.24	1.56	1.641	1.614	1.56	1.641	1.506	1.59	1.506	1.2	1.1
0/90/45 UNDER DIRECT STRESSES	SR = 1/-1	1.534	0.928	0.59	1.49	1.034	1.358	1.49	1.034	1.463	1.31	1.463	1.3	0.53
0/90/45 UNDER DIRECT STRESSES	SR = -1/-1	2.727	4.153	2.41	2.76	2.757	2.65	2.76	2.757	2.814	2.814	2.814	1.154	1.11
0/90/45 UNDER DIRECT STRESSES	SR = 2/1	0.963	0.875	0.82	0.97	0.373	0.98	0.97	0.373	0.939	0.92	0.939	0.9	0.9
0/90/45 UNDER DIRECT STRESSES	SR = 1/0	1.013	0.863	0.72	0.98	0.766	0.94	0.98	0.766	0.941	0.92	0.941	0.496	0.92
55 UNDER DIRECT STRESSES	SR = 0/1	0.97	1.1	0.96	1	0.96	2.25	1	0.96	2.1	2.1	2.15	0.47	1.02
55 UNDER DIRECT STRESSES	SR = 0.75/1	0.44	0.85	0.41	0.76	0.405	1.74	0.76	0.405	1.92	1.82	1.92	0.76	0.74
55 UNDER DIRECT STRESSES	SR = 1.3/1	0.204	0.62	0.21	0.62	0.205	1.43	0.62	0.205	2.24	2.16	2.24	1.3	0.53
55 UNDER DIRECT STRESSES	SR = 3.3/1	0.91	0.65	0.19	0.64	0.163	0.886	0.64	0.163	0.544	0.49	0.53	0.292	0.79
55 UNDER DIRECT STRESSES	SR = 0/-1	1.19	1.055	1.03	1.02	1.027	1.111	1.02	1.027	0.972	0.97	0.972	0.694	0.47
55 UNDER DIRECT STRESSES	SR = -2/-1	0.484	0.461	0.55	0.72	0.485	0.642	0.72	0.485	0.723	0.73	0.723	0.239	0.99
55 UNDER DIRECT STRESSES	SR = 2/1	1.196	1.19	0.815	1.19	0.173	1.076	1.19	0.173	1.327	1.24	1.33	1.154	1.11
55 UNDER DIRECT STRESSES	SR = 1/0	0.655	0.338	0.43	0.57	0.479	0.417	0.57	0.479	0.426	0.43	0.426	0.24	1.08
45 UNDER sr=1/1	SR = 1/1	1.315	0.826	0.14	0.8	0.179	1.275	0.8	0.179	1.31	1.31	1.31	1.356	0.61
45 UNDER SR=1/-1	SR = 1/-1	0.952	0.78	0.771	0.78	0.924	0.771	0.78	0.924	0.771	0.771	0.771	0.539	0.61
0/90 UNDER SR=1/0	SR = 1/0	1.084	0.673	0.48	0.8	1.1	1.051	0.8	1.1	1.051	1.051	1.051	1.054	0.61

Accuracy within  $\pm 10\%$   
 Accuracy within  $\pm (>10<50)\%$   
 Accuracy greater than  $\pm 50\%$

With the success of WWFE I, WWFE II and WWFE III are planned in the pipeline. WWFE II will test failure criteria under tri-axial stresses of fibre reinforced polymer composites and WWFE III will focus on damage, fracture and continuum mechanics theories for fibre-reinforced polymer composites. The preliminary evaluation of WWFE II is similar to WWFE I, suggested that the results are inconclusive. There is no theory that performs the best compared to the rest of the theories.

The dynamic failure models struggled to correlate with actual failure performance. Most of these theories allow input of experimentally obtained parameters to achieve better correlation. Furthermore these state of the art failure theory models are typically not readily available in commercial software. This means that the implementation of such failure model and pre-processing setup will be too taxing with the given timeframe and resources. Even with all the benefits of composite crash structure, compromise for less ideal, simpler solutions has to be explored. These findings strongly indicate the likely reasons why the application of carbon composite in vehicle structures is limited to non-crash energy absorption, which correspond to the findings by Lescheticky from BMW [86]. BMW is currently exploring the correlation of composite simulation to expand carbon composite application into the area outside of the safety cell particularly in crash absorption structure [86]. As a result of the findings, a reasonable approach for EVA was to develop metallic crash structure and the details of the development will be covered in Section 4.5.

### 3.1.8 EVA CFRP Structure Failure Criteria

The review of laminate failure and WWFE shows the limitations in failure prediction and complexity progression of failure in dynamic simulation. This applies to all carbon fibre composite parts in the structure. The limited package space for modern vehicles requires structural surface to conform around tight package restriction. Thus, complex geometric shapes are more common in a vehicle structure than an aircraft. These resulting geometric complexities further complicate the dynamic failure. Literature on how such complexity can be managed to improve structural efficiency and lightweight construction is generally inconclusive and difficult to implement as a correction factor for the development of Project EVA vehicle structure.

In previous section on vehicle structure crashworthiness, the vehicle structure is generally divided into occupant safety cell and crash energy absorption structure, contributing in role of intrusion rigidity and deceleration control respectively. In order to achieve intrusion rigidity during crash, the structure must not fail under crash loads. As a method of simplification by converting dynamic crash loads to equivalent quasi-static crash load, derived in Section 3.1.4. A linear quasi-static approach with conservative interactive failure criteria such as Tsai-Wu or Tsai-Hill can be implemented when developing the occupant safety cell. Thick laminates generally have the tendency to exhibit progressive failure if the laminate comprises of quasi-isotropic layup. The quasi-isotropic layup allows redistribution of the stress to adjacent plies after first ply failure and does not fail catastrophically. This characteristic shows that it is acceptable to have 1 or 2 plies failure within the laminate under crash load conditions. Crash

loads are the peak load requirement of any passenger vehicle structure usually in the range of 20 to 30 times that of normal driving load, thus failure in the structure is less likely to occur if structure meet crash requirements. Crash load cases will be considered as a onetime event. Secondary post-crash impact will not be considered to simplify the development.

Designs for barely visible impact damage (BVID) have to be considered, the close proximity of the structure to road debris brings about possibility for BVID. BVID can cause significant reduction in static strength due to micro impact damage, these micro impact damage results in small delamination and matrix cracking at immediate composite surface reducing strength [87]. Protective covering will be developed at critical structure areas susceptible to damage to limit BVID.

### **3.1.9 EVA CFRP Structure Natural Frequency**

The importance of natural frequency is covered in Section 2.3.3. However due the vehicle structure first bending natural frequency can be approximated with the mass of the vehicle structure and stiffness, this calculation assumes the uniform mass distribution within the structure. The frequency of first mode is calculated similar to the simply supported beam model. For the frequency of the torsional vibration mode, it can be approximated by comparing torsional rigidity of a vehicle with similar final vehicle gross weight, the distribution of mass around the structure is very similar in all sedan vehicle type. Thus benchmarks comparisons can be made to estimate natural vibration frequency in torsional and bending modes which are in acceptable range with stiffness and weight of comparable passenger vehicles.

### **3.1.10 EVA Crash Energy Management Approach**

The metallic crash energy absorption structure for both front and rear will be designed to ensure that it could absorb the collision force in a controlled characteristic over a range of impact angles. The crash structure will have to provide the average crash reaction force identical to quasi-static load calculation obtained in previous section. Stability of axial crushing will be verified through FEA simulation and experimental test. Design of crush initiators have to be verified to ensure low initial peak force and crush initiation occurs at the crash front.

## **3.2 EVA Preliminary Packaging and Design Decisions**

Prototype vehicle structure may seem relatively easy to develop by designing a structure that has sufficient strength to house the main components. However unlike most concept vehicle projects, TUM-CREATE aims to develop a fully functional prototype that satisfy majority of ECE regulations. The level of integration incorporated in the design is unrivalled and comparable to concept vehicles developed by OEMs. The design of the structure is not limited to the vehicle structure requirements reviewed in the previous chapter. There are also considerations for viewing angles, size of A and B-pillars. A multitudes of design ideas were explored to enhance various system concepts, such as use of sandwich composite roof to

provide thermal insulation to reduce cabin cooling requirements, robust structural design that uses the battery pack structure as a crash load path. All to ensure the large 500kg 50 KWh battery is well protected in an unlikely event of a collision and as well as bonnet constructed out glass fibre composite to allow transmission of wireless communication signals. Addition to these requirements, manufacturing and assembly process have to be considered early in the design to ensure that the components can be manufactured and assembled together within tolerance. Waterproofing of the cabin, wire harness cabling and air conditional ducting in the roof and b-pillar are example of the things that affected development the structure. Access holes have to be designed to integrate various vehicle sub-systems. These holes act as a flaw in the structure have to be worked around unless a better solution was discovered or developed. These selected examples are some of the many multi-disciplinary compromises that have to be made at many areas of EVA structure during its development.

### **3.3 Groundwork for Composite Structure Development**

#### **3.3.1 Production Method and Material Selection**

Due to large scale of production, an industrial partner (Admiralty International) was engaged to manufacture the parts according to specification. After considering various manufacturing method based on size of parts, sandwich material, resin system, working time and industrial partner experience, vacuum assisted resin infusion (VARI) production method chosen.

Carbon fibre comes in many forms, different property, different weaves, number of axial layers and area weight. During the process of exploring material possibility, SGL Carbon agreed to sponsor raw carbon fibre material for the construction of the EVA. They offered two options, either 300gsm biaxial NCF (Non Crimped Fabric) (HPT 300 C45 0.3mm/ply) or 600gsm biaxial NCF (HPT 600 C45 0.6mm/ply). The 600gsm will require less physical layers thus is easier to manufacture but at the expense of limited number of more precise ply variations that a thinner ply will provide. The 300gsm biaxial NCF was selected on the basis for lightweight design as it allows greater ply variation and structural efficiency.

Vehicle climate operating limits were defined early in the concept. The vehicle structure has to handle tropical climate and humidity. Benchmark of various existing electric vehicles was conducted and suggests that 80 degrees Celsius is sufficient under tropical operating condition. Through business contacts, we manage to have SIKA as our sponsor for the infusion resin system. Operating temperature, glass transition temperature, working time and viscosity were the main criteria for selection as it is closely tied to the manufacturing process. CR120 epoxy resin system with CR120-3 hardener was chosen as provides up to 90 minutes of working time. This resin system has an upper limit of 120 degrees C and is designed specifically for vacuum infusion process. The high glass-transition temperature after post-curing cycle ensure the part will stay dimensionally stable and have consistent performance under tropical climate.

For structural adhesive, the selection criteria were mostly based on upper operating temperature limit and humidity similar to the selection of resin system. The selected structural adhesive is 3M DP490 two part epoxy.

A list of infusion grade foam core was evaluated and selection was based on shear strength and resin uptake. Airex T92.100 with SealX technology was selected based on its availability, price, density and most importantly resin uptake as thickness of foam core used in the vehicle will be thin and thus resin uptake can form a large percentage of the foam weight.

### 3.3.2 Material Property Testing

Material test defines the basic material failure and the ultimate strength enabling a design engineer to define proper construction at various parts or section of the vehicle. Material and components testing and experiments can be conducted at various hierarchy levels shown in Fig 3.12. Typically basic material information can be used for components development to sub-assemblies development. However, the performance of higher hierarchy level cannot be easily verified and physical experiments have to be carried out for verification and correlation with the design intent.

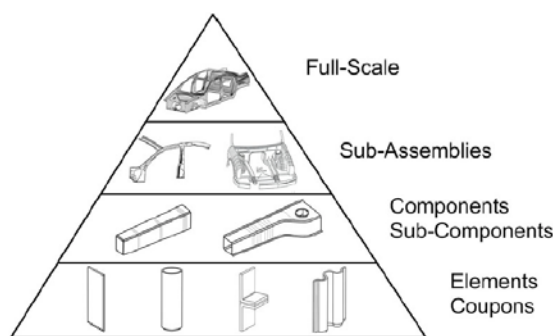


Fig 3.12 Structural components in complexity hierarchy levels [64]

The cost of conducting physical experiments at higher hierarchy levels will be significantly more than lower hierarchy levels. The developed methodology and computer simulations allow us to link basic material properties obtained from lower hierarchy level to the application at higher hierarchy levels. Similar to physical experiments higher hierarchy computer simulation requires higher computation cost. High cost refers to not just monetary terms but also time required. Computation simulation methods are well proven to cut down development time and cost.

#### 3.3.2.1 Property Test for CFRP and Structural Adhesive

There are various forms of material tests, depending on application requirements such as tensile test, compression test, fatigue test, quasi static compressive test, and many more. Handbooks on material testing are available for selecting the standardized test procedures [88]. However standardization of test to classify dynamic failure of composite is still undefined [88].

Physical experiment coupon test is needed because the manufacturing process can introduce defects that affect mechanical properties through fibre misalignment, fibre matrix adhesion, porosity/voids when compared to the perfect material sample. Changes in manufacturing parameters such as temperature, working time, part size, part thickness and vacuum pressure can also drastically affect the quality of the component. Appendix B shows the dimension of the standard test coupon specification planned for tensile laminate strength and adhesive shear test of structural adhesive respectively. The results of these tests will be used as material input data for FEA material model. Table 3.4 shows the test programme that was carried out. The details mechanical test set up are documented by Schwingenschlögl [89].

Table 3.4 An example of a composite mechanical and chemical property test programme [89]

Mechanical Testing					
Material Type	Material Properties	Test Standard	Test Environment	Number of Specimen	Test Configuration
Carbon Laminate : SGL Krumpers HPT 300 C45 (+/-45°) infused with SIKABiresin CR120 Resin System	$E_{it}, \sigma_{it}, \varepsilon_{it}, \mu_{it}$ where $i$ is 1 or 2 fibre direction (Tensile)	EN ISO 527-4	Room Temp	12	RTA
			Hot Wet	12	HWA
	$E_{ic}, \sigma_{ic}, \varepsilon_{ic}, \mu_{ic}$ where $i$ is 1 or 2 fibre direction (Compressive)	EN ISO 14126	Room Temp	12	RTB
			Hot Wet	12	HWB
	$G_{12}, \tau_{12}, \gamma_{12}$	EN ISO 14129	Room Temp	10	RTC
			Hot Wet	10	HWC
Adhesive : 3M Scotch-Weld DP 490 epoxy	$E_m, \sigma_m, \varepsilon_m, \mu_m$	EN ISO 527-2	Room Temp	10	RTD
			Hot Wet	10	HWD
	$G_m, \tau_m, \gamma_m$	EN ISO 14869-2	Room Temp	10	RTE
			Hot Wet	10	HWE

Chemical Testing				
Material Type	Material Properties	Test Standard	Number of Specimen	Comment
FRP	$\phi_f, \phi_v$	DIN EN 2564	9	3 test specimen per plate shall be taken from plates manufactured for RTA, RTB, RTC
FRP	Degree of cure, $T_g$	DIN EN ISO 11357-1 DIN EN ISO 11357-2	9	3 test specimen per plate shall be taken from plates manufactured for RTA, RTB, RTC

The results of the test programme provides the modulus of elasticity, maximum tensile strength, maximum compressive strength, shear stiffness, shear strength and also other properties including density, fibre volume fraction and porosity. To ensure the reliability of the structure in all operating conditions, hot/wet test variant was also conducted. These tests expose coupons to high temperature and moisture prior to mechanical test to ensure the resin and adhesive selection perform adequately in these conditions. High temperature of 70 degrees celsius and high humidity was chosen to depict the tropical condition the vehicle will undergo when carbon structure is exposed to rain and direct sun. The test was conducted externally by an institute in Stuttgart as resources for testing in Singapore does not adhere to tight timeline requirements. The mechanical property obtained from the tests is shown in the Table 3.5 after conversion from NCF test data which were later used in FEA simulation.

Table 3.5 (Top) Equivalent Tape (Lamina) property for FEA simulation and (Bottom) 3M DP490 adhesive performance [89].

Equivalent Uni-direction Layer		Room Temperature	Hot Wet
Young's Modulus in 11-direction, Tensile	$E_{11t}$	114.8 GPa	115.5 GPa
Young's Modulus in 22-direction, Tensile	$E_{22t}$	8.5 GPa	7.0 GPa
Strength in 11-direction, Tensile	$S_{11t}$	1325.7 MPa	1275.0 MPa
Strength in 22-direction, Tensile	$S_{22t}$	38.3 MPa	31.5 MPa
Young's Modulus in 11-direction, Compressive	$E_{11c}$	113.9 GPa	113.8 GPa
Young's Modulus in 22-direction, Compressive	$E_{22c}$	8.5 GPa	7.0 GPa
Strength in 11-direction, Compressive	$S_{11c}$	547.5 MPa	293.5 MPa
Strength in 22-direction, Compressive	$S_{22c}$	191.3 MPa	157.5 MPa
Shear Modulus	$G_{12}$	4.0 GPa	2.3 GPa
Shear Strength	$S_{12}$	59.9 MPa	29.6 MPa
Adhesive			
Young's Modulus	$E_m$	2254.0 MPa	628.3 MPa
Strength	$S$	27.6 MPa	1.4 MPa
Shear Modulus	$G$	625.3 MPa	127.0 MPa
Shear Strength	$\tau$	21.0 MPa	8.0 MPa

Table 3.6 Fibre Volume and Porosity Content [89].

Specimen No.	Fibre Volume $\phi_f$ (%)	Mean (%)	Standard Deviation	Porosity (%)
RTA/HWA – V1-1	49.93	50.71	2.17	9.63
V1-2	49.04			9.65
V1-3	53.16			9.63
V2-1	52.13	51.99	1.35	10.30
V2-2	53.27			7.61
V2-3	50.58			10.09
V3-1	51.92	50.20	1.79	9.56
V3-2	50.33			8.95
V3-3	48.35			8.88
RTC/HWC – V4-1	52.79	52.43	1.26	6.75
V4-2	53.47			8.33
V4-3	51.02			7.18
V5-1	51.72	53.16	1.37	6.74
V5-2	53.32			7.23
V5-3	54.44			7.65
V6-1	53.30	52.11	1.21	6.81
V6-2	52.12			7.39
V6-3	50.89			7.05
V7-1	52.06	51.28	0.79	7.15
V7-2	51.31			6.66
V7-3	50.47			7.05
V8-1	50.18	50.42	0.84	9.00
V8-2	51.36			8.50
V8-3	49.73			9.86
V9-1	50.14	50.34	0.99	8.16
V9-2	49.46			9.11
V9-3	51.42			8.07

From the material test and result, the hot wet conditions have little impact on the stiffness of the coupons. The uneven flatness of the test coupon and the manufacturing error resulting in asymmetric layup in test coupon resulted in lower than expected compression loading strength for fibre direction as numerous compression specimens were invalidated from excessive bending of 0.1 to 0.25 where suggested maximum is 0.1. This asymmetric property was caused by fabrication of the coupon on a flat glass surface, the coupon surface on the vacuum bag side showed unevenness while the coupon surface on the glass side have a very smooth surface. Typical in vacuum infusion process, expected porosity is higher than prepreg, porosity in the region of 2-5% is considered suitable for aircraft grade. However in the specimens test, the porosity is much higher than 2-5%. This porosity decreases the strength of the lamina that relies on matrix strength such as that the compressive strength was lower than expected. According to Birt, [90] every percent increase of porosity decreases interlaminar strength by 7%. The porosity problem was eventually reduced when the dwell vacuum pressure after infusion was decreased and resin degassed prior to infusion. The moisture content and heat were also observed to have significant effect on the shear modulus and strength of the carbon composite. The material property for hot-wet condition is used except for compression



strength in the 11 direction where room temperature is used as the porosity issue is resolved with decrease in vacuum pressure after infusion mentioned before.

The shear strength of adhesive (3M DP490) in Table 3.5 (bottom) given by the manufacturer according to DIN 53283 was 24 MPa if cured for 2h at 65°C and tested at room temperature. The value obtained from testing (DIN EN14869-2) was 21 MPa. The major difference between the tests was the thickness of the bond line. Standard adhesive test uses thickness varying from 0.05 to 0.15mm. The thickness for our test was approximately 1.0mm (the estimate thickness of adhesive in final assembly after inclusion of manufacturing tolerances) further more DIN EN 14869-2 uses stiff adherents which resulted in a much higher peel loads which leads to a reduction in shear strength.



Fig 3.13 (Top) Chemical and mechanical test coupons, (left and bottom right) resin vacuum infusion resin flow test for sandwich structure (bottom left) adhesive test coupon showing failure at the bond surface.

To ensure manufacturability, we have also conducted infusion test as shown in the figure above. We compared a mixture of resin channel designs on the foam core and their effective infusion distance along with placement of peel ply and flow medium. As a result our industrial partner can accurately plan for sufficient resin feed lines to ensure through infusion throughout the part. Fig 3.13 shows the test coupons, the adhesive test coupons and the infusion test.

### 3.3.3 Composite Joining Methods and Adhesive

Most modern composite monocoque are structurally joined together by interlocking panels, typically monocoque structures are made of a number of smaller composite structural panels and are structurally attached together either by adhesive, fasteners or secondary bonding as shown in the exploded view of EVA in Fig 3.14. The strength and durability of these joints are therefore very important. A poorly designed structure connection can be the point of failure. Surface preparation is exceptionally important in adhesive joints and contamination of bond surface will affect bonding strength. Adhesive is strongest when it is loaded in shear but becomes significantly weaker when subjected to peel stress loading. Composite adhesive joints for aerospace applications have been extensively researched by Hart-smith and a few others, topics on mechanics of peel stress are covered quite extensively in literature which was used as reference during the development phase such as Fig 3.15.

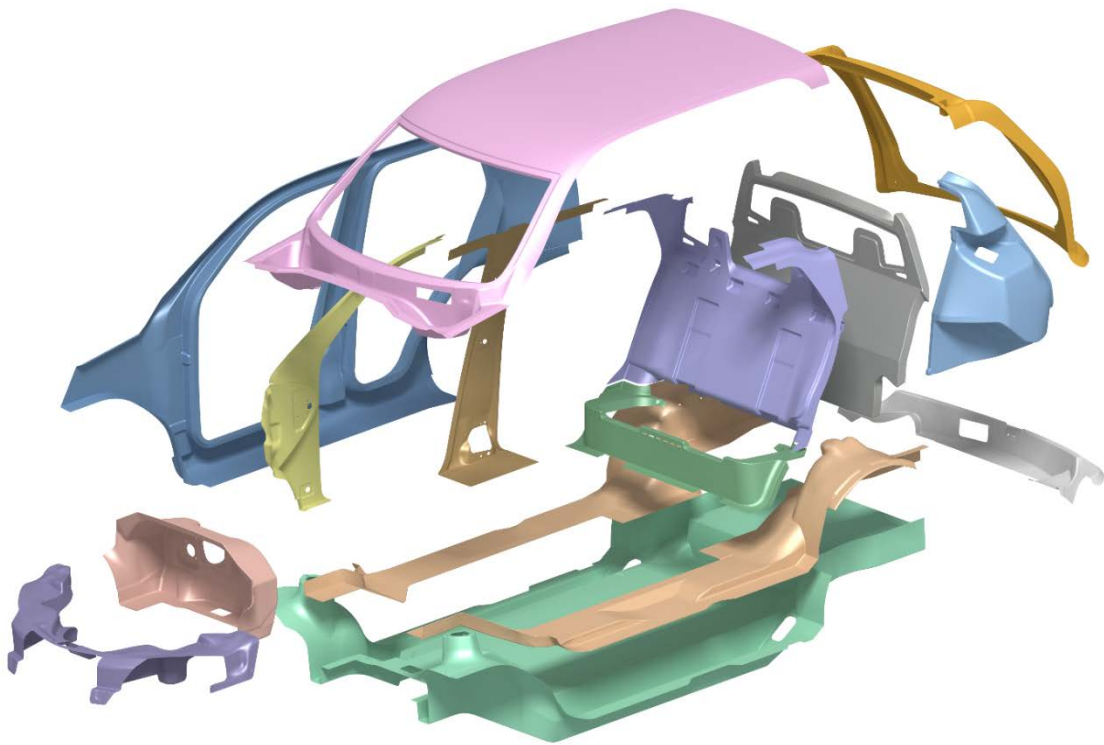


Fig 3.14 Explosion view of the major composite panels that makes up EVA's monocoque structure.

The design of the structure are constructed is a way that when adhesive failed under crash loads the panels will interlock with other panels preventing them from getting dislodged. Adhesive joints in the vehicle are designed with the best ability (while conforming to manufacturability and assembly requirements) to be loaded either in compression or shear. Simulation of peel stress does not make sense as the process of assembly and joining of vehicle structure panels do not allow any control of the gluing edge and the homogeneity of adhesive bond surface cannot be achieved. Thus the idealized FEA simulation will not correlate with the actual component. To ensure adhesive bond strength, conservative FEA simulation will be carried out. To simplify the simulation, adhesive will be considered as

isotropic material and considered to fail if stresses exceed von-mises stress criteria. The interlocking design will serve as a safeguard if adhesive fails under crash impact.

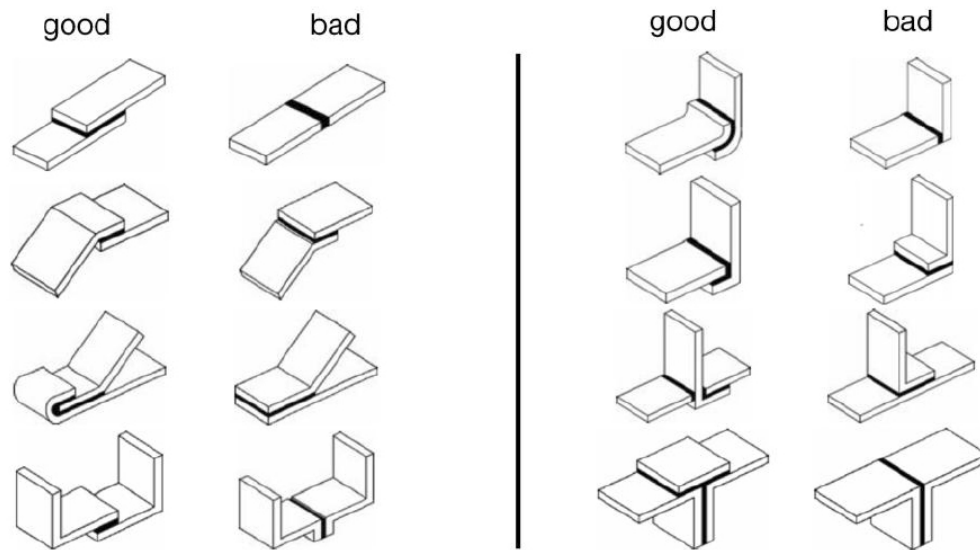


Fig 3.15 Examples of good and bad adhesive joining methods [55]

### 3.3.4 Manufacturing Control

Consideration for manufacturing process and tolerance is extremely important during the development phase. It ensures that the intended manufacturing process will meet the required desired quality and tolerances. For composite, a large variety of factors affects the component quality such as accuracy of hand layup preforms on large geometric complex parts shown in Fig 3.14. Ensuring fibre orientation accuracy for complex shapes can be very challenging. Furthermore the limited size of [0,90] ply shown in Fig 3.16 further complications production. Subsequently the actual orientation layup of the laminate can differ quite significantly from computation model. Other factors such as matrix shrinkage and residual stresses from unbalance plies can affect the part's final geometrical accuracy. These factors are studied and reduced in the design processes. Some components have to be fabricated separately as two different parts to increase production efficiency or reduce cost. In the next section, are some of the constraints employed to increase and control manufacturing quality.

#### 3.3.4.1 Layup and Manufacturing Constraints

SGL Kumpers carbon fibres HPT 300 C45 comes in  $\pm 45^\circ$  biaxials. To ensure ease of layup we will limit angles only to either [0/90], [90/0], [+45/-45], [-45/+45] to reduce complexity. The coordinate systems are aligned towards the vehicle global coordinate unless explicitly stated. Due to the difficulty to hand lay multiple dry fibres plies on geometric complex molds, it is decided that a laminate with maximum of 16 plies will be enforced. If 16 plies (4.8mm) prove insufficient strength, it suggests that the section that failed is geometrically inefficient and the geometric load path should be revised. This aims to reduce excessive material use and increase the efficiency of the vehicle structure. Wearing gloves when handling carbon fibre

prevents contamination of the fibre with organic oils and also prevents skin irritation caused by carbon fibre embedded in the skin. Folding of carbon fibre should be avoided as folding of pre-cut carbon fibre fabric results in fibre breakage. The size of layup should not be too small as placement of these dry fibre plies is difficult and coupling small size with quantity would be difficult to ensure the small plies stay in the correct orientation and position.

- Limited to either 0, 90, +45, -45 layup orientation
- Maximum number of piles is limited to 16 (4.8mm)
- Wear gloves when handling raw materials
- Do not fold carbon fibre fabric
- Minimum layup ply size

### 3.3.4.2 Plies Overlap and Drop Off

Hart smith made numerous research on required adhesive bond length to ensure failure falls outside of the adhesive joints in [61] [60] [91] [59]. He suggested that a good bond length would be 50 to 80 times that of thickness and drop off gradient of 1 in 50. Fig 3.17 shows how ply should be distributed to avoid excessive thickness and enhance load distribution within the overlap region. SGL HPT 300 C45 comes in rolls of 1260mm width in 50m length. Thus to form large plies on large components several small pieces of fabric have to be used as the biggest [0,90] or [90,0] ply that could be formed out of the [+45/-45] roll is approximately only 800mm by 800mm shown in Fig 3.16. Many of these [0,90] or [90,0] required to have a ply overlap to ensure the defined ply is performing as a single piece.

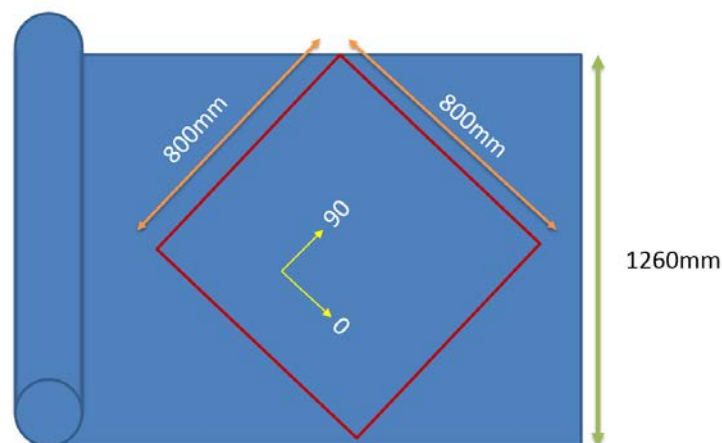


Fig 3.16 Illustration the largest [0,90] ply that could be obtained from a [-45/+45] roll.

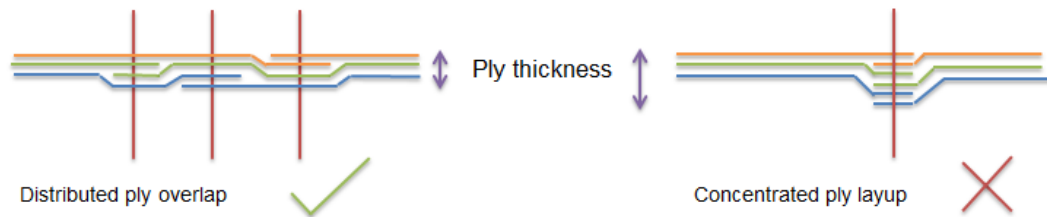


Fig 3.17 Distributed ply overlap to reduce excessive thickness and enhance strength

Using 50-80 times thickness rule Hart-Smith suggested, we can calculate the recommended overlap of 24mm between each ply with each ply is 0.3mm in thickness. However to make up for hand layup inaccuracy and overlapping plies the overlap is increase to 40mm as shown in Fig 3.18 to be on the conservative side. Staggering ply drop off with a gradient of 1 in 50 is enforced to reduce drastic changes in bending stiffness/strength along the laminate.

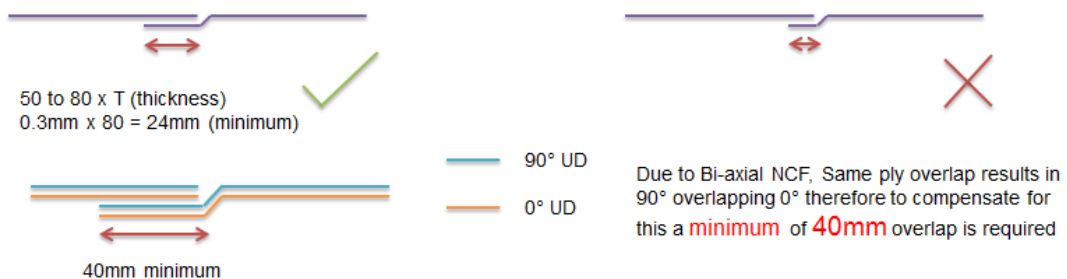


Fig 3.18 Amount of recommended overlap

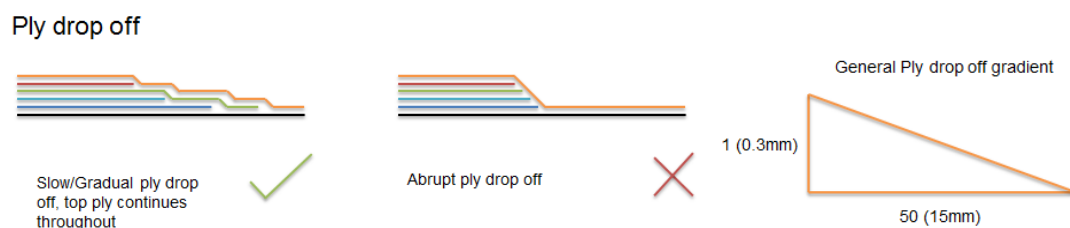


Fig 3.19 Staggering ply drop off.

### 3.4 Concluding Remark

This chapter defines many of the important parameters prior to the next step of detailed structure development of EVA's carbon monocoque structure. First, with the photogrammetry analysis, derived the equivalent quasi-static crash loads that the vehicle structure have to withstand in front and side impact. Next we looked into the state of the art use of composite in passenger vehicles, in literature CFRP is a superior material to absorb crash energy due to the high SEA figures. CFRP crash energy absorption structure can be several times lighter than that of aluminum or steel, however the complexity of failure and CAE development

limitations makes validating of design difficult and expensive. Coupled with the stability requirement in absorbing crash energy from varying angle of impact, it would require a large design space to fit in a crash structure with sufficient high CCR. These two factors are the main limiting factors restricting the proliferation of carbon composite crash structure in the automotive industry. Next, discussion on the suitable simplified failure criteria for EVA's CFRP structure and the subsequent impact on other vehicle structure performance indicators such as natural frequency and residual strength from BVID. Followed by a section giving an example of how the design aims and system integration can compromise the efficient design of vehicle structure members, this has to be accounted for as much as possible in the early stage of design.

Another focus of Chapter 3 was to provide the groundwork for composite structure development, firstly in the area of material selection for carbon fibre fabric and adhesive. Secondly, was the manufacturing and assembly constraints, simplified approaches and guidelines adopted to ensure simplicity of production and subsequently, the quality of the composite parts for assembly. The production methods and parameters were defined, mechanical and chemical test experiments to obtain material properties for CAE development were established and infusion test pieces were conducted to better understand infusion performance.

In the next chapter, we will move on to the next phase of detailed development of EVA's vehicle structure, the workflow of CAE development of both the vehicle structure and aluminium crash energy absorbing structure from geometric design to FEA validation and subsequently the different design phases employed for concurrent engineering development.





## Chapter 4: Development of EVA Vehicle Structure

In this chapter, the detailed development steps and process will focus on covering structural challenges. Solutions to these development challenges will be explained in detail. Considerations and factors that requires detailed attention to satisfy the vehicle structure requirements with development of new prototype such as EVA will be discussed. The development methodology will focus on using FEA simulations as it allows more accurate verification of complex geometry and large structures and lastly the result of the development.

Many of the solutions are not scientifically optimal as a multi-disciplinary problem often does not have optimal solutions or can have multiple solutions. Commercial FEA program such as ABAQUS CAE was used allowing quick pre-processor and post-processing operations while including composite failure criteria such as Tsai-Hill and Tsai-Wu. ABAQUS allow the verification on failure criteria on each lamina ply with principal stresses, stresses in fibre direction and many other parameters. Fig 4.1 shows main development areas of the EVA electric taxi project. The author responsibility is in structure and aerodynamics, but due to the low average speed of the taxi in city, aerodynamics became a low development priority which is superseded by exterior design language.

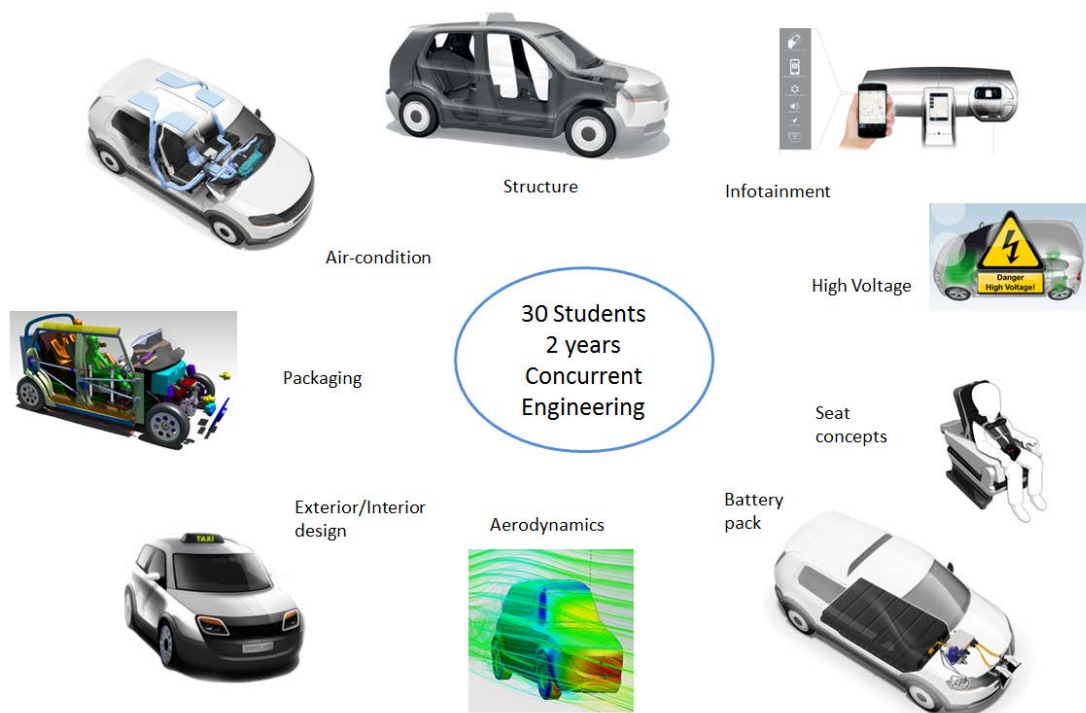


Fig 4.1 Main development topics for EVA electric taxi project.



## 4.1 FEA Simulation Definition of the Materials and Modelling Assumptions

FEA simulation allows the evaluation of elastic structures under load and the defined material test program are conducted concurrently when development work on vehicle structure was commenced. In order to proceed with the initial simulation, rules of mixture (ROM) method was used to calculate the approximate elastic modulus of equivalent uni-directional tape. Initial failure criteria was based on conservative 0.4% maximum strain, this criteria was suggested by an airbus composite engineer as an industrial de facto practice which give an good approximation of the laminate requirements when exact mechanical performance of the composite is not available during the first rough concept and sizing. This 0.4% maximum strain criteria was compared with Tsai-Wu and Tsai-hill criteria when the results of the experimental coupon test established in Section 3.3.2 was received, the comparison shows very good correlation with very minor differences. It offers enough accuracy to highlight structural design weaknesses.

ABAQUS CAE software was chosen for finite element modelling of the vehicle structure. It was chosen due the capabilities of simulating both implicit and explicit simulations without requiring to rebuild the vehicle FEA model. ABAQUS features advance material property model definition and is extremely versatile definition of complex simulation conditions and scenarios. The capabilities of the ABAQUS CAE allow quick verification of the vehicle structure performance requirement. Complimenting ABAQUS CAE, CATIA V5R19 is used to manage the package and for use for creating geometric CAD data.

Simulation load cases for the vehicle structure was defined earlier in Section 3.1.4 on through quasi-static crash load assumption of dynamic crash loads. These loads will be absorbed by the vehicle's crash energy absorption structure. Thus the crash loads are applied to the carbon structure connecting to the crash structure to simulate crash load on the carbon structure. Static implicit simulation will be carried out for development of the composite vehicle structure and dynamic explicit simulation will be carried out for the development of the aluminium crash structure.

### 4.1.1 Fast Layup Changes with Shell Laminate Model

The development of the vehicle structure requires the ease to change composite ply layup, including modification to overlaps and plies definition due to structure revision and updated design boundaries. Thus shell base composite model is chosen so that geometrical data need not be revised when a change of layup thickness was carried out, speeding up modification implementation on the fly. The shell base model will be based on 2D FEA elements which are easier to obtain quality mesh and less likely to have highly distorted elements. 3D elements with low thickness require large element counts to have sufficient accuracy. Mesh sensitivity test was carried out to ensure that mesh size selected does not affect the accuracy of results obtained from the simulation. The ideal mesh size with minimal computation time increase was set at 5-10mm global size.

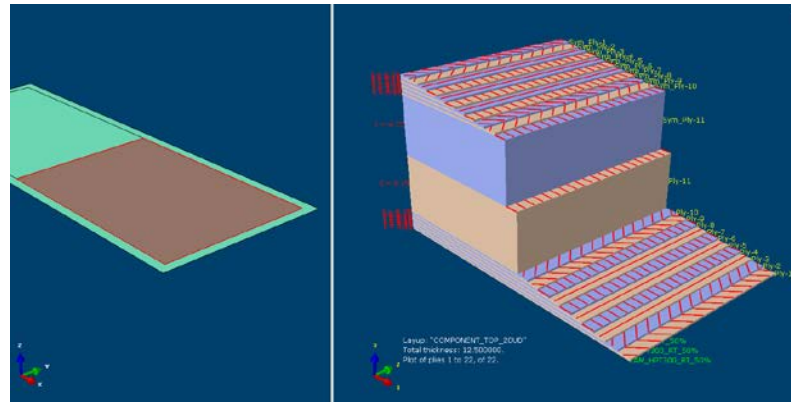


Fig 4.2 Ply stack plot of composite shell

#### 4.1.2 Static Simulation of Dynamic Loading using Inertia Relief

Vehicle crash test occurs within a short duration, the forces generated from the sudden deceleration are results of the structure's resistance to stop due to inertia. The load of crash depends on the inertia of the vehicle including all the components structurally connected which includes occupants in their restraints. Crash loading cannot be accurately simulated with fixed supports boundary condition required in static analysis on opposing ends of the structure shown in Fig 4.3 (left). By fixing the boundary condition at the rear crash structure, crash load path will go through the structure to the fixed boundary condition. In a real crash, vehicle is unconstrained and driven by inertia impact. In order to simulate crash condition we have to employ inertia relief method which is available in ABAQUS.

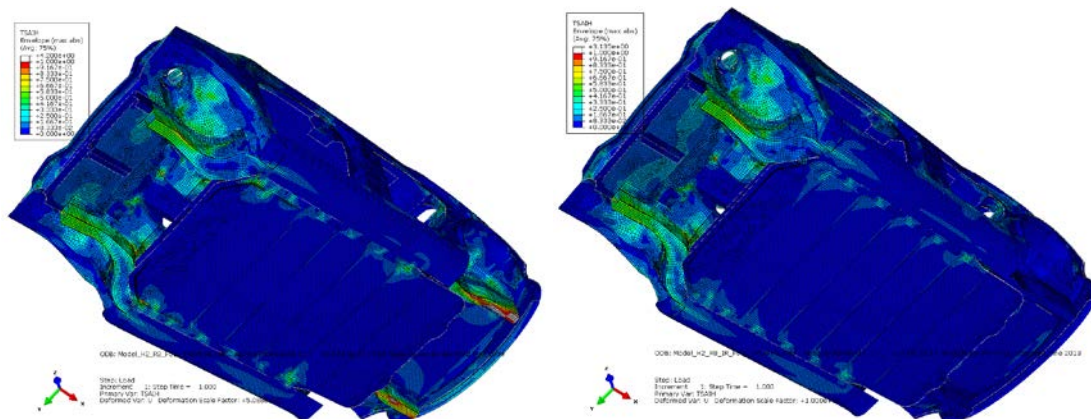


Fig 4.3 (Left) Quasi-static full width frontal crash simulation without inertia relief with fixed support at the rear crash structure (Right) Quasi-static full width frontal crash simulation with inertia relief showing realistic static equivalent of dynamic frontal crash showing low loading in rear crash structure.

Inertia relief is an advanced option in ABAQUS that allows simulation of unconstrained structure in static analysis mode. The basic working principle of how inertia relief work is that the inertia (mass) of the structure is used to resist the applied loadings, that is, an assumption is made that the structure is in a state of static equilibrium even though it is not constrained.

During the convergence calculation for static loading with inertia relief, ABAQUS calculates the forces that result from the mass of each elements and the resulting acceleration is balanced the applied loading conditions and reference frame which replicates dynamic scenario in static loading simulation condition. Fig 4.3 (right) shows the FEA simulation result of full width frontal collision using inertia relief method.

### 4.1.3 Clean-up of CAD Geometry, Meshing and Ply Layup Definitions

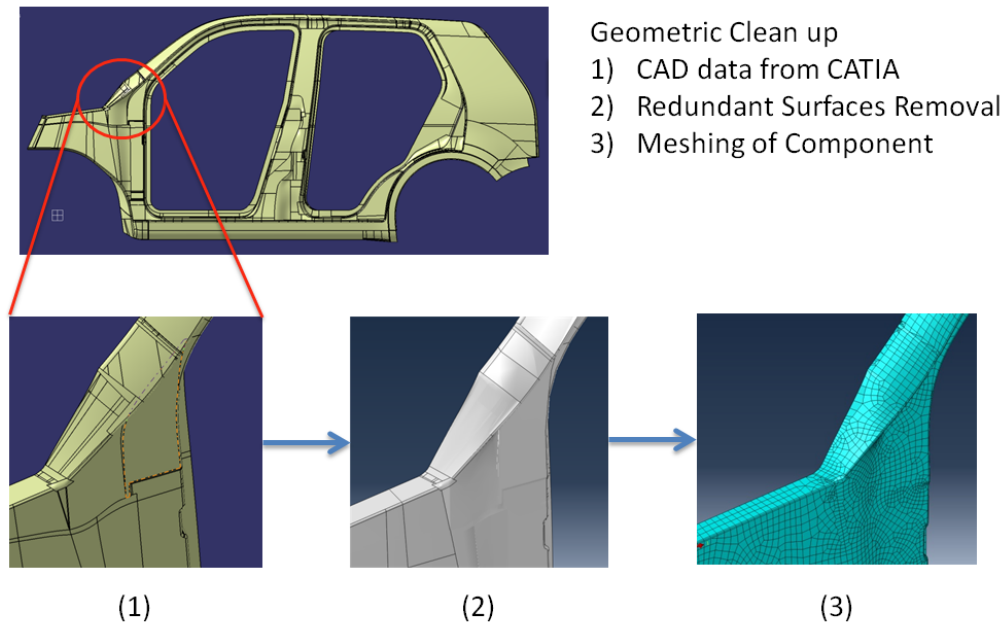


Fig 4.4 Procedure of geometric surface clean up to element generation. In step 2 division or partition line can be drawn to define area of different ply layup or control the characteristic of meshing.

Vehicle structure panels CAD geometric data was created in CATIA V5R19 in order to ensure that it fits within the allocated design space in the package before being imported into ABAQUS CAE for pre-processing setup of the FEA model. The meshing engine in ABAQUS uses geometric division lines within the CAD data to define the mesh generation of elements. The complex surface construction of structural panels and surface offset operations in CATIA V5R19, which generated many small surfaces as shown in Fig 4.4. These small surfaces have to be removed to reduce influence in meshing. Adding on to the difficulty, it was found out during the middle of development that the geometric engine in ABAQUS was not directly compatible from the geometric engine used in CATIA V5R19. Thus during import of geometric CAD data into ABAQUS, panels with compound curvature and many small surfaces are easily affected by ABAQUS geometric translation algorithms and translation between geometric engines often results in geometric errors and imprecise geometries. A large amount of work have to be performed to clean up these geometric errors and inaccuracy using tools provided in ABAQUS. However these tools have limited capability and often struggle to achieve desire outcome. Very often there are some geometric imperfections, which cannot be

corrected and subsequently affects the generation of mesh. The final step to overcoming this problem, meshing tools in ABAQUS was used manually to rectify these erroneous meshes.

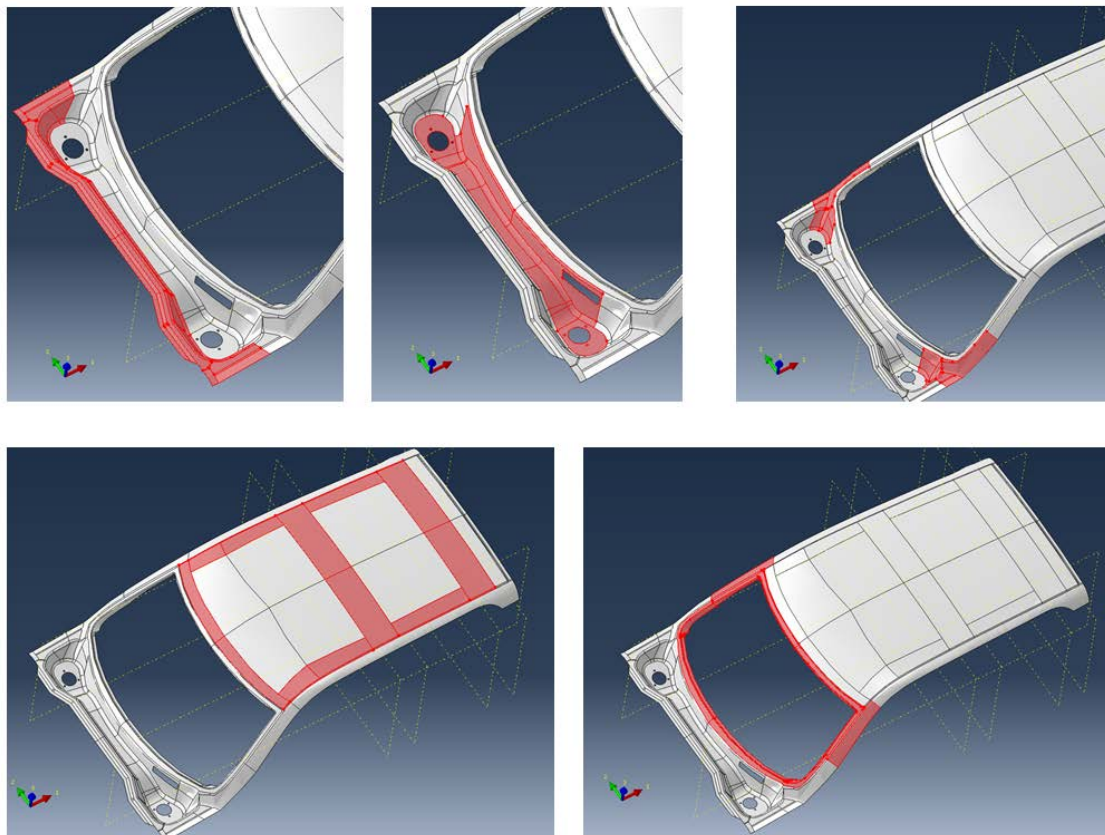


Fig 4.5 An Example of the definition of different ply layup zone in ABAQUS of the windscreen roof structure

RB_CORNER 16UD	RB_CORE 16UD	RB_FLANGE 16UD	RB_WHL_CORNER 24UD	RB_FLANGE_LOW 24UD	RB_CORE_MID 24UD
0	0	0	0	0	0
90	90	90	90	90	90
			0	0	0
			90	90	90
45	45	45	45	45	45
-45	-45	-45	-45	-45	-45
0	0	0	0	0	0
90	90	90	90	90	90
			45	45	45
			-45	-45	-45
45	45	45	45	45	45
-45	-45	-45	-45	-45	-45
	CORE				CORE
-45	-45	-45	-45	-45	-45
45	45	45	45	45	45
			-45	-45	-45
			45	45	45
90	90	90	90	90	90
0	0	0	0	0	0
-45	-45	-45	-45	-45	-45
45	45	45	45	45	45
			90	90	90
			0	0	0
90	90	90	90	90	90
0	0	0	0	0	0
Mold Side	Mold Side	Mold Side	Mold Side	Mold Side	Mold Side

Fig 4.6 Example of the ply book which defines layup in each assigned zone.

Geometric surfaces were used to define the composite ply layup as shown in Fig 4.5 the division lines and partitioning lines provide the means of defining different ply layup. Partitioning lines on the surface of the panels were created by partition function in ABAQUS allowing definition of ply layup including change the ply layup, ply drop off and overlap during the laminate development phase.

Fig 4.6 shows an example of the plybook given to the manufacturer for composite panel production and Fig 4.5 shows the different zones with different ply layup. Fig 4.7 shows how discrete coordinate is used to define the layup direction within the panel, the layup direction is defined to ensure the least possible issue with draping without going into detail of draping simulation.

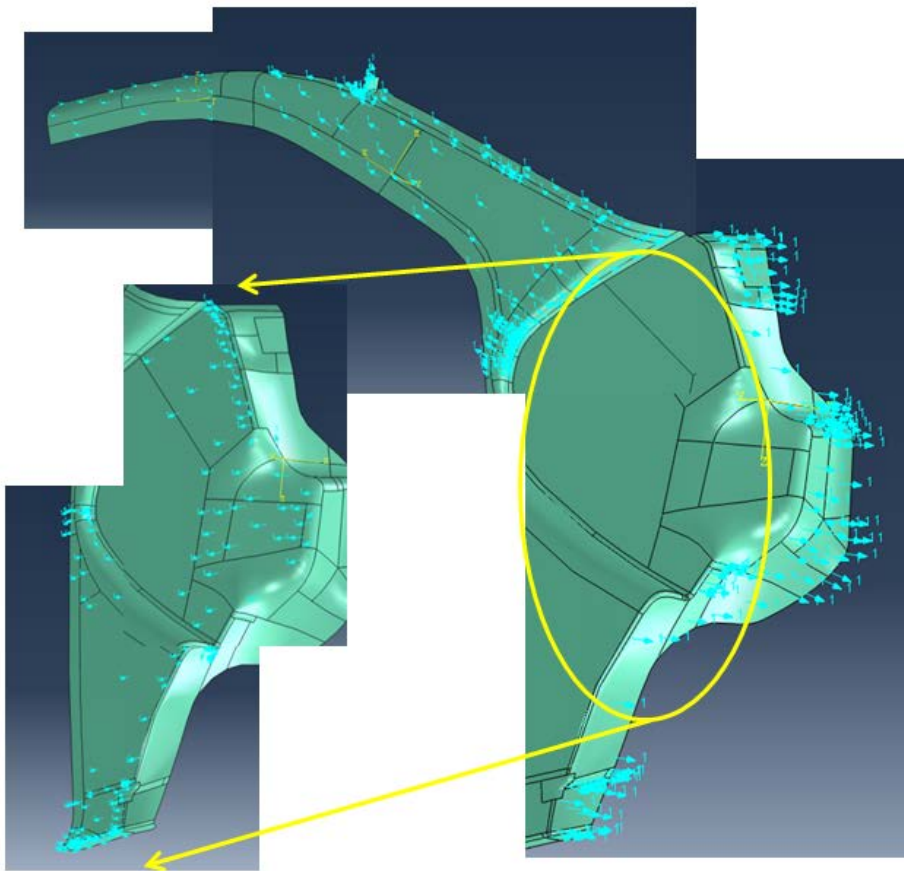


Fig 4.7 The use of discrete coordinates to define layup direction in various region

The division and partition lines also serve as one of the most effective methods to control meshing quality. Mesh size plays a significant role in obtaining required accuracy or resolution and good mesh quality can speed up of convergence of the FEA simulation. The quality of mesh are affected by the element distortion to fit the require geometry constraints, large distortion skews the element excessively and causes mathematical inaccuracy within the element. Multiple literatures are available for reference that discusses methods to ensure mesh



quality. In order to reduce computation cost, quad dominated meshing elements are used for meshing the surfaces, triangular element are used only to allow conformity and reduce distortion in quad mesh. ABAQUS offers meshing tools that is able to check quality of mesh, which are used to ensure that distorted elements do not form more than 2% of the mesh. Ideal mesh quality are often difficult to achieve due to the geometric imperfection inherited from geometric data imported into ABAQUS mentioned earlier.

#### 4.1.4 Constraints Conditions and Assumptions in FEA Model

The composite vehicle structure is formed by structurally joining together a number of carbon composite panels shown in Fig 3.14. Majority of the structure components are adhere together by structural adhesive. Adhesive has a lower young modulus compared to carbon fibre composite panel. When the structured is loaded, the adhesive and carbon composite panels can deform, this changes the stress distribution in composite panel. Thus the connections and constraints between these panels have to be defined in ABAQUS so that the vehicle structure load path can be simulated accurately. The FEA construction method shown in Fig 4.8 was used to simulate the effect of adhesive within the vehicle structure. The thickness of the adhesive is defined at 1mm due to manufacturing and assembly tolerances. The adhered surfaced is tied to the adhesive adhered surface. The tie condition assumes both adhesive and carbon composite panel are connected perfectly and will never come apart. This FEA modelling technique allows the simulation of actual stress distribution between carbon composite panels and adhesive, the stress within the adhesive can be analysed to determine if the adhesive will fail under the applied load.

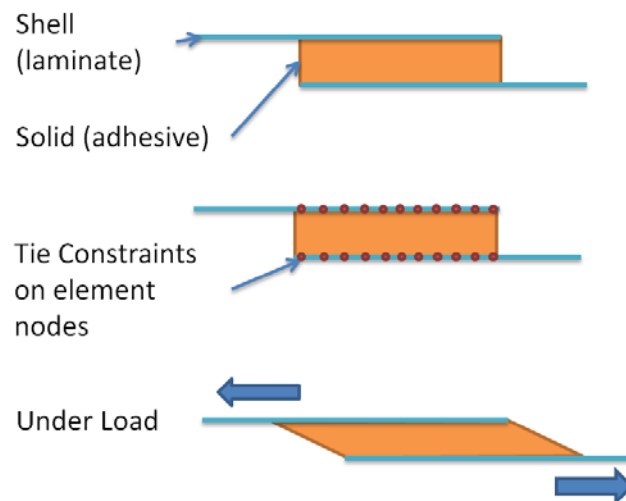


Fig 4.8 (Top) Cross-section illustration of a laminated joint (Middle) Tie constraints on laminate nodes to adhesive nodes (Bottom) The exaggerated shearing deformation shown under joint loading.

Table 4.1 Elements, nodes and element type for H0, H1 and H2 simulation development model.

	Elements	Nodes	S4R	S3	C3D8R	C3D6	C3D10
Model H0	350266	598393	93650	234	185619	1196	39585
Model H1	828291	1353656	249219	5024	184110	2865	387073
Model H2	348592	346489	331041	15448	0	0	0

In the next few sections, more details will be covered for the following 3 simulation model development steps in Section 4.1.6.

Table 4.1 shows the number of elements, nodes and ABAQUS element type used for each model. Elements are sized at globally at 5mm with adaptive localized mesh sizing to fit complex geometry shape. The following list the type of elements.

- S4R – Stress/displacement element, 4-node general-purpose shell, reduced integration with hourglass control, finite membrane strains.
- S3 – Stress/displacement element, 3-node triangular general-purpose shell, finite membrane strains.
- C3D8R – Continuum stress/displacement, 8-node 3 dimensional quadrilateral element with reduced integration.
- C3D6 – Continuum stress/displacement, 6-node 3 dimensional wedge element.
- C3D10 – Continuum stress/displacement. 10-node 3 dimensional tetrahedral element.

Elements generated were analysed for quality with ABAQUS inbuilt mesh analysis tool. Every composite panel has manual mesh control to ensure that the number of excessive skewed elements was kept below 2%. Due to the large complex geometric construction of the part, meshing a model free of skewed elements nearly impossible. Furthermore removing the minute percentage of skewed elements have little improvement to overall simulation result and requires a huge time investment which slows down development. Thus to increase the simulation iteration rate, mesh quality was improved till an acceptable level. To reduce computation cost, shell quad dominated meshing technique was used, in geometric complex sharp corners S3 (shell triangular) element compliments S4R elements to provide better geometric conformity. The complexity of meshing can be seen from the number of S3 elements, as the model develops from H0 to H2 final model the complexity of the geometry increases resulting a large increase in S3 elements. The number of S4R (shell quad) increased with development due to increased number of composite parts.

Due to the time constraints and the limited resources to create solid adhesive elements for the Model H2. The adhesive section was not analysed which explains why the continuum element counts in Model H2 is zero, this decision was made as size of adhesive area is very identical to Model H1 and in Model H1 adhesive simulation results indicates a large safety factor. Furthermore, there are geometric improvement in the structure that loads more adhesive joint in shear. Decreasing the reliance on the adhesive strength, the composite parts in the structure are to be designed to interlock. Thus, in case of adhesive failure the interlocking panels will be wedged into each other, thereby preventing the structure from separation particularly in critical loading conditions. Thus we were very confident in the design of adhesive joints.

### 4.1.5 Load Application in FEA Model

A combination of loading methods are used. For frontal crash loads that goes through the aluminium crash structure, loads are applied in the in-plane direction shown in Fig 4.10 (left). The line loading condition in ABAQUS was used. The outline of the crash structure edge is selected and perimeter calculated and load is applied with reference to global positioning factor. Fig 4.9 and Fig 4.10 shows example of such FEA loading constraints. For large section loading, pressure loading condition in ABAQUS was used as shown in Fig 4.10 (right).

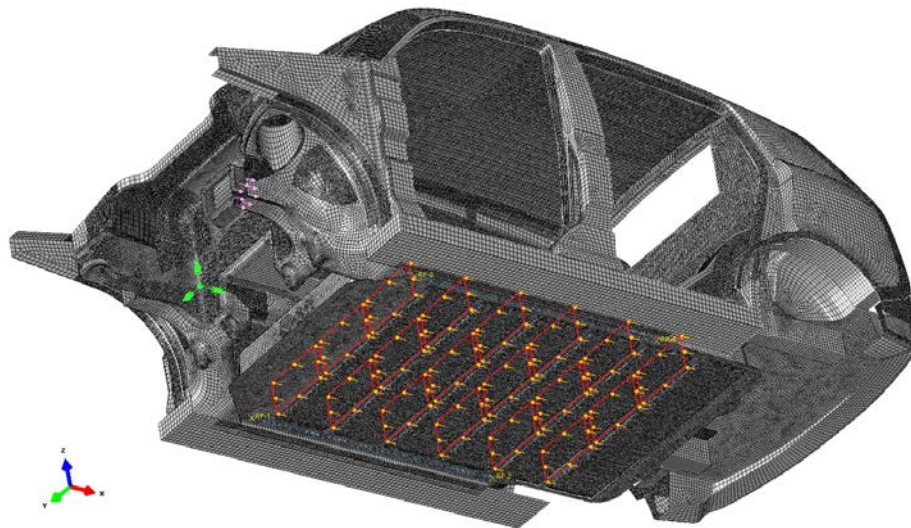


Fig 4.9 The inertia load exerted by the battery cells during frontal offset crash scenario defined using pressure loading condition.

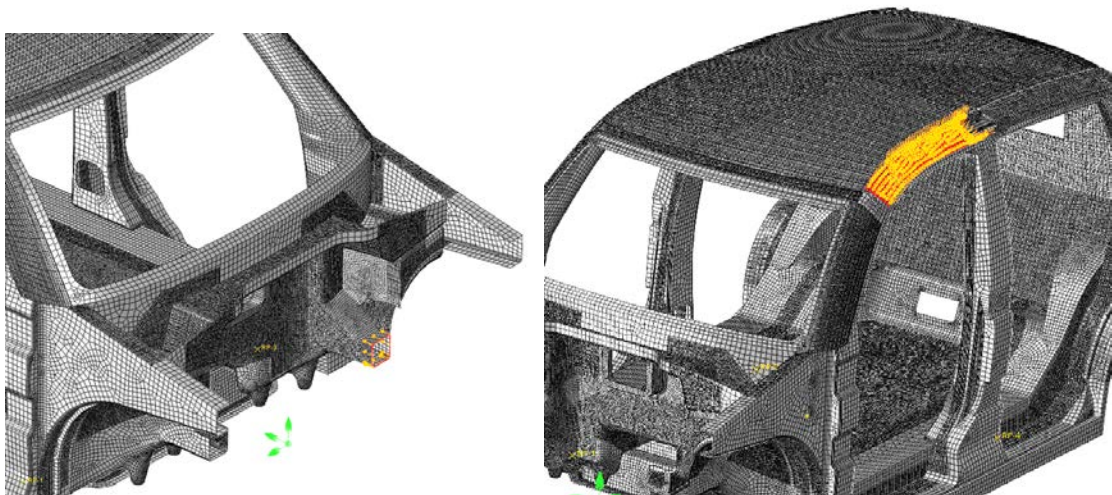


Fig 4.10 (Left) Frontal offset crash structure load on the peripheral of the crash structure mounting using line load condition (Right) Roof crush loading test using pressure loading condition



#### 4.1.6 FEA Model Development Plan and Limitations

The model in ABAQUS CAE can be linked to CATIA for parametric changes to geometry via an associative add-on. However such parametric capabilities falls apart when there are significant changes to geometry that causes disassociation of the parametric associations such as the creation of new surfaces. This means that any geometric design change requires a complete pre-processing of structural panels and the FEA constraints that was defined previously. Pre-processing a new part due to small changes makes updating a model with design changes difficult and time consuming. Ideally, the thicknesses of laminate has to be accounted for during design phase as any change in thickness will require respective geometric surface offset to obtain accurate joint stiffness using the adhesive joint mentioned in Section 4.1.4. Changing the offset will be difficult to achieve during the development which involves ply thickness change. Through some small scale FEA simulation, it is discovered that the absence of ideal offset has only small influence on the performance of overall vehicle structure. Thus, to reduce the time consuming pre-processing rework with every small geometric change, the ideal offset will only be achieve to the best ability as possible without too much emphasis on precise modelling as long as the offset error is not sufficient to cause a large swing of result, due to limited development time.

The difficulty to incorporate new design changes during the development process means that every complete model constructed should have its main purpose and also serve as a feedback for next design iteration. The constructions of the model and its milestone have to be clearly defined. The initial plan outlines two developments Model H0 and H1 Fig 4.11. Model H0 is the first structure concept that will give a good approximation of structure strength, stiffness and layup requirements. It also serves as a simple structure for the concurrent development of battery case structure under crash loads. Initial plans, it would be ideal to carry out only H0 and H1. However sever weakness in H1 structure and the delay in development of doors influenced the setup of H2 simulation model.

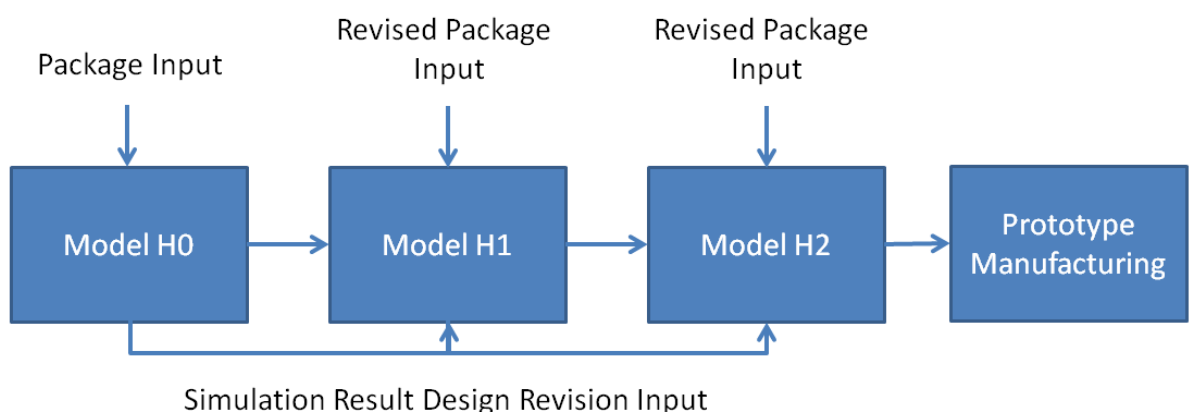


Fig 4.11 Composite Vehicle Structure Development Map

## 4.2 FEA Model H0 (Preliminary)

### 4.2.1 Purpose and Objective of Model H0

The H0 model was the first developed structure when major component packaging location was defined while exterior design surfaces were being designed. The structural model H0 was constructed out of simplistic surface from the available package space, various components were yet to be determined particularly the cross section of the aluminium crash structure and roof would be susceptible to change. This H0 structure model was developed to study the global effect of crash loads distribution on vehicle structure. The simulation results obtained would provide a good indicator and feedback to proceed towards the next step of development. The model was kept as simple as possible without strict restriction on manufacturability (release angle ignored) for initial simulation analysis.

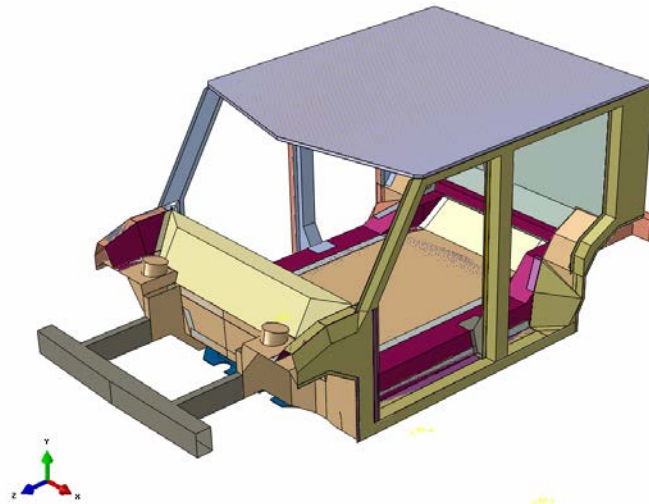


Fig 4.12 H0 Model of EVA taxi concept (with propose layup and structure components)

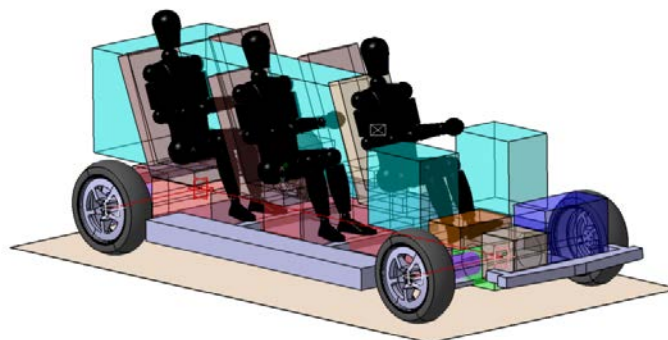


Fig 4.13 Example of early initial package definition that is used to design H0 model

Fig 4.12 shows the simplified initial vehicle structure model based on vehicle package shown in Fig 4.13. The vehicle structure was geometrically constructed with flat surfaces with small

consideration about manufacturability such as molding direction limitation for structure panel part division so that the structure can be a good simplified representation. Quasi-isotropic layup was initially chosen to allow easy and accurate observation of deformation under load and the inherent load path can be clearly analysed as elasticity is consistent in all directions. This initial layup will be varied to ensure that it can handle all crash load cases which depend on how crash load path flows within the structure. Another aim was to identify potential stress concentration and structural weaknesses to feedback into the development of vehicle structure in the next iteration. The composite sandwich effective stiffness effect can be simulated and sized according in this situation while forgoing cross beam structure member shown in Fig 4.14. Furthermore, the first draft location of structural adhesive were modelled within the structure assembly allow us to better understand the type of stress it undergoes in crash load dominated scenarios through FEA simulation.

#### 4.2.2 Simulation Results of Model H0

Due to the amount of simulation analysis conducted, only various major key development analyses will be shown to keep the report concise and short. All areas of the vehicle structure were given the same amount of development effort. During this initial structure development, the basic Rules of Mixture (ROM) was used to calculate the expected elastic properties with material properties from matrix and fibre while experimental material test listed in Section 3.3.2 were being carried out concurrently. Failure criteria follows a maximum strain of 0.4% mentioned in Section 4.1. Fig 4.15 shows the contour plots of the structure with +/- 0.4% strain contour clippings under full width frontal crash in E11 direction. Clipped blue mesh regions indicates possible ply compression failure and while clipped red sections indicates possible tensile failure. Study of the contour plots are conducted for E11, E22, E12 and E13.

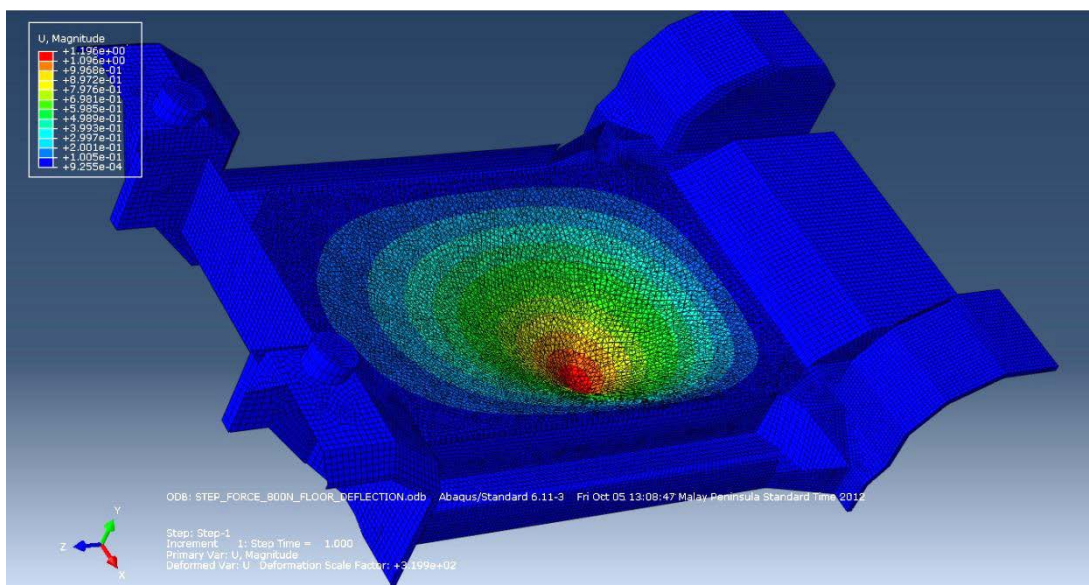


Fig 4.14 Deformation contour plot of the vehicle floor when an area the size of average footwear is subjected to 80kg load.



The progression of H0 model allows better understanding of the bending stiffness and deflection of the sandwich floor shown in Fig 4.14. The vehicle floor design criteria requires minimum deflect of the flooring to enhance the sense of structure stability even when under crash loads in-plane strength are adequate.

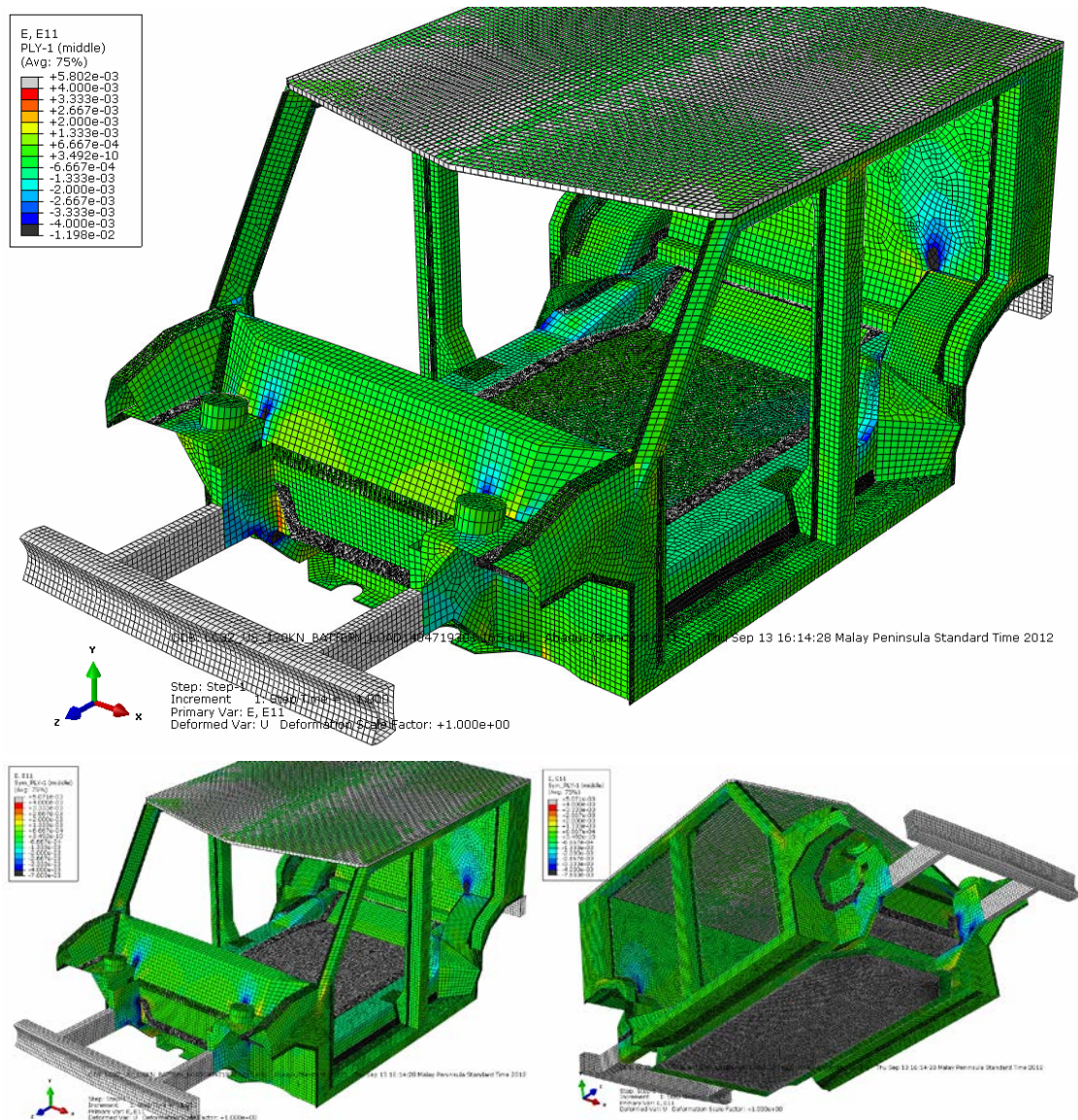


Fig 4.15 (Top) shows the max-strain failure concentration points for the ply 1 at 0.4% strain (bottom left and right) shows symmetric ply 1 failure points at high stress concentration points. (Blue shows compression loading and red shows tensile loading)

The FEA simulation results indicates that the adhesives are not loaded beyond its material strength limit. The adhesive still have significant amount of reserve factor if edge peel stress effect is not considered. Detailed through analyses of the adhesives were not carried out due to lack of manufacturing accuracy to control adhesive edge effect explained in the previous chapter. Thus, the exact failure of adhesive cannot be simulated with sufficient accuracy to obtain results precise enough to conclude its actual performance.

The first series of simulation load cases defined the approximate laminate thickness requirements and at the same time identified structure regions that are highly loaded and inefficient which should be revised in the next design iteration.

### 4.2.3 Structural Design Challenges Identified in Model H0

The H0 construction was very fundamental and does not show the implications for component integration. One of the objectives of model H0 construction was to analysis and size the structure and layup accordingly to the structure requirements. A correction factor will be applied to correct corner/edge effect or fastener effect. However such designs methodology are limited as simplification of geometry such as removing fillets will be impossible as some fillets are built from blended surfaces in latter simulation models. The structure is simply too complex for such simplification to work well. As an example, the lack of doors in the simulation resulted inaccurate loading for side collision.

Another challenge would be how the structure performance will change when holes and functional integration of sub-components are introduced. At the same time the development of the battery case was carried out using fastener load transferred obtained from model H0 side and frontal crash.

## 4.3 FEA Model H1 (Intermediate)

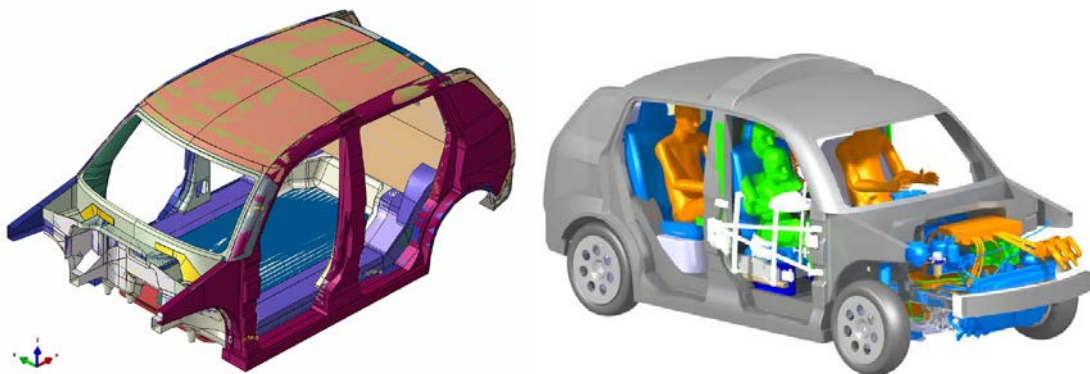


Fig 4.16 H1 Model of EVA Taxi vehicle structure with H1 vehicle package model.

### 4.3.1 Purpose and Objective of Model H1

Simulation model H0 achieved its objective of obtaining approximate required laminate thickness and possible area of failure. Moving on to the next level of development and simulation, Model H1 will focus on the structure performance verification and development on composite layup optimization. Other systems are developed and engineered concurrently with the vehicle structure. The specification freeze of other systems under development meant positioning and engineering specification of many sub-components such as seat belt anchors, steering column, high voltage components, drivetrain and suspension systems can be integrated to the vehicle structure and subsequently new loading points for the structure. The

construction and design of model H1 uses the first draft exterior design surfaces of the vehicle to form the exterior structure design limit.

During the construction of H1 FEA model, material coupon test was completed and test report shows that the elastic properties are within 5% of the values calculated from manufacturer's strength specification values of the fibres and matrix. The experimental coupons ultimate strength allow us to define an accurate failure criteria for the selected manufacturing process. Tsai-Wu and Tsai-Hill interactive failure criteria were employed in Model H1 instead of instead of maximum 0.4% strain criteria used in Model H0.

### **4.3.2 Envelope Contour Plots**

To simplify the presentation of ply failure plots within the thesis, the envelope of section points within the laminate was chosen. The envelope plot of section points shows the summation of ply failure. Thus if any ply in the laminate fails it will be shown as clipped contours. If the section shows significant clipping around region of high stress shown in Fig 4.17 Model H1 front crash rail. This highly stress area is considered to have failed and is unable to withstand the equivalent quasi-static crash loads applied by the crash energy absorption structure. During the development and optimization of composite structure, every ply is analysed for failure

#### **4.3.2.1 Failure Due to Geometric Influence of Model H1**

The initial FEA simulation results were baffling as Model H1 side B pillar have 10 times more deflection than Model H0 even both are configured with the same number of plies and layup. FEA pre-processing setup was check meticulously and all constraints were re-evaluated but no mistakes could be found. The large deformation was then concluded to be likely due to the step geometry within the composite panel, the step geometry sets the panel in a pre-buckled state reducing its ability to transmit loads and induced sensitivity to bending stresses at these step features. Any in-plane load will result in large deformation as in-plane stiffness is reduced dramatically with these steps features.

The choice to proceed deep into component function integration may not be unsuitable as some of these integration adaptations require sharp geometric deviation of load paths resulting in poor structure performance and efficiency. Thus the level of integration design has to be re-evaluated and planned carefully during the start of the design phase. An example of such failure was the integration of the front suspension sub-frame mounting point shown in Fig 4.17 and Fig 4.22.

It was also observed that by changing the young modulus of adhesive results in minimal changes (less than 2%) in the vehicle structure bending and torsional stiffness which indirectly concludes that adhesive plays small part in the transfer of torsion and bending loads, which give a strong indication that the structure panels have good interlocking design. Torsional stiffness was measured at 22.7kNm/degree and bending stiffness are on the higher end of comparative benchmark vehicles.



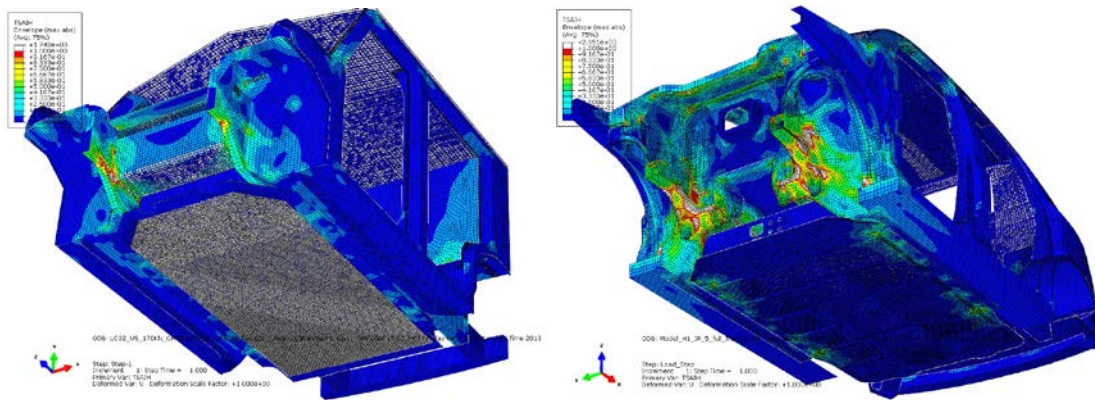


Fig 4.17 Envelope failure plots of (left) Model H0 and (right) Model H1. The envelope plots shows that failure is more widespread on the crash rail of model H1.

#### 4.3.2.2 Results of Multiple Failures of the Composite Vehicle Structure Under Crash Loads of Model H1

There were panel failures in large number of structure areas, the increase in geometrical complexity of the structure along with step features and improper function integration led to weaken and inefficient load path, reducing load carrying capability of the structure. Furthermore integration of components inevitably results in openings and access ports on the structure to ensure functionality. These openings will have significant impact in structural strength if improperly designed.

#### 4.3.3 Solutions to Front Crash Load Path Structure Failure in Model H1

As seen from the simulation results shown in Fig 4.17 and other failure within the structure, geometric complexity decreases the ultimate strength of a composite structure section. In Model H1, the integration design to provide mounting solution for the front suspension sub-frame created a break in the load path resulting in failure. This observation is identical to step features mentioned in Section 4.3.2.1 which geometric features sets the section in a pre-buckled state decreasing its load carrying ability. However due to the complexity of design needs and available structure design space, efficient lightweight design is often hard to achieve and a compromise solution have to be used. This observation influence the limits of structural integration capabilities on main load path of the vehicle structure. As a result, future integration developments of sub-components were carried out with the most direct and simplest load path.

Structure redesigns was carried out at area of structural failure to increase and improve load path characteristic. A few solutions have been explored but the most effective solution was to change the aluminium crash structure attachment point 50mm forward and 50mm downwards as shown in Fig 4.18. This change allow more direct load path with smaller angular changes to frontal crash load path, further more matching the compliance to part 581 crash compatibility voluntary standard and increased package clearance for the mounting of brake booster.

The shifting of front crash structure mounting point is just one of the design changes made to strengthen the vehicle structure and improve its efficiency. Other significant design change is the complete concept changes of the firewall allow decoupling of displacement during crash, preventing brake pedal movement and indirectly stiffen the suspension shock tower stiffener. There also substantial design changes to direct the crash loads to the side rocker sills creating a load path around battery case structure to reduce loading to the battery case in frontal impact.

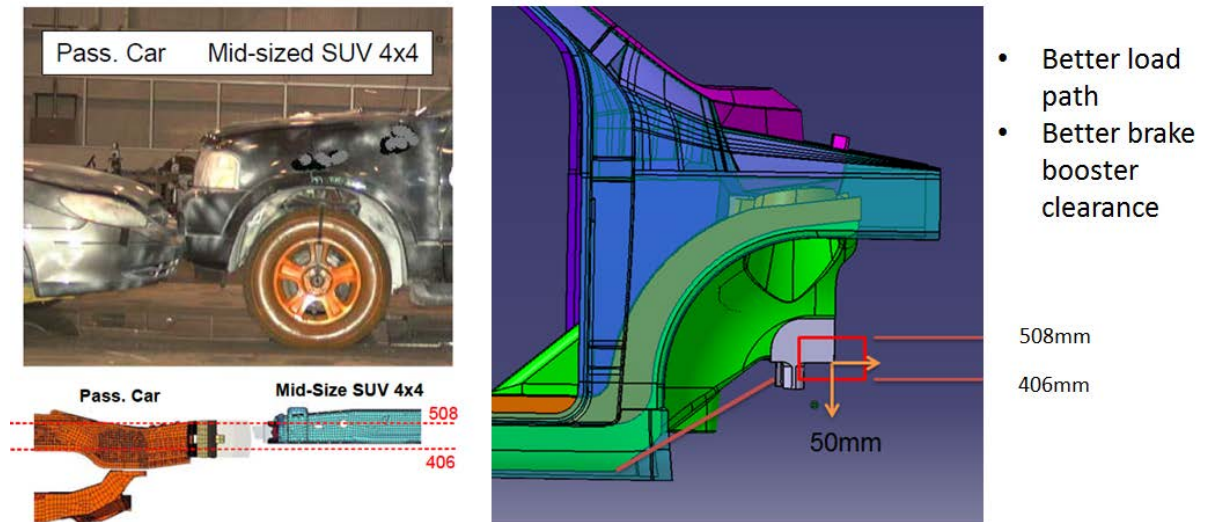


Fig 4.18 (left) Part 581 (NHTSA) crash compatibility, (right) proposed change to crash structure height and allow better load path and brake booster clearance.



## 4.4 FEA Model H2 (Final)

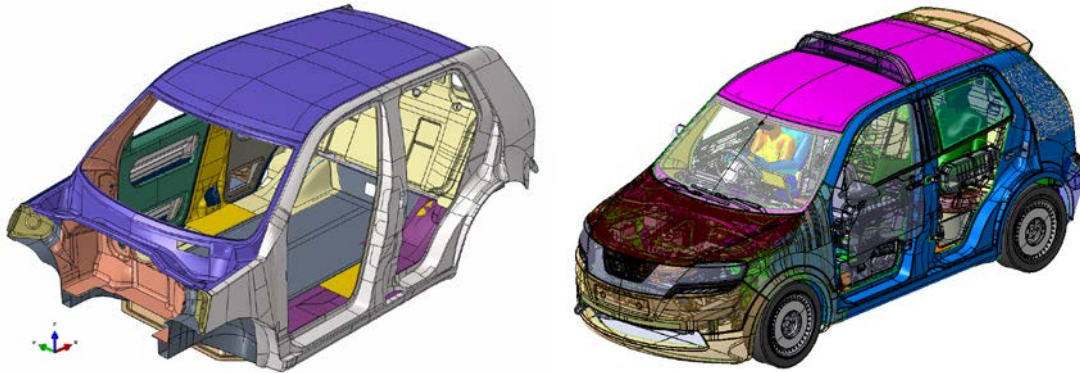


Fig 4.19 Model H2 of EVA Taxi vehicle structure along with H2 vehicle package model

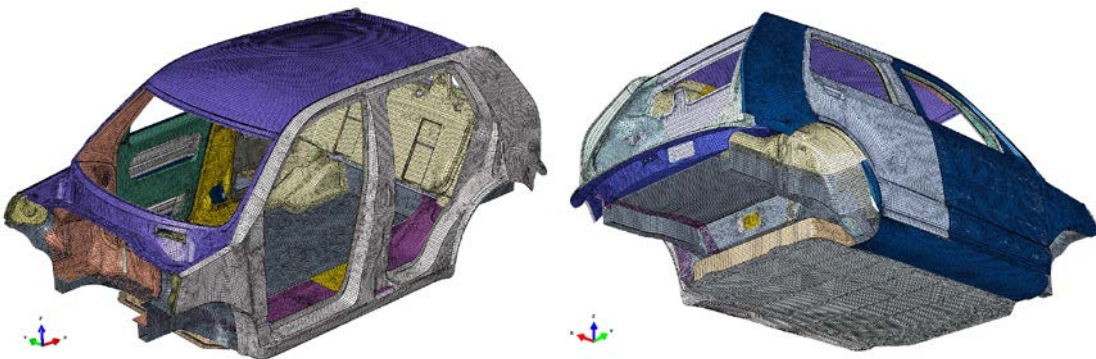


Fig 4.20 Model H2 front and back view in element mesh

### 4.4.1 Purpose and Objective of Model H2

The simulation results of model H1 necessitate the development of model H2 due to its structure inadequacy for equivalent quasi-static crash scenarios. Due to the tight timeline, model H2 will be the last development model before prototype production. Model H2 underwent large number of structural panel revision and changes to improve its load path characteristic and structural efficiency. The increase of structural efficiency can bring about reduction ply thickness for weight reduction. The development of model H2 allowed comparison and verification of the final structure ability to handle crash scenarios particularly front impact with model H1. Model H2 also will incorporate doors with composite side impact protection crash beams. However performance of the doors under impact cannot be verified due to inability to conduct dynamic simulation accurately for composites failure studies as doors become a crash energy absorption structure. Fig 4.19 shows model H2 vehicle structure integrating a much more complicated vehicle page model and Fig 4.20 shows the mesh model of the vehicle structure with battery case attached.

## 4.4.2 Vehicle Structure Performance of Model H2 under Crash Loads

In all crash load scenario simulations, there were significant improvements in the performance of the vehicle structure, shape of the A-pillar was tweaked and revised to reduce its size. There were reduction of composite plies in many area such as roof, front portion of the front suspension shock towers due to the increase in structural efficiency. The increase in stiffness and load path is clearly shown by deformation plot in Fig 4.21. The redesign reduced the total adhesive bond area by improving the design of interlocking structural panels. For example the side panel structure will be assembled from the sides, thus any impact from side either oblique or at an angle will not dislodge the side panel even if the adhesive failed.

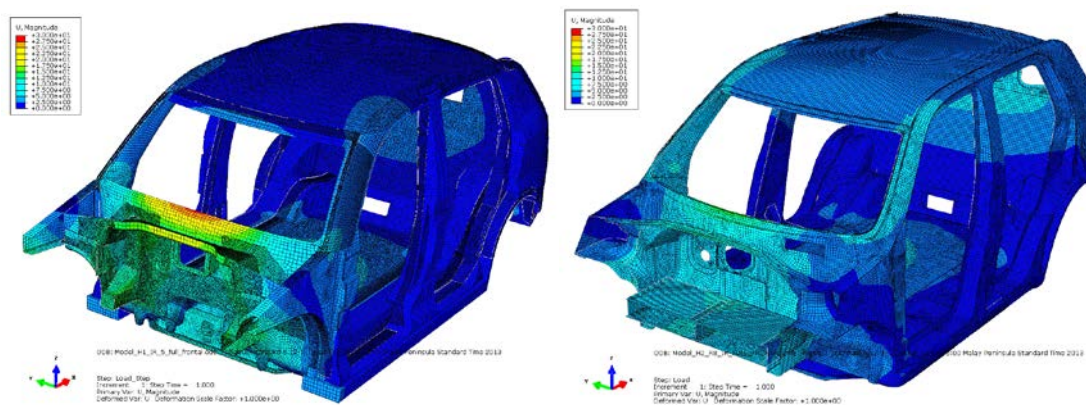


Fig 4.21 Deformation contours of (Left) Model H1 (Right) Model H2 with clipping at 30mm with full width frontal crash.

## 4.4.3 Geometric Structure Design Comparison of Model H0, H1 and H2

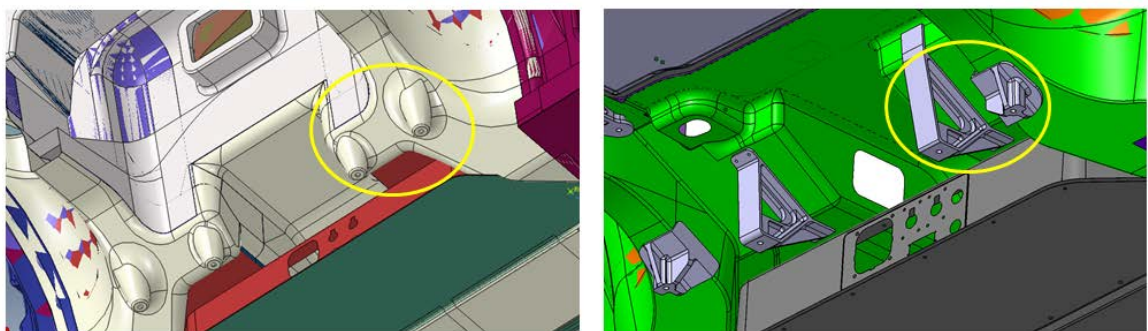


Fig 4.22 Use of aluminium adapters to extend mounting points allowing structure to have a cleaner and smoother load path.

The failure of the front crash rail in model H1 prompts the redevelopment of the attachment points for front suspension sub-frame to improve the load path. The crash structure height was lowered to provide a smooth geometric transition of the crash rail to the rest of the structure,



resulting in a stronger structure as shown in Fig 4.22 and Fig 4.23. The increase of structural strength and stiffness indirectly reduced the loads on the battery case fasteners. The aluminium sub frame adapters were designed to load the adhesive in shear under load to load the adhesive joint efficiently.

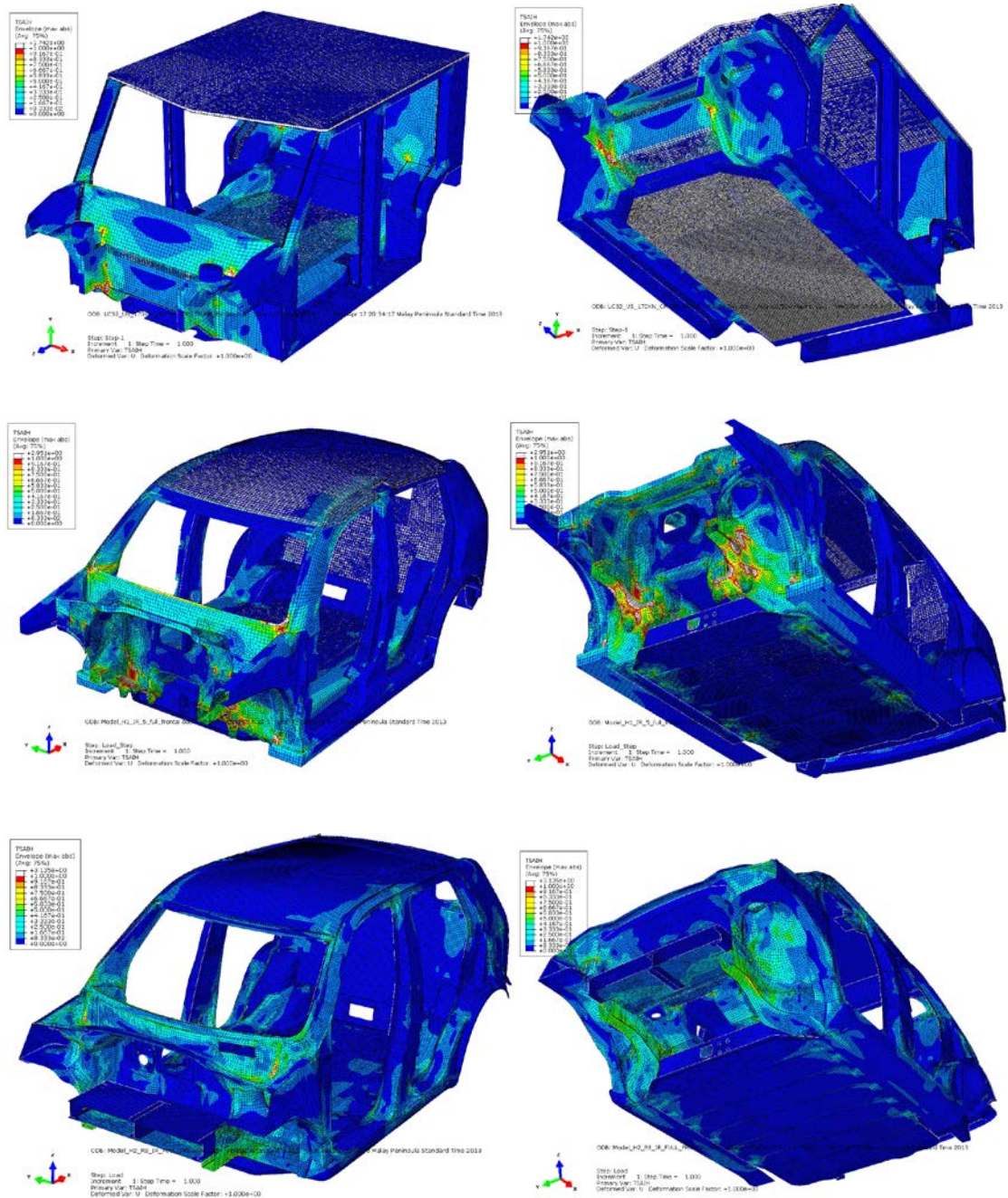


Fig 4.23 Tsai hill envelope plot with clipping set at 1.0 (Top left and Right) Model H0 under full width frontal crash (middle left and right) Model H1 under full width frontal crash and (bottom left and right) Model H2 under full width frontal impact. Model H2 shows significant improvement in strength even when same laminate thickness is used.

Fig 4.23 shows the full width frontal crash scenario for model H0, H1 and H2 showing the improvement in structure crash load capability while reducing stress concentration dramatically. Similar development methodology was used to identify failure location failure location at various parts of the structure in all defined crash load cases. There was great success in improving the vehicle structure strength with the redesign development methodology without increasing laminate thickness; and in some cases there were even reduction of laminate thickness.

In literature review section on carbon composite, the crash stability of carbon composite vehicle structure depends heavily on the compressive strength of the crash structure base. Thus the structures outside of the safety cell such as the rear trunk region were constructed out of thinner laminates with lower strength than the safety cell. This allows the composite structure behind the rear passengers to isolate the damage and increase energy absorption if the crash scenario exceeds the capacity of the EVA's crash structure. The same was done for the front end of the vehicle, auxiliary/secondary crash structure in front of the A-pillar was designed to create additional protection from angled frontal impact and highly offset frontal impact. In a highly offset impact occurs when the crash does not engage the main aluminium front crash structure. The strength of the A pillar will resist such impact force while the front suspension strut structure will act as a secondary crash absorption structure. Stability of this secondary crash structure was also considered by introducing tapered design and thinner laminate at the crash front. However, it was no verified experimentally or by simulation as it is made out of carbon composite.

#### **4.4.4 Side Impact Crash Simulation Result and Novel Side Crash Beam Structure**

For side impact scenario, due to limited space and differing crash mechanics, the employment of energy absorption was limited. The study of side crash mechanics in section 3.1.3 suggested that a strong and stiff structure will theoretically result in lower occupant injuries. However side crash mechanics does not just rely on stiff structure, the design of interior trim must be able to cushion the occupant when they impact the door as shown in Section 3.1.3. Furthermore static implicit FEA simulation struggles to conclude any information and data on crashworthiness performance in such dynamic scenarios.

Not forgoing the objective of the EVA electric taxi project of designing a crashworthy structure. In an effort to stiffen and strengthen the vehicle side structure, a new design method was devised by using carbon fibre Kevlar laminate design of the door crash beam structure. Kevlar also known as aramid fibres are used in bullet proof vest retarding ballistic projectile to Kevlar belt in tires to increase protection from puncture by penetration. The most commonly used Kevlar 49 have identical ultimate tensile strength when compared to carbon fibre. However Kevlar have a lower modulus of elasticity which makes Kevlar composite laminate fails in a differently way compared carbon fibre composite. Kevlar composite fails in a way similar to how metal fails, exhibiting ductile plastic deformation while resisting penetration with the onset of failure. Such characteristic is beneficial to prevent intrusion through the door

during side impact and the ductile plastic deformation property allows redistribution of stress concentration and can possibly increases the ultimate strength capacity of the structure.

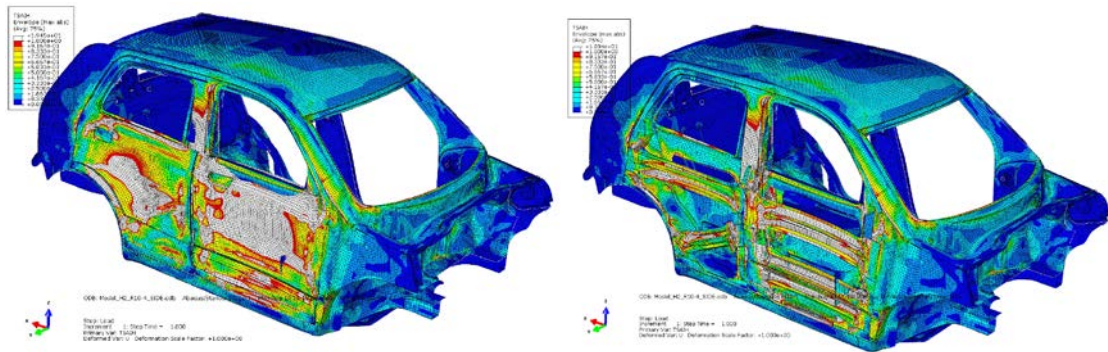


Fig 4.24 Quasi-static side crash load simulation Tsai-Hill envelope plot. (left) with exterior door panel surface (right) with crash beam and door interior panel.

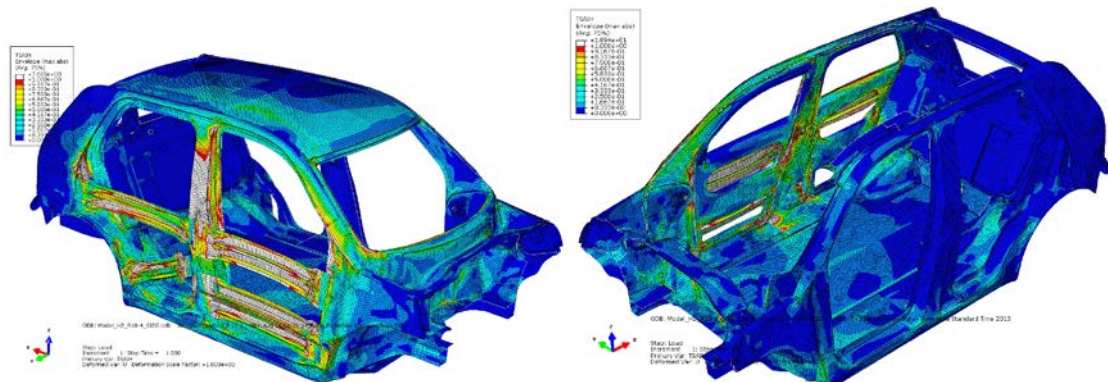


Fig 4.25 Quasi-static side crash load simulation Tsai-Hill envelope plot (Left) crash beam only (right) interior door panel envelope plot.





Fig 4.26 Carbon fibre kevlar composite crash beam of EVA electric taxi prototype.

However due to accuracy limitation of composite simulation, time and resources, verification of such design cannot be simulated or can experimental testing be conducted. Fig 4.24 and Fig 4.25 shows the structure with the envelope plot of implicit side impact FEA simulation using crushing load profile via pressure loading condition of Mobile Deformable Barrier (MDB). Fig 4.26 shows final construction of the carbon kevlar fibre composite crash structure employed in the vehicle while

Table 4.2 shows the plybook and layup of the Carbon Kevlar sandwich front door.

Table 4.2 Plybook and layup of EVA's Carbon Kevlar sandwich front door panel, where FD\_CRASH\_B\_1, FD\_CRASH\_B\_2, FD\_CRASH\_B\_3 the composite crash beams.

Mold Side	Mold Side	Mold Side	Mold Side	Mold Side	Mold Side	Thickness (mm)
FD_EXT	FD_CRASH_EXT	FD_CRASH_MOUNTS	FD_CRASH_B_1	FD_CRASH_B_2	FD_CRASH_B3	
0	0	0	0	0	0	0.15
90	90	90	90	90	90	0.15
0	0	0	0	0	0	0.15
90	90	90	90	90	90	0.15
0	0	0	0	0	0	0.15
90	90	90	90	90	90	0.15
45	45	45	45	45	45	0.15
-45	-45	-45	-45	-45	-45	0.15
90	90	90	90	90	90	0.15
0	0	0	0	0	0	0.15
90	90	90	90	90	90	0.15
0	0	0	0	0	0	0.15
	Kevlar Ply	Kevlar Ply	Kevlar Ply	Kevlar Ply	Kevlar Ply	0.15
	Kevlar Ply	Kevlar Ply	Kevlar Ply	Kevlar Ply	Kevlar Ply	0.15
	Kevlar Ply	Kevlar Ply	Kevlar Ply	Kevlar Ply	Kevlar Ply	0.15
	Kevlar Ply	Kevlar Ply	Kevlar Ply	Kevlar Ply	Kevlar Ply	0.15
			Foam	Foam	Foam	20
		Kevlar Ply	Kevlar Ply	Kevlar Ply	Kevlar Ply	0.15
		Kevlar Ply	Kevlar Ply	Kevlar Ply	Kevlar Ply	0.15
		0	0	0	0	0.15
		90	90	90	90	0.15
			0	0	0	0.15
			90	90	90	0.15
				Kevlar Ply	Kevlar Ply	0.15
				Kevlar Ply	Kevlar Ply	0.15
					0	0.15
					90	0.15
					0	0.15
					90	0.15
					Kevlar Ply	0.15
					Kevlar Ply	0.15
				90	90	0.15
				0	0	0.15
				Kevlar Ply	Kevlar Ply	0.15
				Kevlar Ply	Kevlar Ply	0.15
			90	90	90	0.15
			0	0	0	0.15
		90	90	90	90	0.15
		0	0	0	0	0.15
		Kevlar Ply	Kevlar Ply	Kevlar Ply	Kevlar Ply	0.15
		Kevlar Ply	Kevlar Ply	Kevlar Ply	Kevlar Ply	0.15
			Kevlar Ply	Kevlar Ply	Kevlar Ply	0.15
			Kevlar Ply	Kevlar Ply	Kevlar Ply	0.15
		Kevlar Ply	Kevlar Ply	Kevlar Ply	Kevlar Ply	0.15
		Kevlar Ply	Kevlar Ply	Kevlar Ply	Kevlar Ply	0.15
		Door edge			Door Center	26.6



#### 4.4.5 Result of Bending and Torsion Stiffness Simulation of Model H2

The bending and torsion stiffness benchmarking of model H2 was simulated. The loading constraints and conditions followed industrial standards defined in Section 2.3, the obtained deflection value was measured and computed with the bending and torsional stiffness equations in Section 2.3. The torsional stiffness obtained was 25.2 kNm/degree° and bending stiffness was 14.0 kN/mm shown in Fig 4.27. These numbers matches the upper end of the benchmark spectrum shown in Fig 4.27 which indicates EVA's structure matches the characteristic of vehicles in similar weight class. Thus it was concluded that the performance of the structure will be sufficient as a prototype vehicle.

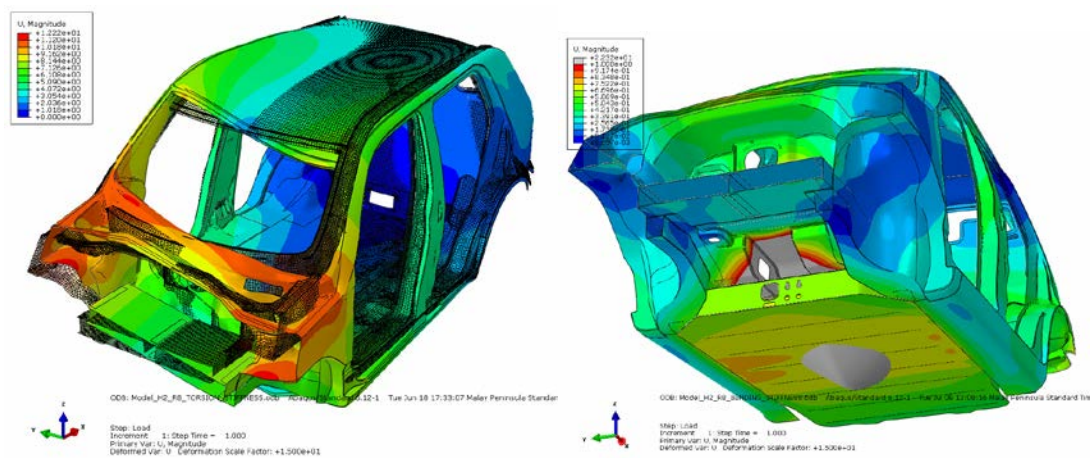


Fig 4.27 (left) Torsional loading deformation plot (right) bending loading deformation plot. (Deformation exaggerated by 15 times)

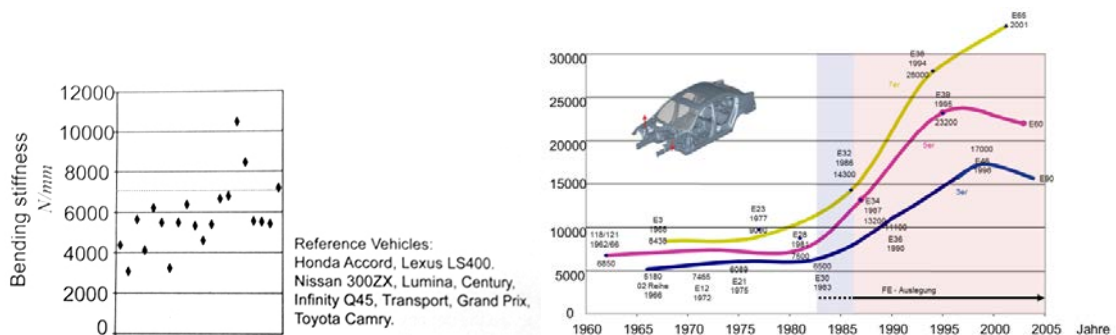


Fig 4.28 (left) bending stiffness benchmark comparison (right) BMW torsional stiffness comparison (Vertical axis in Nm/degree°, horizontal axis in Years).

#### 4.4.6 Development of Auxiliary Components

Besides these development covered in previous section, many auxiliary structure simulation verifications was conducted by the author to ensure function critical components were securely mounted and can withstand crash load or abuse conditions, the list of auxiliary FEA simulation are shown in Fig 4.29. However the detail of the simulation will not be shown to keep focus on the main vehicle structure development.

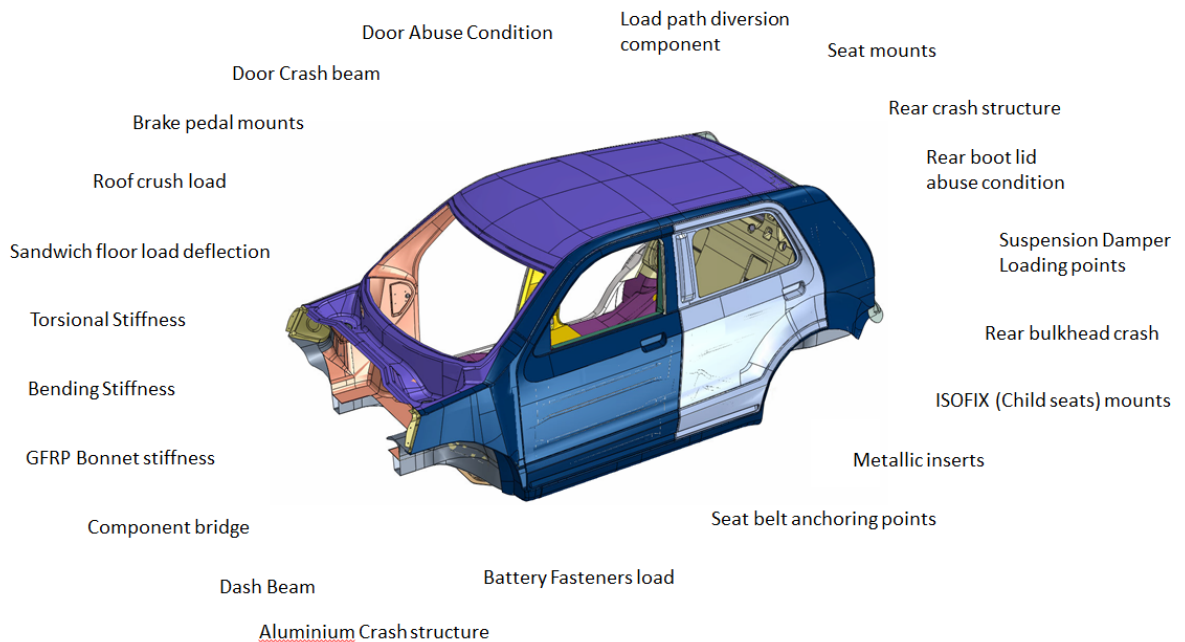


Fig 4.29 Auxiliary FEA simulation conducted to ensure strength of functional critical components in respective load scenarios.

#### 4.5 Front and Rear Aluminium Crash Structure/Crumple Zone

The complete development of the EVA composite vehicle structure model H2 marks the final revision of EVA occupant safety cell. To satisfy the objective of project EVA for crashworthiness, the crash energy absorption structure has to be developed to work as crumple zone section of the vehicle. Statistics shows that the highest percentage of the accidents occurs with frontal impact. Thus the front crash structure cannot be neglected. Since front and rear crash forces are considered identical, the same crash structure design will be implemented in the rear. The choice to go with aluminium crash structure was the ease for simulation as it has low sensitivity to strain rate hardening effect and the strain rate hardening effect can be ignored in simulation without drastically affecting accuracy. Another consideration in the development process was fabrication. There is a possibility to explore custom hydro-formed crash structure profiles but such designs will exceed budget constraints and development timeline, thus only off-the-shelf profiles will be considered during the crash structure development. A large local supplier provided catalogues and the type of profiles they offer

along with information of the profile mechanical properties, reducing the testing and development effort.

#### 4.5.1 Aluminium Failure Model Verification with Published Experimental Data

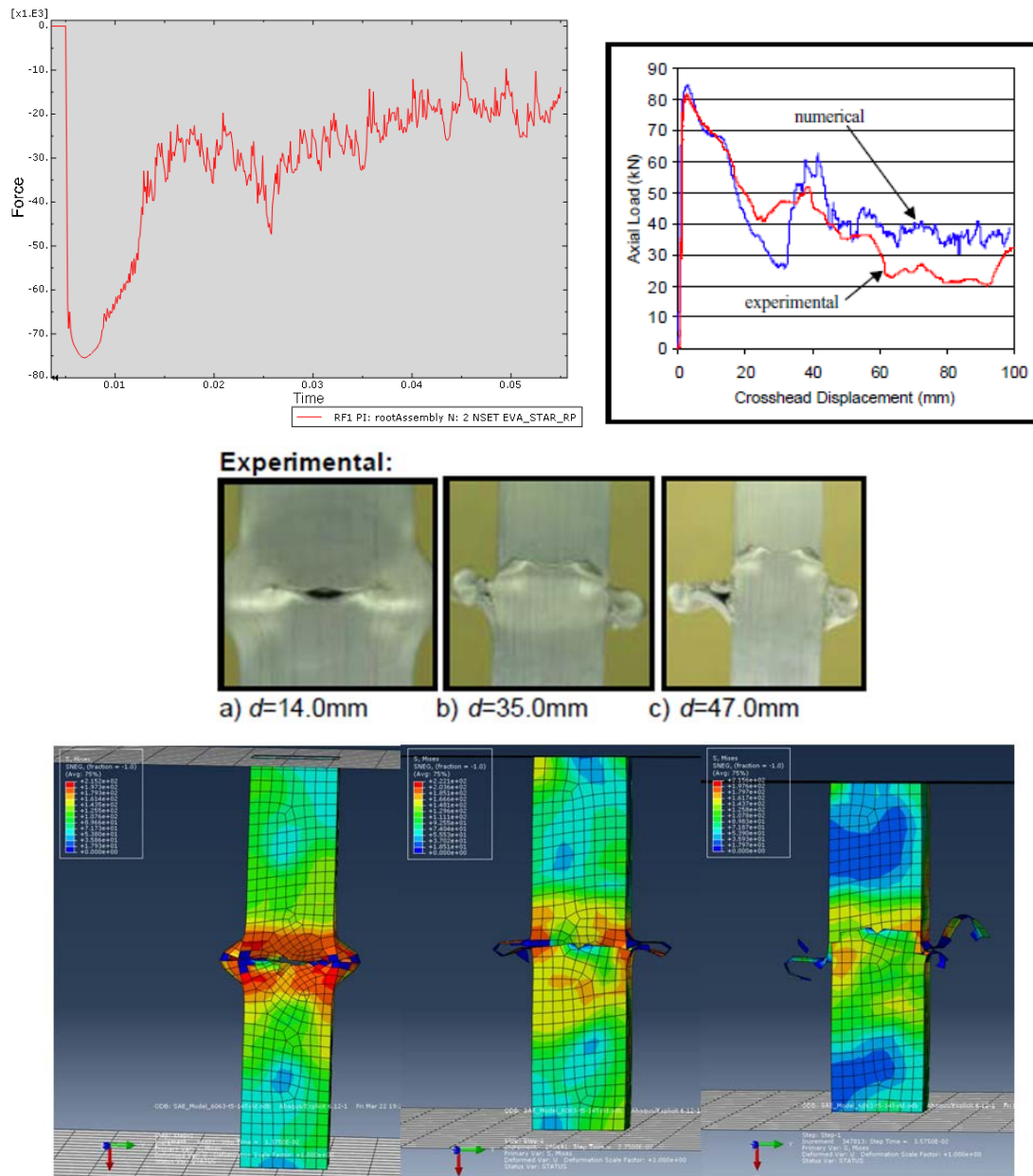


Fig 4.30 (Top right) Force-time plots of FEA simulation (Top left) Force-displacement plot of experimental results. (Middle and bottom) AL6063-T5 FEA material model simulation with comparison with experimental data [92]

The package space (design space) allowance for the crash structure was maximized to ensure the stability of the crash energy absorption and reduces the possibility of premature structure buckling via varying a variety of thin wall profiles. In section 2.6.1 we reviewed the

mechanics behind the progressive axial crushing of ductile metallic profiles and identified the key requirement performance characteristic and how such collapse was controlled. Using the material information given by the supplier, different variations or combination of profile size and wall thickness was evaluated for stability of energy absorption and average crush reaction force through dynamic FEA simulation. To ensure that the simulation correlate with actual real-life performance, a research paper publish by Arnold [92] will be used as reference for comparison. It contains AL6063-T5 experiment results which is the same material provided by the supplier. Dynamic explicit FEA simulation was conducted in ABAQUS to compare against published experiment data. The simulation results show good correlation with visual comparison and force-displacement plots of experimental results shown in Fig 4.30.

#### 4.5.2 Crash Structure Detailed Geometry Development

With the verification of the aluminium material model, the evaluation of suitable combination of aluminium profile was evaluated for crushing/folding stability and average reaction force generated. The most suitable combination was two 3 inches (76.2mm) by 2 inches (50.8mm) rectangular profile with 3mm wall thickness. To ensure stability of combined structure, the folding mechanism has to be asymmetric between two profiles. To trigger folding mechanism a geometric feature have to be devised to create sufficient out of plane load to initiate the folding of profile, this was best achieved by milling a 10mm wide 1mm deep groove. This groove causes out of plane bending stress in direction perpendicular to the groove when in-plane load is applied. Thus allowing the two profiles to fold asymmetrically alternating grooves are machined on the long and short dimension of the respective profile as shown in Fig 4.31.

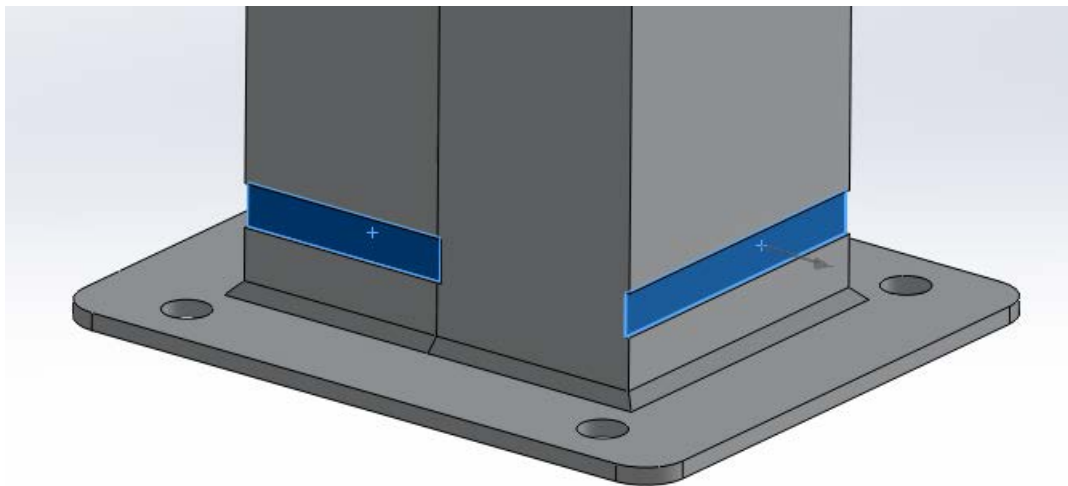


Fig 4.31 Alternative machined groove to trigger asymmetric folding (blue)

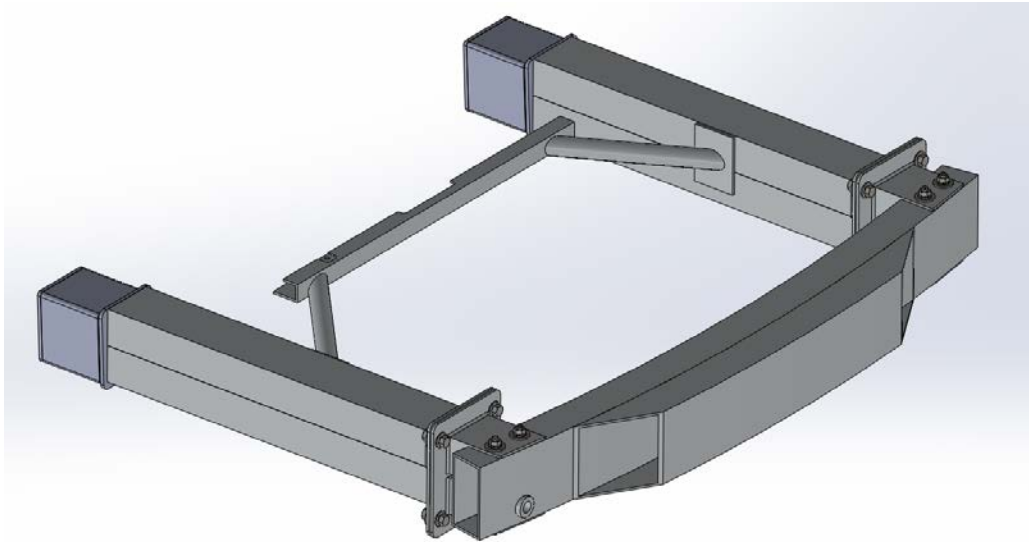


Fig 4.32 Subassembly of front crash structure with easily replaceable bumper assembly.

The construction of the front and rear crash structures are constructed in a similar manner as crash load forces for rear crash and frontal crash are identical. The crash structure system also features a low speed crash system integrated into the bumper as shown in Fig 4.32. The low speed crash system was designed to absorb low speed impact up to 15kmh minimizing or preventing damage to the main crash rail by having a lower crushing load compared to the main crash rail allowing low cost replacement. This mitigates the low speed crash force to reduce the amount of structural damage, similar to how a padded elbow and knee guard works.



### 4.5.3 Experimental Test Specimens and Simulation Verification

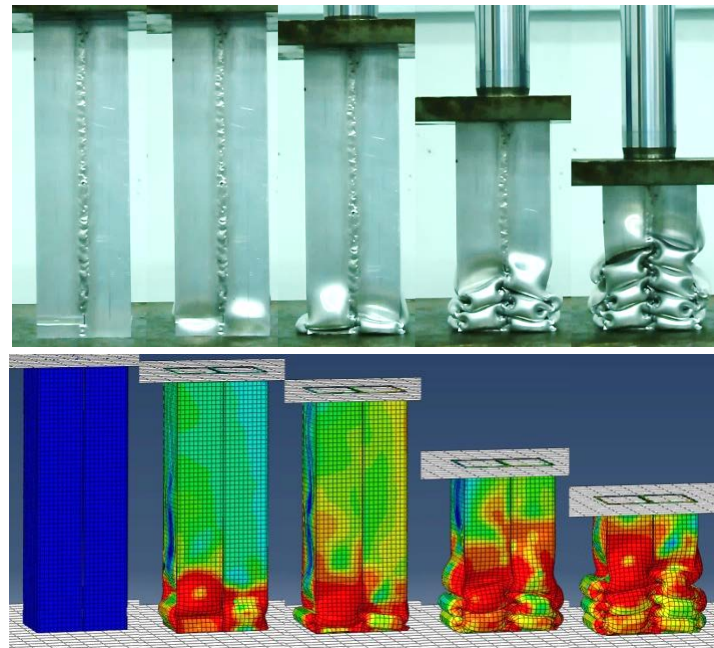


Fig 4.33 Quasi-static crushing of TUM-CREATE electric taxi aluminium crash structure for crash initiator design verification (above) experiment, (below) Explicit FEA simulation in ABAQUS.

Main crash rail specimens were produced to experimentally verify dynamic simulation data shown in Fig 4.33. Due to the tight timeline restriction, scientific setup using load cell to data log force displacement plot was not possible as the author was unable to obtain a load cell capable of measuring large forces with peak loads of 150kN force during the crash structure 2 months development timeframe. As an alternatively solution, the author have access to a hydraulic press with capacity of 50 tons (500kN), It was used to crush the specimens quasi-statically. A pressure gauge was used to calculate the reactive force exerted by the crash structure onto the press, video capture of this pressure gauge was performed along with the crushing of the specimen. The multiplication of pressure gauge and piston area gave the instantaneous reaction load. This approximate plot tallied very closely with the figures achieved in FEA simulation.

The crash structure was further developed to ensure robustness under varying angle of impact. A target of  $\pm 15$  degrees was set. In angled impact simulation, it was observed that the crash structure would not crush axially without lateral support, the crash structure would bend plastically at the base attachment point and breakoff prematurely resulting its inability to fully absorb crash energy. A variety of design options was explored and narrowed down to centre bracing of the crash structure as shown in Fig 4.32. The centre bracing was structural mounted onto the main structure, the centre brace is made from 1 inch diameter (25.4mm) with wall thickness of 3mm. Fig 4.34 and Fig 4.35 shows the ABAQUS dynamic explicit simulation

crushing of aluminium crash structure in 0 degree and 15 degree impact respectively. Fig 4.35 shows that under 15 degree angled impact, the aluminium crash structure remained stable.

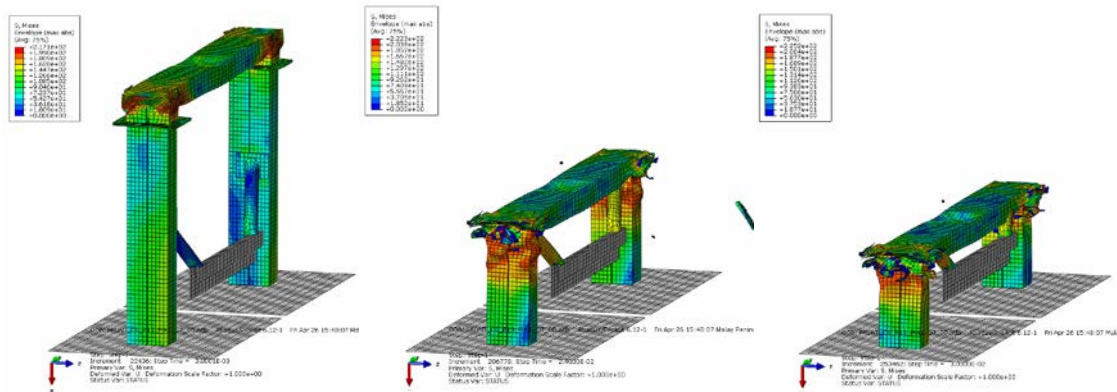


Fig 4.34 (left) crushing of low speed crash structure (middle) progressive folding of main crash beam (right) Progressive folding not affected by centre comp bracing

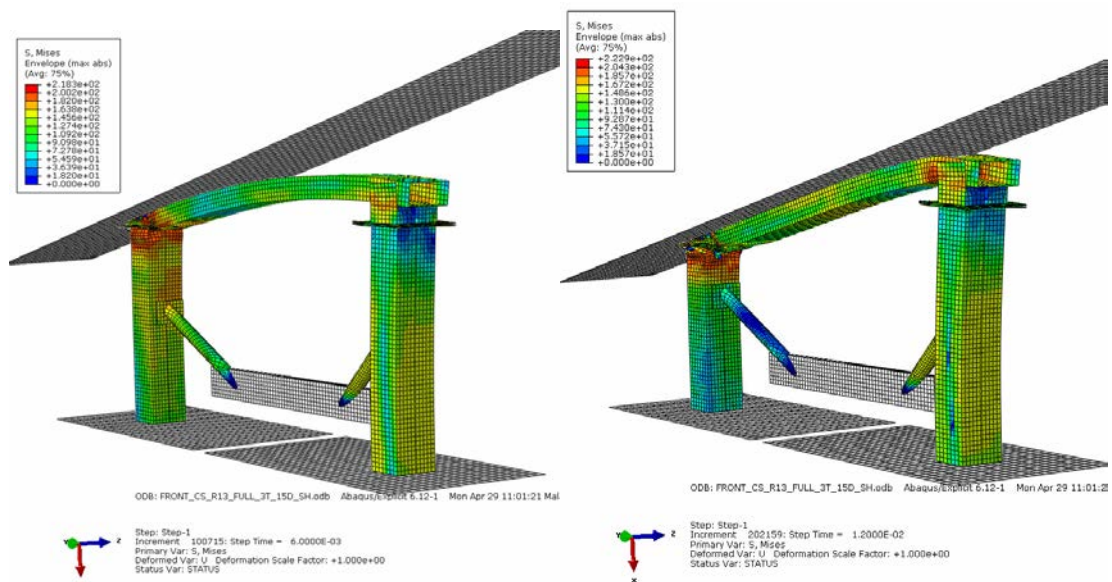


Fig 4.35 (Left) 15 degree angled impact (Right) stability of crash structure maintained

The force vs time plots are shown in Fig 4.36 and Fig 4.37, both of which are performed at the same velocity. In Fig 4.36, the combination of low speed impact crush structure and bumper results in a low initial mean absorption force shown in the polynomial trendline. Once the main crash rail was triggered, the average sustained crash load averages maintains in the region between 250kN and 300kN before maxing out at 350kN near the end of the crash duration. This average crash reaction force obtained is similar to the equivalent quasi-static crash load obtained using photogrammetry analysis in Section 3.1.2. In Fig 4.37, it is observed that the initial total reaction force for 15 degree impact is much lower than that of 0 degree impact, as the impact only engages one side of the crash rail. As the second crash rail engages, the total

reaction force raises. This characteristic was also observed in FEA simulation of 5 degrees and 10 degrees impact angle.

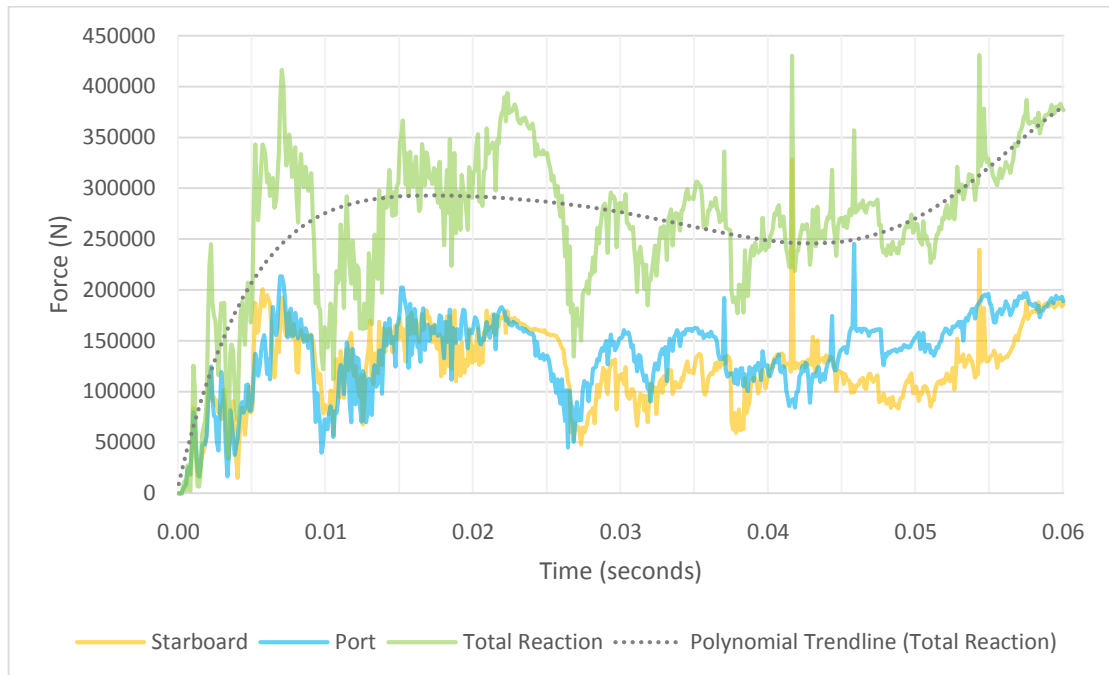


Fig 4.36 Force vs time plot for frontal impact at 0 degrees.

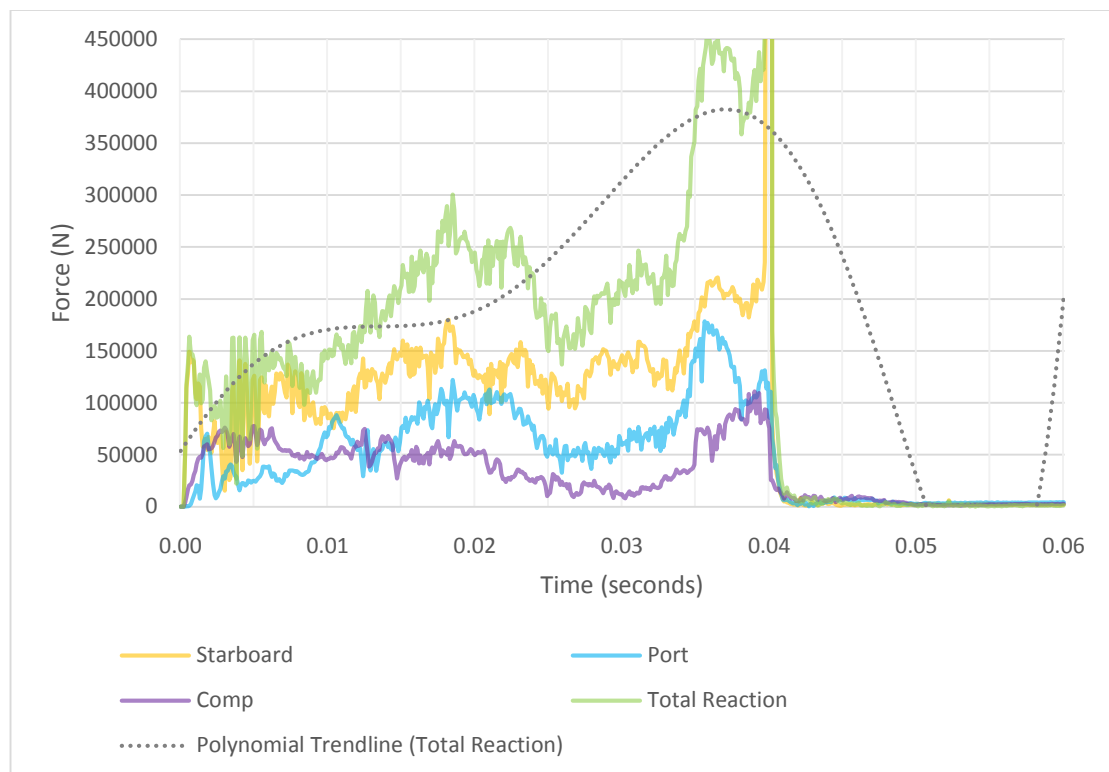


Fig 4.37 Force vs time plot for frontal impact at 15 degrees.



In Model H2 FEA simulation, the front crash structure attachment points is loaded with equivalent quasi-static crash loads derived in from Section 3.1.2. The safety factor available in EVA's composite structure will be able to withstand the occasional 400kN force spikes during the aluminium crash structure energy absorption process. The final aluminium crash structure design offering good energy absorption characteristics and stability in crushing. Fig 4.38 shows the final design of the aluminium crash structure for EVA.



Fig 4.38 Project EVA electric taxi aluminium crash structure.

## 4.6 Concluding remark

In this chapter, the development methodology of the vehicle structure was covered in more detail. First, the pre-processing methodology from CAD was defined and the use of shell FEA model for versatility quick layout changes, followed by CAD data import and geometrical clean up and simplification for meshing. Inertia relief boundary conditions was also used in FEA to ensure realistic equivalent quasi-static crash load simulation on the structure. As a method to increase speed of development, the author employed 3 development stages, Model H0 to H2. Each development model had a specific structural goal to achieve, H0 was used to size the laminate thickness and structure sections. H1 and H2 verify the structure after integration of system components. This method reduces the need to update every small design changes. This is the most time consuming as the geometric data in the FEA model cannot be modified parametrically as almost all the design changes made during EVA's development was not parametric. Throughout the development of the structure, the author observed that geometric complexity have a large impact in the final strength and load paths of the structure. The vehicle structure from Model H1 to H2 structure was optimized significantly, particularly in the way panels are joined. By analysing the load path distribution of the failed areas, subsequently solutions were developed to improve the efficiency of the joints and load paths to strengthen the structure. In an effort to keep report more concise, the thesis covered only the detailed load path management of the front crash structure was covered as it was one of the most relevant solution that depict the design impact of load path geometry. The author carried out multiple FEA analysis of various system components listed in Section 4.4.6. The FEA simulations allowed the author to have a complete overview of the structure response under crash loads and thus effectively make design changes to the vehicle structure. EVA's vehicle structure was benchmarked in simulation on its torsional and bending stiffness performance with vehicles in the same class. Subsequently, the aluminium crash energy absorbing structure was developed using dynamic FEA simulation and was tested experimentally to match the dynamic crash absorption requirement of EVA. The development of the doors and its integrated crash beams followed shortly, however its actual performance cannot be evaluated. The vehicle structure aim was to develop the vehicle to include as much design safety as possible within the limited design timeframe. The simplification of forces and simulation methodology allow the author to achieve this aim. In the next chapter, the author will discuss about his contribution to the manufacturing and assembly of EVA and in the final chapter the conclusion and possible further research direction.



---

## Chapter 5: Manufacturing and Assembly of EVA

---

### 5.1 Manufacturing and Final Assembly

In this chapter, the manufacturing and assembly section will be mostly pictorial however it will not be covered in detail as manufacturing and assembly is not the main focus of this thesis. In this section, the author will touch briefly on his contribution, roles and responsibilities in the manufacturing and assembly of the vehicle structure.

While working on the development of the vehicle structure, the author worked closely with industrial partners to ensure the design manufacturability and assembly of the vehicle structure. He also participated actively in the design meeting every week, discussing and providing solutions to structural challenges, or structural compromises to meet design and system integration requirements. Furthermore, he supervised and oversaw interns and students working on the vehicle components, providing advices and design parameters on composite components such as the composite structure within the vehicle seats.

During the manufacturing testing phase, the author was actively participating in the infusion test samples, fabrication of mechanical test coupons, observing the layup procedures to better understand the manufacturing limitations. The author also gained a significant experience by helping out in the manufacturing of a few major components, laying up the carbon fibre plies, vacuum bagging the parts and taking down notes. He was also present during the infusion process to ensure the correct infusion parameters was used.

During the assembly of the body-in-white, the author was present to ensure the precise alignment of the body panels are within acceptable tolerances on the assembly jig and the preparation of gluing surfaces was carried out properly.

Manufacturing of EVA carbon composite vehicle structure are pictorially presented in Fig 5.1. In Fig 5.2 shows the assembly process of the sub-system components of EVA electric taxi. The author also participated actively in the assembly of the vehicle components to the body-in-white structure, ensuring the vehicle will be completed in time for Tokyo Motorshow. The assembly of the components required significant amount of work as some components cannot be fitted in and modification of the components have to be carried out.

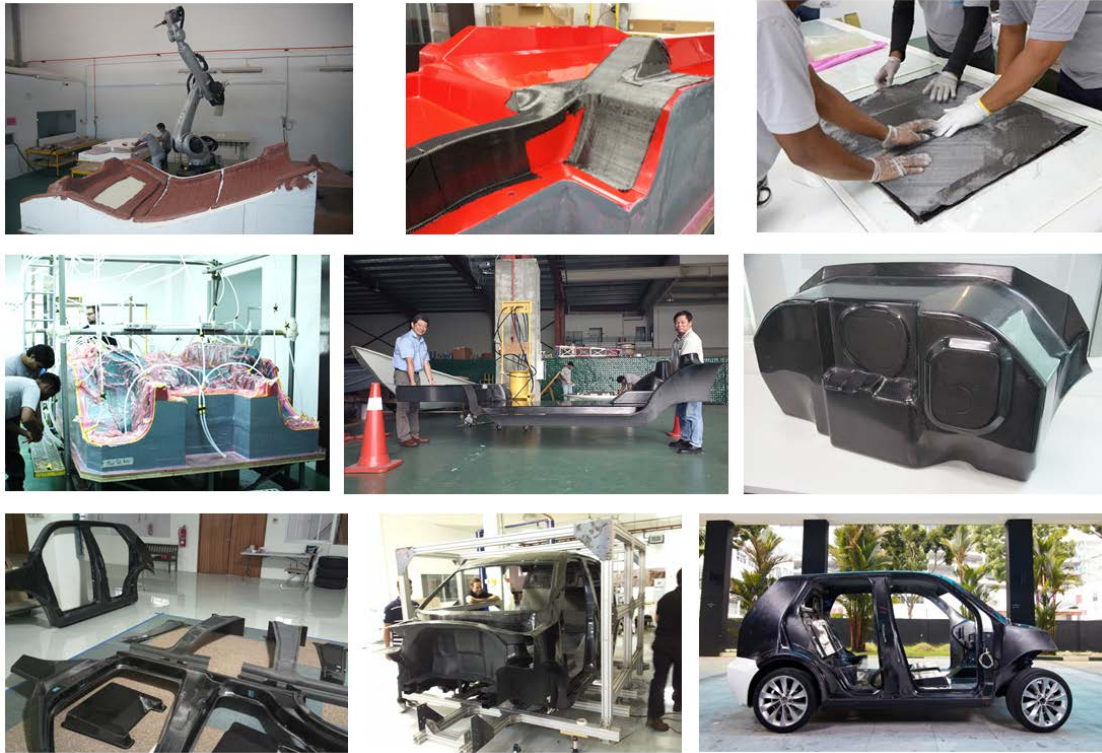


Fig 5.1 Manufacturing and assembly sequence of EVA BIW structure (Caption below)

1. *(Top right)* Kuka CNC robot machining carbon fibre composite panel tooling mold.
2. *(Top middle)* First play layup on main tub tooling mold.
3. *(Top right)* Layup of sandwich panel for test infusion.
4. *(Middle left)* Infusion of the vehicle main structural tub.
5. *(Middle)* Completed vehicle main structural tub.
6. *(Middle right)* Firewall carbon composite panel
7. *(Bottom left)* Carbon composite panels waiting to be assembled together.
8. *(Bottom mid)* Structural panels joint together using 3M DP490 adhesive on custom assembly jig.
9. *(Bottom right)* Completed EVA electric taxi body-in-white (BIW).





Fig 5.2 Component assembly of EVA Electric Taxi (Caption below)

1. *(Top left)* Rolling BIW structure test fitted with interior door panels
2. *(Top middle)* EVA in preparation for paint job.
3. *(Top right)* Vehicle component assembly at TUM CREATE automotive workshop.
4. *(Middle right)* EVA test fitted with front bumper.
5. *(Middle center)* Interior of EVA taxi
6. *(Middle right)* Photo-shoot of EVA.
7. *(Bottom)* Assembled EVA ready to be shipped to Japan for Tokyo Motor Show 2013.



Fig 5.3 Snippets of author working with EVA.

1. *(First row left)* Author sitting beside installed aluminium crash structure
2. *(First row middle)* View of the vehicle structure being assembled in the assembly jig.
3. *(First row right)* Authors and colleagues taking a photo with EVA after finish of final paintjob.
4. *(Second row left)* Dry hand layup of rear bootlid
5. *(Second row middle)* Transporting EVA for photoshoot
6. *(Second row right)* Author at Tokyo Motor Show 2013 with EVA
7. *(Third row left)* Bonding of internal and external bootlid panels at Admiralty International
8. *(Third row middle)* Taking a break from EVA assembly



9. (Third row right) Author trimming carbon composites panel
10. (Bottom) EVA project team members and industrial partners

## 5.2 Tokyo Motorshow 2013

After assembly, EVA Taxi was shipped to Japan and was officially launched at Tokyo Motor Show 2013. During which the electric taxi concept is showcased and was rigorously tested by visitors.



Fig 5.4 Compilation of pictures from the launch of EVA electric taxi at Tokyo Motor Show 2013.

1. (Top left) EVA exhibition booth crowded with visitors
2. (Top right) Children exploring the features of EVA
3. (Middle) EVA alone at the exhibition booth
4. (Bottom left) Demonstration of the convertible child seat
5. (Bottom right) Visitors exploring components in the motor bay



### 5.3 Vehicle Structure Performance by Physical Evaluation



Fig 5.5 Illustration of the carbon composite vehicle structure of EVA electric taxi prototype.

The complete body in white vehicle structure weight in at 220kg including metallic inserts and suspension sub-frame adapters mounts. During the assembly process structure the structure held up to rough handling and there are no noticeable flexing or weak points in the vehicle structure. However crashworthiness of the vehicle cannot be verified, physical inspection of crash critical components are very strong and rigidly attached such as anchoring points for seat belts. Preparation for driving is still underway, and further verification of the structure can only occur when driving test starts. In the next Chapter, we would conclude the observations and findings of the thesis.

---

## Chapter 6: Conclusions

---

### 6.1 Conclusions

The development of EVA electric taxi was challenging especially with the lack of design literature for crashworthy carbon composite vehicle structure. Information on carbon composite design have to be brought in from aircraft industries standard practices, Formula 1 race cars, type of vehicle structure design, metallic vehicle design, motorsport crash safety to detailed analysis of vehicle crash mechanics and vehicle crash standards. Information from these sectors are compiled together and analysed to develop a methodology that can be implemented for the development of a prototype vehicle structure. The understanding of failure modelling, particularly in fibre composite dynamic failure and non-linear ductile material behaviour allow the author to grasp the limitations and accuracy of such failure model to set realistic targets in the development. The development skills does not only include structural strength verification but also establishing methods to identify structural weakness and finding an efficient solution within tight design space by redirecting load path or changing the laminate layup. The simplification of crash loads into equivalent quasi-static crash loads was a new methodology to further simplify and speed up development. This is particularly useful for EVA's development, as accurate performance or highly efficiency engineering of vehicle structure is not required as development time for prototype as a fully functional proof of concept is usually short. Emphasise on development is to ensure safety and functionality of the prototype, whereby the accuracy of the simplified method is more than sufficiently and conservative.

The observation of step features and geometric complexity weakening the overall structure significantly are normally not covered in any vehicle structure literature. Coupled with these findings and design requirements, along with the understanding of manufacturing processes and tolerances allowed the author to develop efficient solutions. Many of the important, vehicle structure literature, development considerations and assumptions are highlighted chronologically from Chapter 2 and 3. The author also learnt to use of published experimental data to verify accuracy of material failure model to further proceed with development of the aluminium crash structure. Observation and findings from EVA's structure development enriched this thesis with practical design challenges for composite vehicle structure. Thus, this thesis would be very informative for development of any carbon composite vehicle structure, be it Shell Eco Marathon vehicle, Human Powered Vehicles (HPVs) or a fully functional vehicle concept.

In the development of the methodology, many assumptions and simplifications are made to allow quick approximate structure verification particularly under crash loads. This is one of the most important advantage anyone can have when developing a safe fully functional vehicle prototype which normally comes with low development resources and short timeframe. The simplified development methodology approach allows the structural designer to reach a

relatively efficient structure design quickly with just a few iteration, however it does not allow the designer to reach a highly developed efficient structure design. This is one drawback of simplified approach, but proved to be very useful for development of proof of concept prototype vehicles such as EVA, where development time is limited.

To develop and build the first fully functional electric taxi prototype in Singapore was challenging as there are limited local automotive industry, having to work closely in a team with people from different disciplines exposed the author to many different vehicle design specialization such as vehicle exterior/interior design and high and low voltage electrical systems. The experience was not just limited to vehicle structure development work but also learning the soft skills required to work well in a team.

This is a rare project opportunity as few university projects involves this level of exposure. Furthermore being able to oversee the fabrication and materialization of the author's engineering design into a fully functional prototype is heartwarming. The author now has a deep understanding of the amount of engineering work and design consideration that goes into any road worthy vehicle.

## 6.2 Recommendations for Future work

The methodology considerations, assumption and understanding of the requirements of crashworthy vehicle structure resulted in the successful development of EVA electric taxi. During the development process, the author identified many limitations and possible future research topics. Carbon composite crash structures have huge potential in lightening vehicle structure but the complexity of dynamic failure and stability under crushing cause many manufacturers to stick to traditional proven metallic ductile crash structures. With the improvement in simulation technology, manufacturing process, composite design validation via simulation will move the trend towards composites.

One potential area of research could be how load path design and geometrical features can be quantified numerically for optimal composite structure efficiency. As observed during development, geometrical effects on structural strength are far greater than the strength of the layup. Structural stiffening methods used for metallic structure does not work well for composites as composites does not have plasticity to mitigate stress concentration. By quantifying the strength factors of step features or angle of load path or even minimum feature radius can be useful in the initial phase and sizing. If these features can be quantified, it can be used to develop a geometry efficient structure quickly as one of the challenges in H0 model was to develop a realistic load path section.

Topology load path optimization can also be employed in the methodology to identify best position to place structural members and subsequently its required cross section size. This can be particularly useful during package definition during the project development. Further outlook on how these geometric complexity in carbon fibre composite can be characterize as one of the factor to rate vehicle structure efficiency.

The automotive industry will eventually move towards to employ multi material design and improvement in composite production will bring on incentive to focus applicability of composite in vehicle structure. The integrated Kevlar carbon composite used in the doors for crash protection can be further researched upon and characteristic of dynamic failure of such laminate can be useful to fine tune requirement for ductility and stiffness while keeping weight low.

### **6.3 Conferences and Publications by the Author**

The author has published conference papers on development methods of carbon composite vehicle structures.

- Raymond Khoo, A/P Ng Heong Wah - FEA simulation of a CFRP vehicle structure JEC ASIA 2013 (Singapore) Speaker
- Raymond Khoo, A/P Ng Heong Wah - EVA – The first electric vehicle specifically designed as a taxi for tropical megacities. Tackling the challenges of heat and humidity on EVs. E-mobilia World 2014 (Kuala Lumpur, Malaysia) Keynote Speaker
- Sebastian Bender, Vinoth Pannirsilvam, Raymond Khoo, Pablo López Hidalgo, Maximilian Tschochner, Pratik Sheth, Sebastian Osswald, Daniel Gleyzes, Heong Wah Ng, Markus Lienkamp, Concept of an Electric Taxi for tropical megacities COFAT 2014 (Germany)

---

## References

---

- [1] TUM CREATE, "Research," 2012. [Online]. Available: <http://www.tum-create.edu.sg/research/research>. [Accessed 30 May 2013].
- [2] Land Transport Authority of Singapore, "Singapore Land Transport Statistics in Brief 2013," LTA, Singapore, 2013.
- [3] IIHS, "IIHS 50th anniversary demonstration," Insurance Institute of Highway Safety, 2009.
- [4] C. Bare, D. Peterson, M. Marine and K. Welsh, "Energy Dissipation in High Speed Frontal Collisions," *SAE International*, 2013.
- [5] USARTL, "Aircraft Crash Survival Design Guide," USARTL, 1980.
- [6] R. Austin, "Lower extremity injuries and intrusion in frontal crashes," National Highway Traffic Safety Administration, Washington, DC, 2012.
- [7] Carhs, "Safety companion 2013," in *Safety companion 2013*, Germany, 2013.
- [8] Audi, "Audi TT space frame," Audi, [Online]. Available: [http://www.audi.com.au/au/brand/en/models/tt/tt\\_roadster/equipment/audi\\_space\\_frame.html](http://www.audi.com.au/au/brand/en/models/tt/tt_roadster/equipment/audi_space_frame.html). [Accessed 20 10 2013].
- [9] M. Nakao, "Collapse of Tacoma narrows bridge," University of Tokyo, Tokyo, 1996.
- [10] D. E. Malen, Fundamentals of automobile body structure design, Warrendale, USA: SAE International, 2010.
- [11] M. Pfestorf and J. V. Rensburg, "Functional Properties of High Strength Steel in the body in white," Great Designs in Steel Seminar, 2005.
- [12] S. Braess, Handbook of automotive engineering, SAE International, 2005.

- [13] G. P. Jäger and M. Tschochner, *Axle system sourcing : Simulation and integration for an electric taxi*, Singapore: TUM CREATE, 2012.
- [14] J. C. Brown, A. J. Robertson and S. T. Serpento, "History : the underfloor chassis frame," in *Motor vehicle structures : concepts and fundamentals*, Butterworth Heinemann, 2002, p. 29.
- [15] Boron Extrication, "2011 Audi A8 Body Structure Safety Cage," 29 10 2010. [Online]. Available: <http://www.boronextrication.com/2010/10/29/2011-audi-a8-body-structure-safety-cage/>. [Accessed 20 11 2013].
- [16] European Aluminium Association, "The aluminium automotive manual," European Aluminium Association, 2013.
- [17] A. MacKenzie, "50 years of McLaren: 1963-2013," 29 10 2013. [Online]. Available: <http://www.gizmag.com/50-years-mclaren/26807/>. [Accessed 30 11 2013].
- [18] E. Loveday, "Overview of BMW i3 lifedrive tech," 17 10 2011. [Online]. Available: <http://green.autoblog.com/2011/10/17/overview-of-bmw-i3-lifedrive-tech/>. [Accessed 2 12 2012].
- [19] Caricos, "2012 BMW i3 Coupe Concept," 20 10 2011. [Online]. Available: [http://www.caricos.com/cars/b/bmw/2012\\_bmw\\_i3\\_coupe\\_concept/](http://www.caricos.com/cars/b/bmw/2012_bmw_i3_coupe_concept/). [Accessed 14 10 2013].
- [20] K. Makino, "Advanced requirements for fuel efficient cars by creating efficient body," *SAE International*, 2011.
- [21] ICCT, "Global comparison of light-duty vehicle fuel economy/GHG emissions standards," The international council on clean transportation, 2012.
- [22] B. K. Zuldema, "On the Role of body-in-white weight reduction in the attainment of the 2012-2025 US EPA/NHTSA fuel economy mandate," ArcelorMittal Global research and development, 2013.
- [23] C. R. Knittel, "Automobiles on Steroids : Product attribute trade-offs and technological progress in the automobile sector," *American Economic Review*, pp. 3368-3399, 2012.

- [24] N. Lutsey, "Review of technical literature and trends related to automobile mass-reduction technology," Institute of Transportation Studies, University of California, Davis, 2010.
- [25] M. Gillies, "Volkswagen unveils seventh-generation golf in berlin," 4 sept 2012. [Online]. Available: <http://www.media.vw.com/newsrelease.do;jsessionid=34282B007EB6F52F499BF3B89EF75C90?&id=1205&mid=1>.
- [26] J. Vondruska, "Golf 7 Tech highlights," 24 Aug 2012. [Online]. Available: <http://www.vwvortex.com/features/technical-features/golf-7-technicalpreview/>.
- [27] A. Stoy, "2013 Land Rover Range Rover sheds weight with all-aluminum unibody," 9 June 2012. [Online]. Available: <http://www.autoweek.com/article/20120906/carnews/120909922>.
- [28] Aluminum.org, "Jaguar, Land Rover to go All-aluminum," 2010. [Online]. Available: <http://www.aluminum.org/AM/Template.cfm?Section=Home&CONTENTID=29338&TEMPLATE=/CM/ContentDisplay.cfm>. [Accessed 6 May 2012].
- [29] National Climate Change Secretariat, "National Climate Change Strategy 2012," National Climate Change Secretariat, Singapore, 2012.
- [30] WorldAutoSteel, "Future Steel Vehicle Phase 2," EDAG, 2011.
- [31] International Aluminium Institute, "Improving sustainability in the transport sector through weight reduction and the application of aluminium," The Aluminum Association, 2007.
- [32] J. Nolan, "The relative safety of large and small passenger vehicles," NHTSA Mass-size safety symposium, Washington, DC, 2013.
- [33] Institute for carbon composite (LCC), "Composite materials and structure property relationship," Technical University of Munich, Munich, 2011.
- [34] J. Shaw and B. Zuidema, "New high strength steels help automakers reach future goals for safety, affordability, fuel efficiency and environmental responsibility," SAE

*Technical Paper*, 2001.

- [35] World Steel Association, "Advance High Strength Steel Application Guidelines," 2009.
- [36] T. B. Stoughton, "A General forming limit criterion for sheet metal forming," *International journal of mechanical sciences*, pp. 1-27, 2000.
- [37] E. Billur and T. Altan, Challenges in forming advanced high strength steel, Engineering research center for net shape manufacturing (ERC/NSM).
- [38] H.-S. Kim, "New extruded multi-cell aluminium profile for maximum crash energy absorption and weight efficiency," *Thin-walled structures*, vol. 40, pp. 311-327, 2002.
- [39] T. Wierzbicki and W. Abramowicz, "On the crushing mechanics of thin-walled structures," *Journal of Applied Mechanics*, vol. 50, no. 4a, pp. 727-734, 1983.
- [40] B. Dipaolo, P. Monteiro and R. Gronsky, "Quasi-static axial crush response of a thin-wall, stainless steel box component," *International Journal of Solids and Structures*, vol. 41, pp. 3707-3733, 2004.
- [41] M. F. Ashby, Material selection in mechanical design, Fourth edition, Butterworth-Heinemann, 2010.
- [42] B. Klein, "Werkstoffwertung," in *Leichtbau-Konstruktion: Berechnungsgrundlagen und Gestaltung*, Vieweg+teubner, 2009, p. 31.
- [43] T. Edison, "Electric Lamp". US Patent 223,898, 27 Jan 1880.
- [44] J. Sloan, "Carbon fiber market: Cautious optimism," in *Composite World's Carbon Fiber conference 2009*, 2009.
- [45] M. Zhou, R. Fleury and W. Dias, "Composite design optimization - from concept to ply-book details," in *8th world congress on structural and multidisciplinary optimization*, Lisbon, Portugal, 2009.
- [46] Boeing, "787 Dreamliner program fact sheet," Boeing , [Online]. Available: <http://www.boeing.com/boeing/commercial/787family/programfacts.page>. [Accessed



03 01 2014].

- [47] I. Daniel and O. Ishai, Engineering mechanics of composite materials 2nd edition, Oxford University Press, 2006.
- [48] V. Calard, "Formulas and equations for classical laminate theory," Centraliens, 2011.
- [49] Zoltek, "Zoltek prepreg," 07 2011. [Online]. Available: <http://www.zoltek.com/wp-content/uploads/2011/07/Prepreg.png>. [Accessed 03 12 2013].
- [50] Institute for carbon composite (LCC), "Lecture : production technologies for composite parts," Technical university of munich, munich, 2012.
- [51] F. Mayer, "Analysis and implementation of a parametric vehicle body component out of CFRP," TUM CREATE, Singapore, 2013.
- [52] Institute for carbon composite (LCC), "Lecture : analysis and design of composite structures," Technical university of munich, Munich, 2012.
- [53] L. J. Hart-Smith, "The Ten-Percent Rule for preliminary sizing of fibrous composite structures," *SAWE Journal*, vol. 5, no. 2, pp. 10-16, 1993.
- [54] L. J. Hart-Smith, "Design and analysis of adhesively bonded joints in fibrous composite structures," McDonnell Douglas.
- [55] K. Dreschsler, R. Hinterholz, C. Hahn and A. Altmann, "Analysis and Design of Composite Structures," Lehrstuhl für Carbon Composite (LCC), Munich, 2011.
- [56] L. Hart-Smith, "Mechanically-fastened joints for advanced composites - Phenomenological considerations and simple analyses," *Fibrous composites in structural design*, vol. New York, no. Plenum Press, pp. 543-574, 1980.
- [57] D. Liu, Y. Tang and W. Cong, "A review of mechanical drilling for composite laminates," *Composite structures*, vol. 94, pp. 1265-1279, 2012.
- [58] R. F. Gibson and S. Thoppul, "Experimental and numerical characterization of relaxation in bolted composite joints," in *Composite materials and joining technologies*

for composites, volume 7 : proceedings of the 2012 annual conference on experimental and applied mechanics, 2012.

- [59] L. Hart-Smith, "The Critical factors controlling the durability of bonded composite joints - surface preparation and the presence or absence of pre-bond moisture," in *MIL-HDBK-17 & FAA Meeting*, Seattle, 2004.
- [60] L. J. Hart-Smith, "Surface preparations for ensuring that the glue will stick in bonded composite structures," McDonnell Douglas, South Carolina, 1993.
- [61] L. J. Hart-Smith, "Adhesively bonded joints for fibrous composite structures," McDonnell Douglas, London, 1986.
- [62] Direct industry, "Bighead load bearing threaded inserts," Direct industry, [Online]. Available: URL: <http://www.directindustry.com/prod/bighead-bonding-fasteners/load-bearing-threaded-inserts-15331-442142.html>. [Accessed 22 05 2013].
- [63] J. Ucsnik, "lightweight design," in *Mischbau-Fügetechnik für Metall- Composite-Lasteinleitung*, 2013, pp. 24-29.
- [64] G. Barnes, I. Coles, R. Roberts, D. O. Adams and D. M. G. jr., "Crash Safety Assurance Strategies for future plastic and composite intensive vehicles (PCIVs)," Volpe National Transportation Systems Center, Cambridge, 2010.
- [65] A. Puck, Festigkeitsanalyse von Faser-Matrix-Laminaten: Modelle für die Praxis, München; Wien: Hanser, 1996.
- [66] Z. Hashin and A. Rotem, "A Fatigue failure Criterion for fibre reinforced materials," *Journal of Composite Material*, vol. 7, pp. 448-464, 1973.
- [67] V. D. Azzi and S. W. Tsai, "Anisotropic Strength of Composites," *Experimental Mechanics*, pp. 283-288, 1965.
- [68] O. Hoffman, "The brittle strength of orthotropic materials," *Journal of Composite Material*, pp. 200-206, 1967.
- [69] C. Chamis, "Failure Criteria for Filamentary Composites," in *Composite Materials :*

*Testing and Design, STP 460*, Philadelphia, 1969.

- [70] P. Camanho and F. Matthews, "A progressive damage model for mechanically fastened joints in composite laminates," *Journal of Composite Materials*, vol. 33, pp. 2248-2280, 1999.
- [71] I. Shalif and F. Chang, "An accumulative damage model for tensile and shear failures of laminated composite plates," *Journal of Composite Materials*, vol. 29, pp. 926-981, 1995.
- [72] WorldAutoSteel, "Future Steel Vehicle Phase 1," EDAG, 2009.
- [73] EuroNCAP, "European New Car Assessment Programme - Frontal impact testing protocol," EuroNCAP, 2013.
- [74] Insurance Institute for highway safety, "Small overlap frontal crashworthiness evaluation crash test protocol," Insurance institute for highway safety, Arlington , 2012.
- [75] K. J. Craig, N. Stander, D. Dooge and S. Varadappa, "Automotive crashworthiness design using response surface-based variable screening and optimization," *Engineering computations : international journal of computer-aided engineering and software*, vol. 22, no. 1, pp. 38-61, 2005.
- [76] W. J. Witteman, "Improved vehicle crashworthiness by control of the energy absorption for different collision situations," University of Eindhoven, 1999.
- [77] H. G. Herrmann, C. Mohrdieck and R. Bjekovic, "Materials for the automotive lightweight design," in *FKA/IKA Conferences New advances in body engineering*, Aachen, Germany, 2002.
- [78] USF1 team, "US F1 Team - Nose Crash Test," US F1 Team, 9 Jan 2010. [Online]. Available: <http://www.youtube.com/watch?v=Mc0wFyCIDfE>. [Accessed 30 12 2013].
- [79] C. McGregor, R. Vaziri and X. Xiao, "Finite element modelling of the progressive crushing of braided composite tubes under axial impact," *International Journal of Impact Engineering*, vol. 37, pp. 662-672, 2010.

- [80] T. PH., "The crush behavior of pultruded tubes at high strain rates," *Journal of composite materials*, vol. 24, p. 594, 1990.
- [81] H. D., "Unified approach to progressive crushing of fibre-reinforced composite tubes," *Composites science and technology*, vol. 40, pp. 377-421, 1991.
- [82] A. Stahl, "Crash relevant composite vehicle structure in the DLR vehicle concept NFS," in *Composite Forum - Lightweight structures*, 2010.
- [83] P. Soden, A. Kaddour and M. Hinton, "Recommendations for designers and researchers resulting from the world-wide failure exercise," *composite science and technolgy*, vol. 64, pp. 589-604, 2004.
- [84] M. Hinton, A. Kaddour and P. Soden, *Failure Criteria in Fibre-reinforced-polymer composite*, Elsevier, 2004.
- [85] M. Hinton, S. Kaddour, P. Smith, S. Li and P. Soden, "Failure criteria in fibre reinforced polymer composites : can any of the predicitive theories be trusted," in *NAFEMS World Congress*, Boston, 2011.
- [86] J. Lescheticky, G. Barnes and M. Schrank, "System level design simulation to predict passive safety performance for CFRP automotive structures," *SAE International*, 2013.
- [87] A. J. Fawcett, "Damage Tolerance and the Composite Airframe (787 dreamliner)," Boeing, 2007.
- [88] Department of Defense, MIL-HDBK-17-1F : Composite material handbook : Volume 1. Polymer matrix composite guidelines for characterization of structural materials, Department of Defense, 2002.
- [89] A. Schwingenschlögl, "Material Property Testing TUM CREATE RP 9 WP A3," TUM CREATE, Singapore, 2012.
- [90] E. A. Birt and R. Smith, "A Review of NDE methods for porosity measurement in fibre-reinforced polymer composites," *Insight*, vol. 46, no. 11, pp. 681-686, 2004.
- [91] L. Hart-Smith, "Mechanically-fastened joints for advanced composites - phenomenological considerations and simple analyses," in *Fibrous Composite in*

*Structural Design*, New York, Plenum Press, 1980, p. 543.

- [92] B. Arnold and W. Altenhof, "Finite Element Modeling of the axial crushing of AA6061 T4 and T6 and AA6063 T5 structure square tubes with circular discontinuities," *SAE Technical Paper*, 2005.
- [93] W. T. Hollowell, H. C. Gabler, S. L. Stucki, S. Summers and J. E. Hackney, "Updated review of potential test procedures for FMVSS 208," NHTSA, 1999.
- [94] Insurance Institute for highway safety, "Side impact crashworthiness evaluation crash test protocol (version VI)," Insurance Institute for highway safety, Arlington, 2012.
- [95] Euro NCAP, "European New Car Assessment Programme - Side impact testing protocol," EuroNCAP, 2012.
- [96] EuroNCAP, "European new car assessment programme - pole side impact testing protocol," EuroNCAP, 2011.
- [97] Insurance Institute for highway safety, "Crashworthiness evaluation roof strength test protocol (version II)," Insurance Institute for highway safety, Arlington, 2012.
- [98] BSI, *BS EN ISO 527-4 Plastic - Determination of tensile properties*, BSI, 1997.
- [99] BSI, *Structural Adhesives - determination of shear behaviour of structural bonds part 2 : thick adherends shear test (ISO 11003-2:2001, modified)*, BSI, 2011.
- [100] S. Palanivelu, W. V. Paepegema, J. Degrieck, D. Kakogiannis, J. V. Ackeren, D. V. Hemelrijck, J. Wastiels and J. Vantomme, "Comparative study of the quasi-static energy absorption of small-scale composite tubes with different geometrical shapes for use in scarifical cladding structures," *Polymer Testing*, no. 29, pp. 381-396, 2010.
- [101] B. Jason C., R. A. John and S. Stan T., *Motor Vehicle Structures : Concepts and Fundamentals*, Butterworth Heinemann, 2002.
- [102] G. Barnes, "CZone Composite crush predictions," in *49th MIL-HDBK17 meeting*, Santa Monica, 2005.

- [103] H. Puck, "Festigkeitsanalyse von fasern-matrix-laminaten," Hanser, 1996.
- [104] U. Polimeno and M. Meo, "Detecting barely visible impact damage detection on aircraft composite structures," *Composite structures*, vol. 91, no. 4, pp. 398-402, 2009.
- [105] T. O'Kane, "2008 Mercedes-Benz C-Class Achieves Top Score In US Safety Test," the motor report australia, 10 12 2008. [Online]. Available: [http://www.themotorreport.com.au/content/image/1/4/14439\\_merc\\_c\\_class\\_crash\\_test\\_thumb-4b77abb5ef6f8.jpg](http://www.themotorreport.com.au/content/image/1/4/14439_merc_c_class_crash_test_thumb-4b77abb5ef6f8.jpg). [Accessed 13 12 2013].
- [106] Delorean Museum, "Delorean Museum," [Online]. Available: <http://www.deloreanmuseum.org/car.html>. [Accessed 10 12 2012].
- [107] A. Tsaousis, "car scoops," 10 02 2013. [Online]. Available: <http://www.carscoops.com/2013/02/vw-group-mqb-mega-platform-is-huge-game.html>. [Accessed 3 10 2013].
- [108] Formula 1, "2014 pre season testing," 20 1 2014. [Online]. Available: <http://www.formula1.com>.
- [109] R. J. B. R. Peter Furrer, "Aluminum crash management systems," in *2004 SAE World Congress*, Detroit, Michigan, 2004.





---

## Glossary

---

ABAQUS	Explicit and implicit FEA simulation software
Advanced high strength steel	Special grade of steel that is above 300MPa
Airbags	Inflatable bag that deploy in vehicle impact to cushion occupant from impact forces
Anisotropic	Non homogenous material mechanical properties
A-Pillar	The first pillar to the roof of a vehicle structure reference from front
Barely Visible Impact Damage	Localized damage that cannot be detected visually resulting in reduction of static strength
Bending Stiffness	Value to indicate performance in bending mode
Black Metal Design	Quasi-isotropic layup of carbon fibre to mimic homogenous material
Body in White	Bare body structure of a vehicle excluding doors
B-Pillar	The second pillar to the roof of a vehicle structure reference from front
Brittle	A material that fails without plastic deformation
Cabin	Vehicle occupant area
Carbon Composites	Carbon Fibre Composite
Chassis	Suspension systems and powertrain components
CO <sub>2</sub>	Carbon Dioxide
Composites	Combination of two or more material that comprises of at least one reinforcing material
Computation fluid dynamics	Simulation of fluid behavior using mathematical model
Continuum Damage Mechanics	A method of finite element simulation on material failure
Coupons	Test coupon for testing mechanical properties
C-Pillar	The third pillar to the roof of a vehicle structure reference from front
Crash compatibility	Injury risk when colliding with a different class of vehicle
Crashworthiness	A structural that can absorb crash energy to reduce or prevent injury
Crumple zone	An allocated space/zone used to absorb crash energy
Crush Compression Ratio	Composite crush strength and compressive strength
Czone	A simulation method to predict dynamic composite failure
Delamination	Layered separation between layers of fibres and matrix material
Ductile	Material that undergoes large plastic deformation
Electronic stability control	An active electronic program that maintain stability of vehicle by optimally applying brake on each individual wheel
Elements	Elements in finite element analysis

Fasteners	Mechanical clamping, locking device to attach two components together
Fatigue (material)	Fail of material due to excessive cycling stress load
Fibre Volume Fraction	Volume ratio of reinforcing fibre in the composite
Fibre Wash out	movement of fibre due to violent injection particularly in resin transfer moulding
Fragmentation	Breaking up in small pieces
Future steel vehicle	A research development program to identify weight saving capabilities using state of the art steel
Green house Gases	Gases that traps heat
Hyper Elastic	Material that enlarges many times its length without failure or plastic deformation
Inter-laminar	Interaction between laminar layers
Intrusion	Deformation inwards
ISOGRID	Stiffening shapes (hexagon) typically
Laminar	A layer of composite structure that have identical reinforcement
Laminate	A combination of laminar
Layup	How reinforcing fabric is placed
Light weight index	An index to classify vehicle structure efficiency
Lightweight	Performance with minimal amount of weight
Matrix Material	Material that supports reinforcement materials
Megacities	A metropolitan area with a total population in excess of 10 million people
Mobile Deformable Barrier	A dummy vehicle with aluminium honeycomb crash structure
Monocoque	A structural design that utilize strength of exterior skin as a unit to provide support
Multi body simulations	Computer simulation of response between mass bodies
OPTISTRUCT	Altair group optimization software package
Orthotropic	Symmetric material properties in 3 direction
Perform	Shaped reinforced fabric for manufacturing
Plasticity	Degree of plastic deformation
Plies	Layers of lamina
Ply book	The complete layup of the family group
Porosity	Void in a material
Powertrain	The systems that paramounds the
Pre-preg	Pre-impregnated reinforcing fabric with resin
Resin Transfer Moulding	A composite manufacturing process
Rigid Barrier	A crash barrier without deformable structure
Roll over	A vehicle that flipped or impacted the roof

Safety Cell	the stiff vehicle structure that encompass the cabin
Safety Glass	Temperglass that shatters into small bis when breakage
Sandwich Construction	Layer construction of composites with a lightweight high shear streangth material
Specific energy absorption	Specific Energy absorptiong
Sub-systems	Systems that is within the system
Topology	Geometric layup
Unibody	Similar to monocoque, unit body
Vehicle footprint	Plan projection view limits

## Appendix A

---

# Crash Standards Selected for Development of EVA Vehicle Structure

## Full Width Crash Test.

---

This test is performed by U.S. NCAP (FMVSS 208), is one of the most demanding. The test simulates a violent frontal collision against a rigid wall, engaging the entire front crash structure. This full engagement of the crash structure will result in the highest deceleration on the safety cell. The criteria for performance are determined by the crash test dummy's injury criteria [93].

---

## Offset deformable barrier (ODB) and Small Overlap Barrier (SOB)

---

Misaligned frontal collision or offset frontal collision into another vehicle or road side obstacles are more likely to happen than a full width engagement collision. The 40% offset deformable barrier crash test is introduced to test the structure stability of the vehicle structure in an off axis impact. Vehicles that perform well in this test are able to withstand off balanced crash forces while minimize intrusion and deformation in passenger cabin [93] [73]. The IIHS introduced the 20% small overlap barrier test in Oct 2012 to promote safety in crashes where the main front energy absorbing beam will be missed. [74]

---

## Mobile Deformable Barriers (MDB)

---

Mobile deformable barriers side crash test are primary used to test the ability of the vehicle to protect occupants in a side impact particularly the head and torso. The lack of crumple zone in doors meant that side airbags plays a major role in reducing injuries. IIHS and U.S. NCAP utilize a larger MDB that mimic side impact by a large truck to test head protection. [94] [95]

---

## Pole Crash Test

---

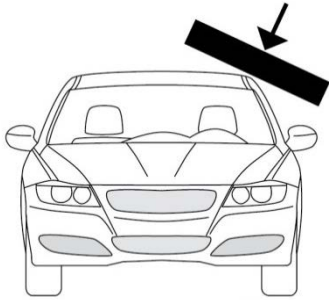
Pole test is particularly similar to MDB tests, which relies significantly on the performance of the air bag. The pole test simulates side impact with a pole like object, simulating impact with a tree or lamppost [96].

---

## Roof Crush Test

---

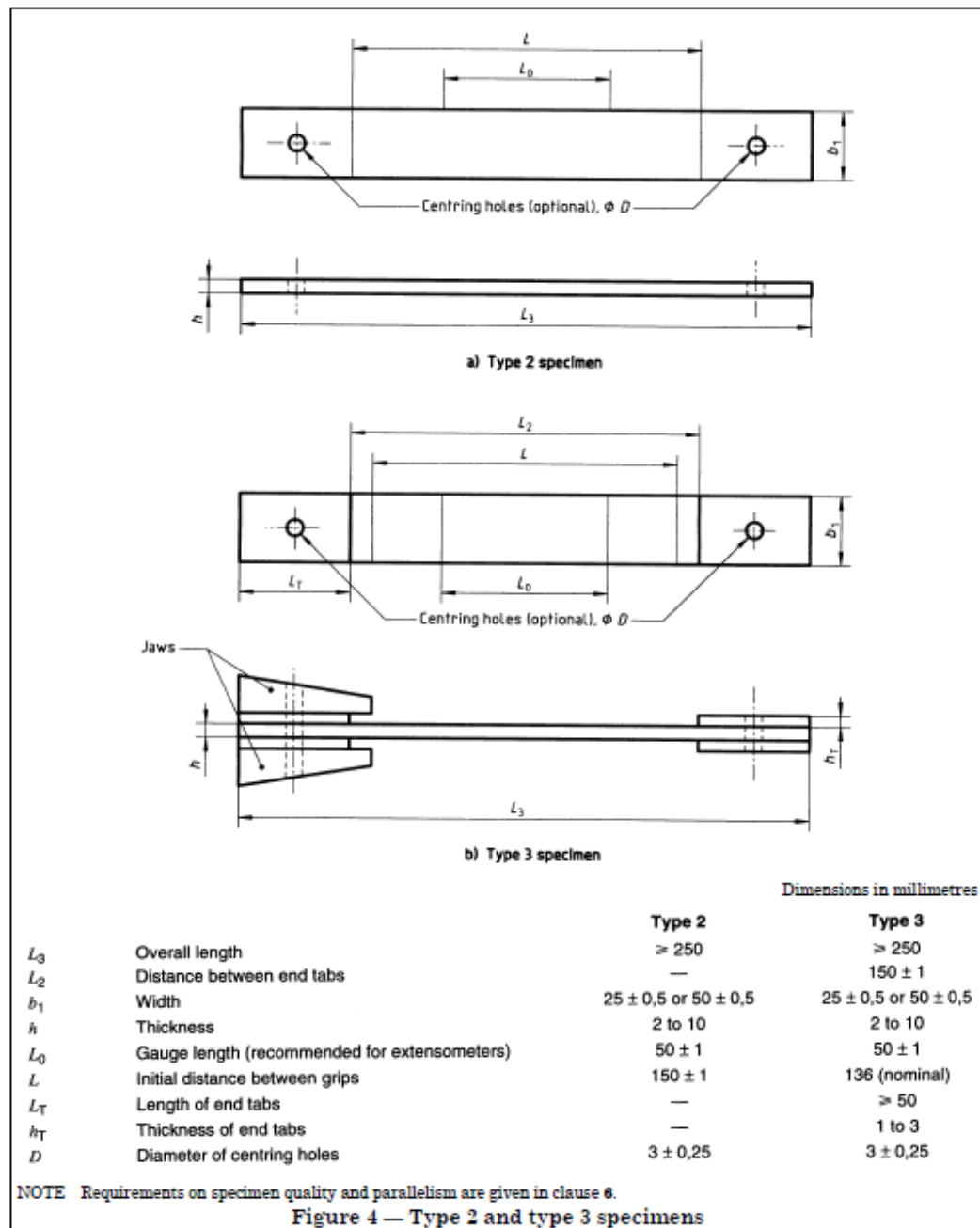
The roof crash test (FMVSS 216a) is only conducted by IIHS. It evaluates the strength of the roof with predetermined displacement (127mm), the rating are usually rated in strength to vehicle weight ratio. Vehicles that perform well in this test generally have roof strength that can withstand 4 times the weight of the vehicle. This test is to ensure the roof is strong enough to provide survival space in an event of a rollover [97].



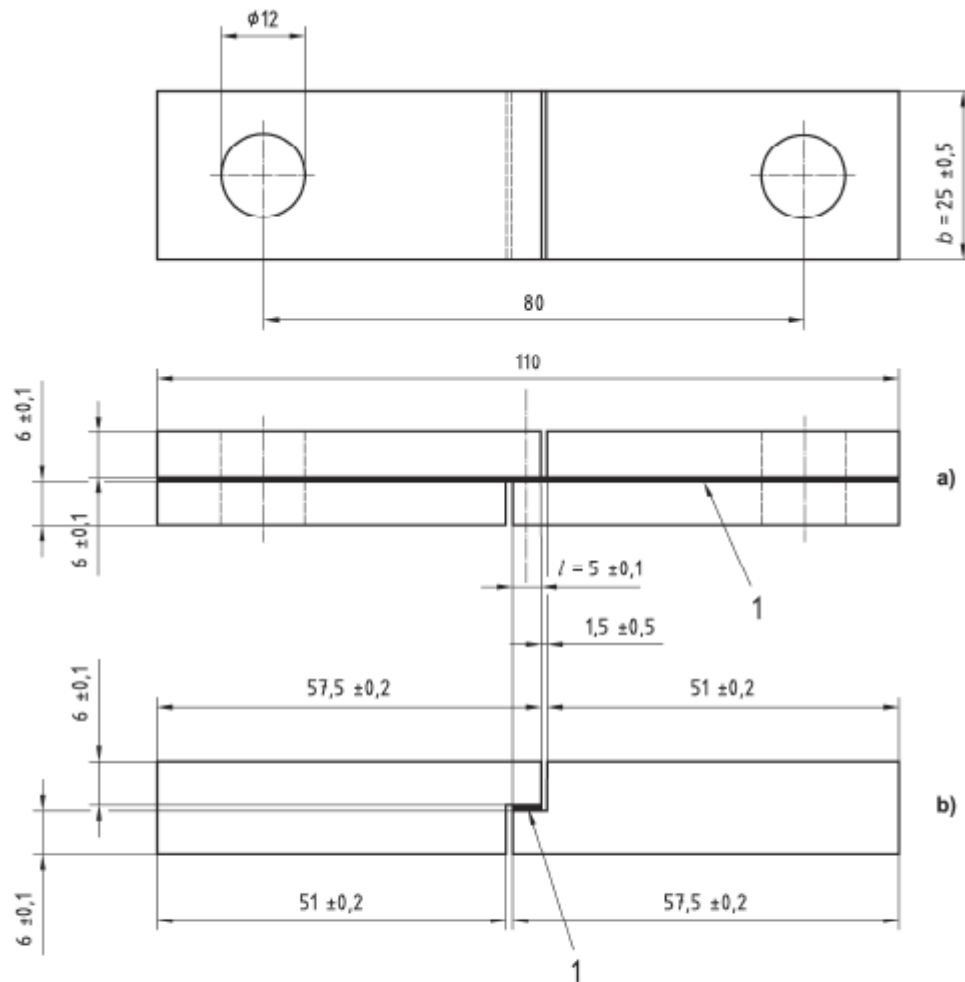
Roof crush test IIHS (FMVSS 216a)

## Appendix B

Type 2 and type 3 coupon specimen specification for EN ISO 527-4:1997 test for determination of tensile properties of orthotropic fibre-reinforced plastics. [98]



Specification of different coupon test sample EN 14869-2:2011 Standard for structural adhesives - determination of shear behaviour of structural bonds: Part 2 Thick adherends shear test [99]



#### Key

- a) Bonded adherends
- b) Machined adherends
- 1 Adhesive bond
- $b$  Width of adhesive
- $l$  Length of adhesive

Figure 1 — Specimen dimensions and configuration